Aus dem Munich Cluster for Systems Neurology (SyNergy) am Institut für Schlaganfall- und Demenzforschung (ISD)
Institut der Ludwig-Maximilians-Universität München

Vorstand: Prof. Dr. med. Martin Dichgans


# Dissecting the role of UBQLN2 in amyotrophic lateral sclerosis and frontotemporal dementia using multi-omics profiling

Dissertation

zum Erwerb des Doktorgrades der Naturwissenschaften

an der Medizinischen Fakultät der

Ludwig-Maximilians-Universität zu München

vorgelegt von

Laura Rebekka Strohm

aus

Münsingen

2022

Gedruckt mit Genehmigung der Medizinischen Fakultät

Der Ludwig-Maximilians-Universität München

| | |
|---|---|
| Betreuer: | Prof. Dr. rer. nat. Christian Behrends |
| Zweitgutachter(in): | Prof. Dr. rer. Nat Axel Imhof |
| Dekan: | Prof. Dr. med. Thomas Gudermann |
| Tag der mündlichen Prüfung: | 30. März 2023 |

# Table of Contents

# Summary

Amyotrophic lateral sclerosis (ALS) and frontotemporal dementia (FTD) are two entangled neurodegenerative diseases that were shown to form a disease continuum. Besides common mutations in chromosome 9 open reading frame 72 (*C9orf72*), fused in sarcoma (*FUS*) and transactive response (TAR) DNA-binding protein of 43 kDa (*TDP-43*), also mutations in ubiquilin 2 (*UBQLN2*) are known to cause ALS/FTD. Interestingly, most ALS/FTD-associated mutations are in or close to the PXX repeat motif of UBQLN2. This region is not present in any other member of the ubiquilin protein family. The main cellular function of UBQLN2 is the shuttling of ubiquitinated cargo to the proteasome for degradation. Accordingly, disturbances in the ubiquitin-proteasome system (UPS) are one of the most studied mechanisms in UBQLN2-associated pathologies. Despite intensive research, the specific pathomechanism of ALS/FTD-linked UBQLN2 mutations remains elusive.

Hypothesizing that mutations in UBQLN2 lead to alterations of cellular components regulated by UBQLN2, we performed a multi-omics screening. Systematic proteomic and transcriptomic analyses of patient-derived UBQLN2 mutant lymphoblast cell lines (LCLs), CRISPR/Cas9-engineered HeLa cells harboring the same mutations and their wild-type counterparts revealed changes in ALS/FTD-associated pathways, such as RNA metabolism or mitochondrial function. Additionally, we uncovered a strong enrichment of a protein which was poorly characterized in the context of ALS/FTD: the microtubule-associated protein 1B (MAP1B). Based on the consistent up-regulation in all analyzed data sets and its importance in the modulation of cytoskeletal dynamics in neuronal cells, further experiments within this thesis focused on MAP1B. To clarify if MAP1B up-regulation can be ascribed to a UBQLN2 loss-of-function or gain-of-function, a CRISPR/Cas9-mediated UBQLN2 knockout (KO) HeLa cell line was generated. As in UBQLN2 mutant cells, a strong increase in MAP1B was detected in UBQLN2 KO cells. The relevance of this finding was further substantiated by depletion of Ubqln2 in primary hippocampal and cortical rat neurons. Also, in these neuronal cells a MAP1B elevation was observed. Consistent with MAP1B's capacity to associate with microtubules, we found an increase in microtubule mass in UBQLN2 KO cells.

In a phosphoproteomic screen of the LCLs, we discovered that ALS/FTD-linked mutations in UBQLN2 result in a hypophosphorylation of serine 439 (S439) in FUS. Phosphorylation of this site was reported but not further dissected before, even though it is in the zinc finger domain of FUS which is crucial for RNA-binding. We found that modulation of this phosphosite not only regulates FUS-RNA-binding but also MAP1B protein abundance. In summary, this work provides first evidence for increased mRNA and protein abundance of MAP1B caused by ALS/FTD-linked UBQLN2 mutations as a result of a UBQLN2 loss-of-function mechanism. In

addition, this work links phosphorylation of S439 to FUS' RNA-binding capacity and to ALS/FTD. Thus, this thesis further interconnects three main pathogenic mechanism of ALS/FTD: dysfunctional protein homeostasis, disturbed RNA metabolism and cytoskeletal defects.

# Zusammenfassung

Amyotrophe Lateralsklerose (ALS) und Frontotemporale Demenz (FTD) sind zwei eng miteinander verknüpfte, neurodegenerative Erkrankungen, welche als zwei Ausprägungen eines Krankheitskontinuums betrachtet werden. Neben den häufigeren genetischen Ursachen von ALS/FTD wie Mutationen in Chromosome 9 Open Reading Frame 72 (*C9orf72*), Fused in Sarcoma (*FUS*) und Transactive Response (TAR) DNA-binding protein of 43 kDa (*TDP-43*), können auch Mutationen in Ubiquilin 2 (*UBQLN2*) ALS/FTD verursachen. Hierbei wurde festgestellt, dass die meisten dieser Mutationen nahe oder in der PXX-Region von UBQLN2 liegen, einer Region, welche in keinem anderen Mitglied der Ubiquilinfamilie zu finden ist. In der Zelle ist UBQLN2 hauptsächlich für den Transport von ubiquitinierten Substraten zum Proteasom zuständig, wo diese dann abgebaut werden. Entsprechend wurden UBQLN2-Mutationen in der Vergangenheit vor allem hinsichtlich ihrer Auswirkungen im Ubiquitin-Proteasom-System (UPS) untersucht. Trotz intensiver Forschung ist der Pathomechanismus von ALS/FTD-assoziierten UBQLN2-Mutationen noch nicht vollständig aufgeklärt.

Basierend auf der Annahme, dass Mutationen in UBQLN2 zu Veränderungen von zellulären Komponenten führen, haben wir ein Multi-Omics Screening durchgeführt. Systematische proteomische und transkriptomische Analysen von aus Patienten isolierten lymphoblastoiden Zelllinien (LCLs), CRISPR/Cas9-editierten HeLa-Zellen, welche die gleichen Mutationen in UBQLN2 tragen, sowie deren Wildtyp-Gegenstücke, zeigten Veränderungen in ALS/FTD-assoziierten Mechanismen, wie dem RNA-Metabolismus oder der mitochondrialen Funktion auf. Zudem haben wir eine starke Erhöhung des Mikrotubuli-assoziierten Proteins 1B (MAP1B), einem Protein welches bisher kaum im Kontext von ALS/FTD erforscht wurde, aufgedeckt. Die konsistente Erhöhung in allen Datensätzen, sowie die Bedeutung von MAP1B für die Regulation des Cytoskeletts in Neuronen veranlasste uns dazu dieses Protein genauer zu untersuchen. Zunächst wurde ermittelt, ob die validierte Erhöhung von MAP1B auf einen Funktionsverlust oder einen toxischen Funktionsgewinn von UBQLN2 zurückzuführen ist. Hierfür wurde mithilfe von CRISPR/Cas9 eine UBQLN2-Knockout (KO)-HeLa-Zelllinie generiert. Wie bereits in den UBQLN2-Mutanten, haben wir auch bei den UBQLN2-KO-Zellen eine starke Erhöhung von MAP1B festgestellt, was einen Funktionsverlust von UBQLN2 als Ursache dieser Erhöhung nahelegt. Die Relevanz dieser Erkenntnisse wurden durch die Verminderung von Ubqln2 in hippocampalen und kortikalen primären Rattenneuronen unterstrichen, in welchen ebenfalls eine Erhöhung von MAP1B gemessen wurde. Im Einklang mit der Rolle MAP1B‘s als Mikrotubuli-assoziiertes Protein, haben wir zudem eine erhöhte Menge an α-tubulin in UBQLN2-KO-Zellen zeigen können.

Darüber hinaus haben wir in einem phosphoproteomischen Screening der von Patienten isolierten LCLs mit Mutationen in UBQLN2 eine Hypophosphorylierung von FUS Serin 439 (S439) entdeckt. Obwohl bekannt ist, dass diese Stelle in FUS phosphoryliert werden kann und sie in der für die RNA-Bindung essenziellen Zinkfingerdomäne von FUS liegt, wurde diese Position bisher noch nicht genauer untersucht. Wir haben gezeigen, dass die Modulation dieser Phosphorylierungsstelle sowohl die FUS-RNA-Bindekapazität als auch die Proteinmenge von MAP1B regulieren kann.

Diese Arbeit beschreibt erstmalig eine Erhöhung von MAP1B auf mRNA- und Proteinebene infolge eines Funktionsverlusts von UBQLN2 ausgelöst von ALS/FTD-assoziierter UBQLN2 Mutationen. Zudem verknüpft sie die Phosphorylierung von FUS S439 mit ALS/FTD und mit FUS‘ RNA-Bindekapazität. Somit verbindet diese Arbeit drei wichtige Krankheitsmechanismen von ALS/FTD: eine funktionsgestörte Proteinhomöostase, einen gestörten RNA-Stoffwechsel und eine Beeinträchtigung des Cytoskeletts.

# Abbreviations

| | |
|---|---|
| ABD | Actin-binding domain |
| ACN | Acetonitrile |
| AcOH | Acetic acid |
| ACTB | Actin, cytoplasmic 1 |
| Ac-tubulin | Acetylated α-tubulin |
| AD | Alzheimer's disease |
| ALS | Amyotrophic lateral sclerosis |
| ATG proteins | Autophagy-related proteins |
| BafA | Bafilomycin A1 |
| BCA | Bicinchoninic acid |
| BSA | Bovine serum albumin |
| Btz | Bortezomib |
| C9orf72 | Chromosome 9 open reading frame 72 |
| CCNF | Cyclin F |
| CHMP2B | Charged multivesicular body protein 2b |
| DAPK-1 | Death-associated protein kinase-1 |
| DMEM | Dulbecco's modified eagle's medium |
| DPR | Dipeptide repeat |
| DTT | Dithiothreitol |
| EMSA | Electrophoretic mobility shift assays |
| ER | Endoplasmic reticulum |
| ERAD | ER-associated degradation |
| FBS | Fetal bovine serum |
| FMRP | Fragile X mental retardation protein |
| FTD | Frontotemporal dementia |
| FUS | Fused in sarcoma |
| GABARAP | γ-aminobutyric acid receptor associated protein |
| GAN | Giant axonal neuropathy |
| GAPDH | Glyceraldehyde-3-phosphate dehydrogenase |
| GO | Gene ontology |
| GRN | Progranulin |
| GSK3 | Glycogen synthase kinase-3 |
| HC | Heavy chain |
| HDR | Homology-direct repair |
| hnRNP | Heterogenous nuclear ribonucleoprotein |
| HSP70 | Heat shock protein 70 |
| HSP90 | Heat shock protein 90 |
| IAA | Iodoacetamide |
| IAP | Integrin-associated protein |
| KD | Knockdown |
| KO | Knockout |
| LB | Lysogeny broth |
| LC1 | Light chain 1 |
| LC2 | Light chain 2 |
| LC3 | Light chain 3 |
| LCL | Lymphoblast cell line |

| | |
|---|---|
| LC-MS/MS | Liquid chromatography with tandem mass spectrometry |
| LIR | LC3-interacting region |
| LLPS | Liquid-liquid phase separation |
| $Log_2FC$ | $Log_2$ fold change |
| MAP | Microtubule-associated protein |
| MAP1B | Microtubule-associated protein 1B |
| MAPT | Microtubule-associated protein tau |
| MBD | Microtubule-binding domain |
| mTORC | Mammalian target of rapamycin complex |
| Neo | Neomycin |
| NES | Nuclear export signal |
| NLS | Nuclear localization signal |
| OPTN | Optineurin |
| ORF | Open reading frame |
| OXPHOS | Oxidative phosphorylation |
| PCR | Polymerase chain reaction |
| PD | Parkinson's disease |
| PFN1 | Profilin 1 |
| PQC | Protein quality control |
| pS439 | Phosphorylated FUS residue serine 439 |
| PTM | Post-translational modifications |
| RBP | RNA-binding protein |
| RNASeq | RNA sequencing |
| RNP | Ribonucleoproteins |
| RRM | RNA recognition motif |
| RT-qPCR | Real-time quantitative PCR |
| shRNA | Short hairpin RNA |
| SILAC | Stable isotope labeling by amino acids in cell culture |
| SMCR8 | Guanine nucleotide exchange protein SMCR8 |
| SOD1 | Superoxide dismutase 1 |
| SQSTM1/p62 | Sequestosome 1 |
| STAGE | Stop and go extraction |
| STI-1 like | Stress-induced protein 1-like motifs |
| TBK1 | TANK-binding kinase 1 |
| TBP | Tata-binding box |
| TBS | Tris-buffered saline |
| TBST | Tbs-tween-20 |
| TDP-43 | Transactive response DNA-binding protein of 43 kda |
| TFA | Trifluoroacetic acid |
| TIMM44 | Translocase of inner mitochondrial membrane 44 |
| TREM2 | Triggering receptor expressed on myeloid cells 2 |
| TUBA4A | Tubulin alpha 4a |
| Ub | Ubiquitin |
| UBA | Ubiquitin-associated |
| UBL | Ubiquitin-like |
| UBQLN/Ubqn | Ubiquilin |
| UBQLN2 | Ubiquilin 2 |
| UBQLNL | Ubiquilin-like |
| UPS | Ubiquitin-proteasome system |

| | |
|---|---|
| VAPB | Vesicle-associated membrane-protein-associated protein B |
| VCP | Valosin-containing protein |
| WDR41 | WD repeat-containing protein 41 |
| WT | Wild-type |
| ZnF | Zinc finger |

# 1 Introduction

## 1.1 Amyotrophic lateral sclerosis and frontotemporal dementia

Amyotrophic lateral sclerosis (ALS) is the most common motor neuron disease in adults with a median prevalence of 4.8 per 100,000. It is rare before age 50, but in the middle-to-late 50s incidence rates increase [1]. ALS is defined by the degeneration of the upper and lower motor neurons resulting in progressive muscle atrophy. With respect to the affected motor neurons, the clinical presentation of ALS is diverse. In general, early manifestations include muscle weakness of the limbs, but occasionally cases are bulbar with slurred speech and difficulty in swallowing [2]. Ultimately, paralysis of the respiratory muscles leads to death due to respiratory failure on average 3-5 years after disease onset [3]. In the early 2000s, it was reported that a significant subset of individuals with ALS also presented cognitive impairment which met the criteria for frontotemporal dementia (FTD) [4, 5].

FTD, formerly known as Pick's disease, is a leading type of early-onset dementia and particularly common in patients younger than 65 years. It is caused by the degeneration of the frontal and temporal cortical lobes. Two main clinical variants of FTD are distinguished: the behavioral variant and primary progressive aphasia. The latter is subdivided in the non-fluent variant and the sematic variant [6]. Early symptoms of patients with the behavioral variant are personality and behavioral changes as well as apathy, whereas in patients with primary progressive aphasia mainly language is impaired [7]. Over time, all FTD patients develop global cognitive impairments and motor deficits. The disease duration is about 8 years after which patients typically die from pneumonia or secondary infections [6].

It was not only reported that some ALS patients develop FTD-like symptoms but vice versa, about 15% of FTD diagnosed patients show over time symptoms characteristic of ALS [8]. However, the overlap between these two diseases is not limited to clinical features but includes pathological and genetic characteristics. A common pathological hallmark of a variety of neurodegenerative diseases, including ALS and FTD, is aberrant protein accumulation and aggregation. One major aggregation-prone protein, whose ubiquitinated and hyperphosphorylated form was found in cytoplasmic inclusions in ALS and FTD, is the transactive response (TAR) DNA-binding protein of 43 kDa (TDP-43) [9, 10]. Aggregates of this RNA-binding protein (RBP) were detected in in more than 90% of ALS and over 40% of FTD patients (Figure 1-1). Another RBP, fused in sarcoma (FUS), can also be found in aggregates in both diseases, however to a much lesser extent [11, 12]. FUS is observed in cytoplasmic inclusions in approximately 9% of FTD and in less than 1% of ALS cases [13].

In general, both ALS and FTD can occur either based on a familial history or sporadic. While approximately 5% of all ALS cases were reported as familial, the proportion is with 20-50% higher in FTD [14-17]. In the last decades, multiple genes were linked to ALS, FTD or both (Fig. 1B). However, the classification is not always clear and varies between publications [13, 18-22]. Mainly associated with the clinical phenotype of ALS are mutations in in the genes encoding for TDP-43 and FUS [23-29] as well as superoxide dismutase 1 (SOD1), vesicle-associated membrane-protein-associated protein B (VAPB), Optineurin (OPTN), heterogeneous nuclear ribonucleoprotein A1 and A2/B1 (hnRNPA1 and hnRNPA2B1) and profilin 1 (PFN1) [27-33]. Mutations, which are likewise linked to clinical phenotypes of ALS and FTD include those in chromosome 9 open reading frame 72 gene (*C9orf72*), cyclin F (*CCNF*), sequestosome 1 (*SQSTM1*/p62), TANK-binding kinase 1 (*TBK1*), tubulin alpha 4a (*TUBA4A*), ubiquilin 2 (*UBQLN2*) and valosin-containing protein (*VCP*) [34-41]. Primarily FTD associated are mutations in triggering receptor expressed on myeloid cells 2 (*TREM2*), charged multivesicular body protein 2b (*CHMP2B*), microtubule-associated protein tau (*MAPT*) and progranulin (*GRN*) [42-47].

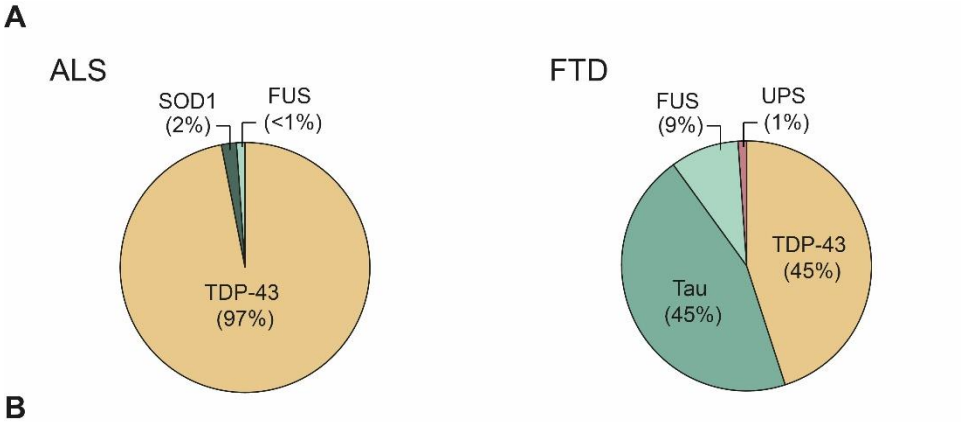


**Figure 1-1: The ALS-FTD continuum – schematic illustration of shared and distinct pathological and genetic features.**
**(A)** Pathological protein inclusions are a hallmark of several neurodegenerative diseases including ALS and FTD. Inclusions containing mainly TDP-43 or FUS are found in ALS and FTD. Tau proteinopathies are exclusively found in FTD patients, while SOD1 protein inclusions are specific for ALS. Less than 1% of FTD inclusions are primarily positive for ubiquitin-proteasome system (UPS) markers. **(B)** Pure ALS and pure FTD are the two extremes of the ALS-FTD continuum. A variety of genes linked to FTD, ALS or both are depicted and assigned based on their main association. Adapted from Ling et al. (2013).

Due to the pathological as well as genetic overlap between ALS and FTD, these diseases are considered to form a neurodegenerative disease continuum. This ALS/FTD continuum also includes shared pathogenic pathways which are involved in disease initiation and progression.

### 1.1.1 Multiple pathogenic mechanisms are linked to ALS/FTD

Although the exact disease mechanisms are still elusive, genes implicated in ALS/FTD offer valuable insight in the complex underlying pathological processes. In the recent years, excessive whole-genome sequencing and whole-exome sequencing resulted in the discovery of a variety of novel ALS/FTD genes [48]. Today, more than 50 genes are associated with either or both diseases [49]. Clusters of those genes operate in a subset of molecular processes; primarily in RNA metabolism, protein homeostasis, mitochondrial function and cytoskeleton dynamics (Figure 1-2).

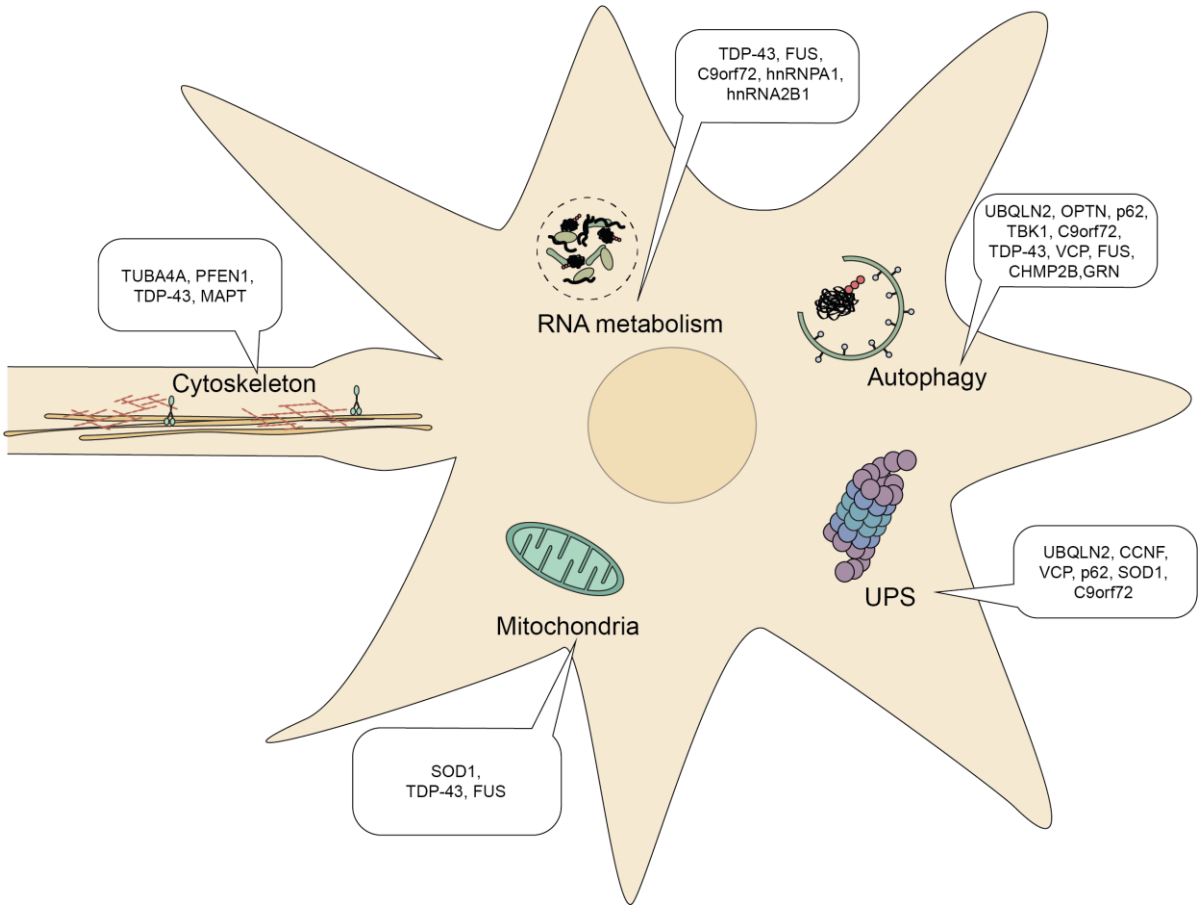


**Figure 1-2: ALS/FTD linked genes elucidate key underlying mechanisms of the disease.**
ALS/FTD-linked genes, noted in Figure 1-1, can be grouped in four categories depending on the cellular pathway they are involved in: RNA metabolism, protein homeostasis (including UPS and autophagy), mitochondrial function and cytoskeleton dynamics. UPS, Ubiquitin-proteasome system.

#### 1.1.1.1 Disturbed RNA Metabolism in ALS/FTD: of FUS and TDP-43

The fact that the two main aggregating proteins in ALS/FTD, FUS and TDP-43, are RBPs implies a central role of RNA metabolism in disease pathogenesis. Besides those two, several more ALS/FTD-associated genes are implicated in RNA metabolism, for example heterogeneous nuclear ribonucleoprotein A1 and A2/B1 (*hnRNPA1* and *hnRNPA2B1*).

However, since FUS and TDP-43 are the most studied RBPs and play a role in multiple steps of RNA processing, this paragraph focuses on these two. In healthy neurons, FUS and TDP-43 are mainly localized to the nucleus, but they can also shuttle to the cytoplasm [50, 51]. Both are assigned to the heterogenous nuclear ribonucleoprotein (hnRNP) protein family and harbor one or more RNA recognition motif (RRM), a low complexity domain and a nuclear localization signal (NLS) [52] (Figure 1-3). The low complexity domains influence protein self-assembly, which can result in liquid-liquid phase separation (LLPS) from an aqueous environment [53]. In addition to the RRM, FUS contains a zinc finger (ZnF) domain, which is also capable of binding RNAs [54].

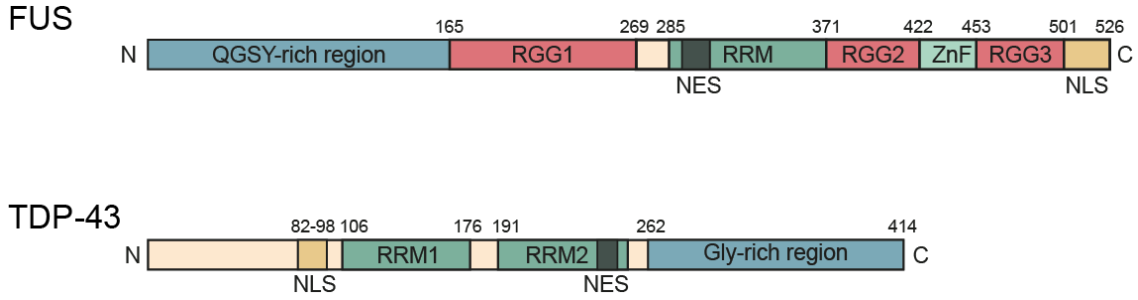


**Figure 1-3: FUS and TDP-43 protein structures.**
FUS and TDP-43 share common motifs. Both include an RNA recognition motif (RRM; dark green), a low-complexity domain (QGSY-region and GLY-rich region, respectively; blue), a nuclear localization signal (NLS; yellow) as well as a predicted nuclear export signal (NES; dark green). In addition, FUS harbors three Arginine/Glycine rich regions (RGG, dark red) and a zinc finger domain (ZnF; light green). Arabic numbers indicate amino acid position of the motifs.

FUS and TDP-43 are implicated in multiple steps of RNA processing. They have roles in transcription, pre-mRNA splicing, mRNA stability, mRNA trafficking, translation and in stress granules (Figure 1-4). TDP-43 was initially characterized as a transcriptional repressor of transactivation response (TAR) element of the human immunodeficiency virus type 1 [55]. Later, it was reported to associate with sites of transcription and to interact with transcriptional regulators [56, 57]. One of these transcriptional regulators is FUS [58]. FUS can associate with RNA Polymerase II and its general transcription factor IID but it can also interact with additional transcription complexes and bind to single-strand DNA promoters [59-64]. FUS and TDP-43 regulate the splicing of several hundred non-coding and protein-coding RNAs. Yet, FUS and TDP-43 have distinct functions in splicing and bind to different RNA targets [65]. TDP-43 induces, for example, exon skipping or exon inclusion, autoregulates itself and represses cryptic exons [66-75]. In contrast, FUS influences splicing through binding to preferentially long introns of pre-mRNAs and interaction with components of the spliceosome machinery [76-79]. Furthermore, FUS and TDP-43 are able to destabilize and stabilize various mRNA transcripts by binding to or close to the 3'UTR [65, 73, 75, 80-82]. Due to the substantial distance of the nucleus in the cell body to the dendrites and axons as well as the high polarization of neurons, mRNA transport and local translation is especially critical in this cell type. mRNA transport is

controlled by RBPs which recognize specific mRNAs and associate with them to ribonucleoproteins (RNPs) which often assemble into RNP granules. Some RNPs enable transport by direct contact with motor proteins whereas others are transported indirectly via vesicles [83]. For instance, TDP-43 was shown to co-purify with several proteins involved in mRNA transport and to modify RNA transport along axons [84-86]. Also, FUS has been implicated in mRNA trafficking. It was shown to be associated with microtubule as well as actin motor proteins and to be crucial for the transportation of several mRNAs to dendrites [87, 88]. Furthermore, FUS and TDP-43 were reported to modulate protein translation. They interact with translation regulators as well as with ribosome subunits [58, 89-91]. One common interactor of FUS and TDP-43 is fragile X mental retardation protein (FMRP), which acts as a translational repressor [92-96]. Colocalization of FUS, TDP-43 and FMRP is especially visible during stress conditions, such as heat stress or sodium arsenate treatments. Under these conditions, RBPs undergo LLPS mediated by intrinsically disordered low-complexity domains forming so called stress granules. Stress granules are membrane-less organelles whose main function is the temporal blockage of translation and storage of mRNAs during stress conditions by clustering translating initiation factors, non-RNA-binding proteins, RBPs and non-translated mRNAs [13, 97].

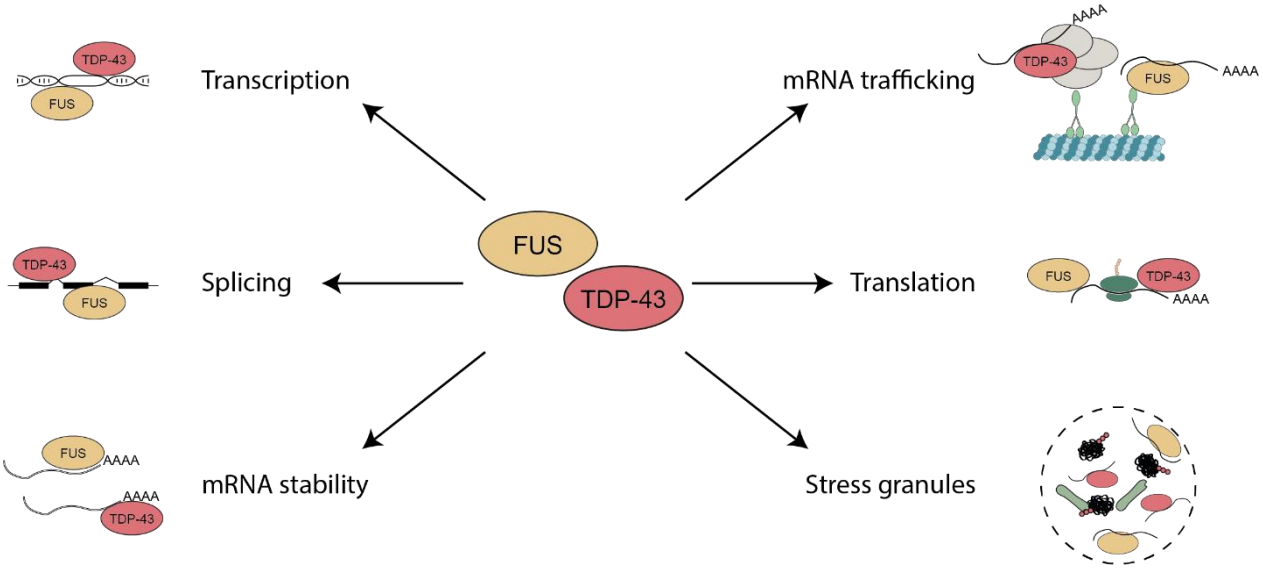


**Figure 1-4: Schematic diagram of known cellular roles of FUS and TDP-43.**
The RNA-binding proteins FUS and TDP-43 are involved in multiple processes. In the nucleus they are involved in transcription, while in the cytoplasm they regulate splicing, mRNA stability, mRNA trafficking, translation and the formation of stress granules.

Due to the widespread roles of FUS and TDP-43 in RNA processing, pathogenic mutations in FUS and TDP-43 severely impact RNA metabolism. It is suggested that mutations in FUS and TDP-43 result in both gain- and loss-of-function of the proteins. Mutated FUS and TDP-43 cause alterations in mRNA splicing, transport, stability and translation [75, 80, 90, 98, 99]. However, mutations in FUS and TDP-43 can also give rise to mislocalization and abnormal

protein aggregation in the cytoplasm [100-102]. Evidence shows that pathogenic protein aggregates colocalize with stress granules markers and that mutations in FUS and TDP-43 result in increased stress granule formation during stress [103-105]. Indeed, stress granules are considered as a seed for toxic protein aggregation [106].

#### 1.1.1.2 Importance of the cytoskeletal system in neurons and its derogation in ALS/FTD

Neurons are highly polarized cells. Typically, they develop several dendrites and a single axon which can extend beyond one meter. Due to this extreme polarization and size, neurons depend highly on the cytoskeleton which is among others required for efficient communication and transport between the cell body and the axon tip. The cytoskeleton is made up of actin filaments, intermediate filaments and microtubule filaments. The latter forms tracks on which several cargos such as mitochondria or lysosomes are transported. Microtubules are composed of α- and β-tubulin heterodimers and have a tubular structure. Myriad proteins bind to microtubules; while motor proteins such as dynein and kinesin transport various cargos along these tracks [107-109], microtubule-associated proteins (MAPs) influence the interaction with other cellular components and stabilize microtubules [110, 111]. Besides MAPs, post-translational modifications (PTMs), such as detyrosination and acetylation of tubulins, play an important role in modulating microtubule dynamics [112-115]. The constant assembly and disassembly of microtubules, an alteration between growth and shrinkage referred to as dynamic instability, provides microtubules with a high organizational flexibility. This flexibility is crucial for neurons, since it enables migration and promotes connectivity to other cells [116].

Due to the high dependency of neuronal integrity on the cytoskeleton system, it is not surprising that impaired cytoskeletal functions are linked to several neurodegenerative diseases. A well-known example is the hyperphosphorylation and abnormal aggregation of the microtubule-associated protein tau in Alzheimer's disease (AD), which leads also to microtubule depolymerization [117, 118]. Alterations in the cytoskeleton system can result in a variety of severe consequences in neurons, including loss of neuronal polarity and morphology, impaired signal transduction and intracellular transport deficits [119].

Transport deficits of vesicles and mitochondria are for example reported for ALS-associated SOD1 mutants [120, 121]. In recent years, the list of ALS/FTD-linked genes which are involved in the cytoskeleton system has been growing rapidly. In addition to the microtubule-associated protein tau, it includes subunits of motor proteins, cytoskeletal modulators as well as an α-tubulin isotype (*TUBA4A*) [39, 41, 122-125]. The number as well as the multifaceted roles of those genes highlight cytoskeleton disturbances as a key molecular mechanism in ALS/FTD.

#### 1.1.1.3 Protein degradation systems and their impairment in ALS/FTD

A hallmark of several neurodegenerative diseases is the accumulation and aggregation of proteins due to impaired protein degradation. Under physiological conditions, protein quality control systems prevent such events. Two main systems are primarily responsible for this task; namely the ubiquitin-proteasome system (UPS) and autophagy. In principle, both pathways result in the degradation of proteins (Figure 1-5). The UPS process starts with a multi-step, catalytic process that attaches one or multiple ubiquitin (Ub) molecules to proteolytic substrates [126]. Firstly, ubiquitin is activated in an ATP-dependent manner by an E1 enzyme. In this reaction a ubiquitin adenylate is formed which is then transferred to a cysteine residue of the E1 enzyme, which in turn passes Ub on to the Ub-conjugating enzyme, the E2 enzyme. Then, an E3 Ub ligase catalyzes the transfer of Ub to substrate proteins. Multiple rounds of ubiquitination are possible, which can lead to a wide spectrum of distinct Ub chains. Ubiquitinated proteins are either directly bound by Ub receptors at the proteasome or recognized by shuttle factors, which bring them to the proteasome [127]. Ub-shuttle factors harbor ubiquitin-associated (UBA) and ubiquitin-like (UBL) domains, which enable them to bind ubiquitinated substrates as well as Ub receptors at the proteasome. Irrespective of the mode of recognition, the proteolytic substrates are deubiquitinated and unfolded prior to degradation. These first steps occur at the 19S regulatory particle of the proteasome followed by the translocation of the substrate protein into the 20S core particle. In this barrel-shaped, proteolytic cylinder proteins are degraded into short peptides [128]. In this way the proteasome degrades regulatory and short-lived proteins as well as damaged and misfolded proteins [129]. However, the proteasome channel is relatively narrow, and thus cannot degrade protein aggregates or organelles. These are degraded, amongst other substrates, by the autophagy-lysosome pathway.

Autophagy, Greek for “self-eating”, describes the delivery of proteolytic substrates to the lysosome. Three different branches of autophagy exist: microautophagy, chaperon-mediated autophagy and macroautophagy. Of those, macroautophagy (hereafter called autophagy) is historically the most prevalent form and describes the engulfment of cytosolic substrates by a double-membrane structure which then fuses with a lysosome [130]. Most cells exhibit basal levels of autophagy, however, stress stimuli such as nutrient deprivation or proteotoxic stress can enhance the autophagy pathway. While starvation induces bulk degradation to provide new building blocks, other stimuli trigger selective autophagosomal degradation of specific substrates such as protein aggregates or damaged mitochondria. After autophagy initiation by the serine/threonine-protein kinase ULK1 complex, numerous ATG (autophagy-related) proteins orchestrate the formation of the phagophore, a double-membraned cup-shaped structure [131]. Phosphatidylethanolamines of the growing phagophore membrane become

conjugated with ubiquitin-like human ATG8 (hATG8) proteins [132]. The hATG8 family consists of microtubule-associated protein 1 light chain 3 (LC3) and γ-aminobutyric acid receptor associated protein (GABARAP) subfamilies. This so called ATG8 lipidation is necessary for cargo recruitment to the forming autophagosome. Like in the UPS, ubiquitination of substrates can serve as a degradation signal for selective autophagy. Autophagy receptors simultaneously bind cargo tagged with this “eat-me-signal” and hATG8s to which they bind through a LC3-interacting region (LIR) motif. In this way, autophagy receptors bridge cargo and autophagosomal membranes [133]. Cargo sequestration is followed by closure of the double-membrane autophagosomes and their subsequent fusion with lysosomes generating autolysosomes. Finally, lysosomal enzymes digest the autophagosomal cargo and the degradation products are released into the cytosol [134].

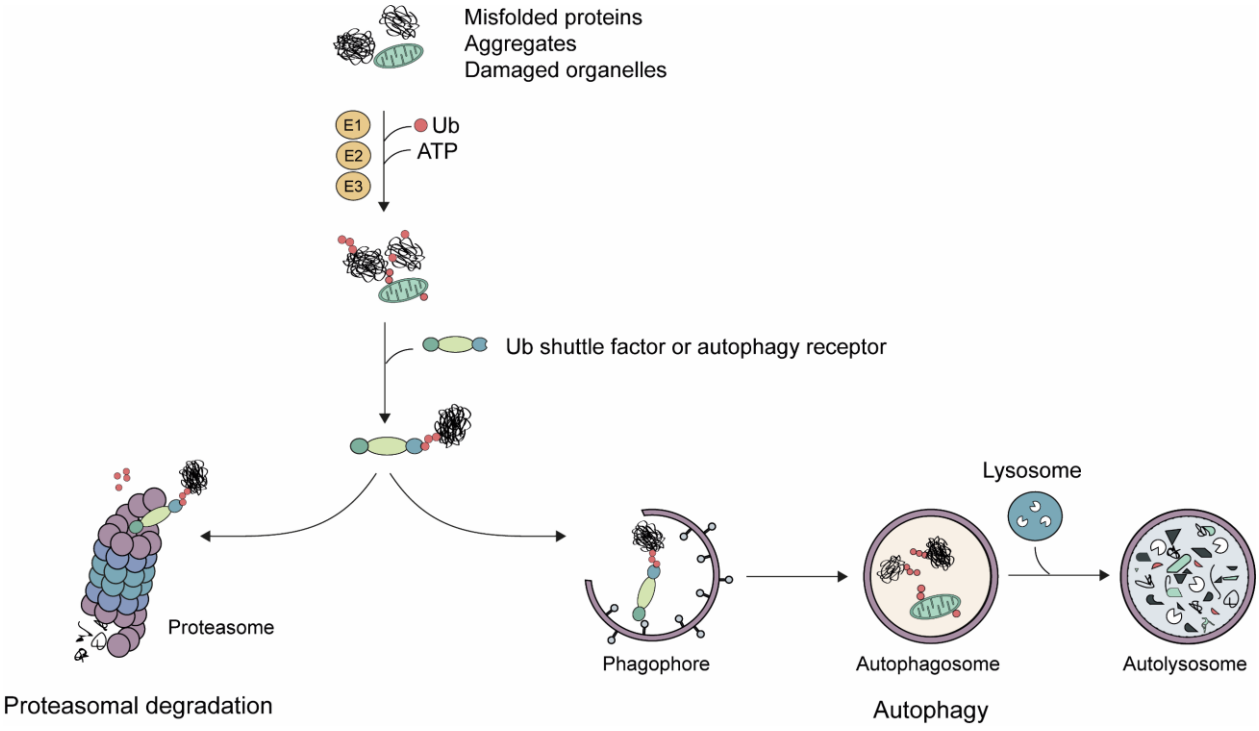


**Figure 1-5: The UPS and autophagy are the two main cellular protein degradation systems.** Ubiquitination of damaged organelles, misfolded, or aggregated proteins occurs through an enzymatic cascade. After activation by an ATP-depended activation enzyme (E1), ubiquitin (Ub) is transferred to a conjugating enzyme (E2). A ligase (E3) mediates the Ub transfer to substrates. For proteasomal degradation, ubiquitinated substrates can either be directly recognized by Ub receptors at the proteasome or targeted to the proteasome via Ub-shuttle factors. Among other `eat-me-signals´, autophagy receptors recognize Ub chains and recruit cargo to the forming phagophore. The phagophore matures into an autophagosome, which ultimately fuses with lysosomes followed by degradation of the enclosed cargo. UPS, Ubiquitin-proteasome system.

The accumulation of protein aggregates in individuals with ALS/FTD suggests a failure of protein quality control. This notion is substantiated by numerous observations of which only a few are outlined hereafter. For instance, it was reported that expression of SOD1 mutations reduced proteasomal activity in a motor neuron-like cell line [135] Complementary, proteasomal inhibition enhanced SOD1 aggregation and toxicity in mice [136, 137]. ALS/FTD-

linked mutations in CCNF, an E3 ligase, was shown to result in an accumulation of ubiquitinated proteins, including TDP-43 [47]. Interestingly, C9orf72, the most common genetic cause for ALS/FTD, functions in a complex with WD repeat-containing protein 41 (WDR41) and the guanine nucleotide exchange protein SMCR8 to regulate autophagy initiation and autophagsosome maturation [138-140]. ALS/FTD-associated mutations were also described in the autophagy receptors SQSTM1/p62, OPTN and UBQLN2, which all target ubiquitinated substrates to either proteasomes or autophagy [32, 36, 141].

### 1.1.2 The ALS/FTD-linked protein UBQLN2

In 2011, Deng and colleagues identified five missense mutations in UBQLN2 in families with ALS [35]. Since then, UBQLN2 and its association with ALS was intensively studied. UBQLN2 belongs to the family of ubiquilin proteins which are present in all eukaryotes [142]. In humans the UBQLN family consists of five members, namely UBQLN1-4 and the ubiquilin-like protein (UBQLNL). Pairwise protein sequence similarity revealed a percentage identity of 29.47% to 74.76% between family members (Figure 1-6A). UBQLN1 and UBQLN2 are the most closely related members, whereas UBQLN3 and UBQLNL are most distant from the other family members (Figure 1-6B).

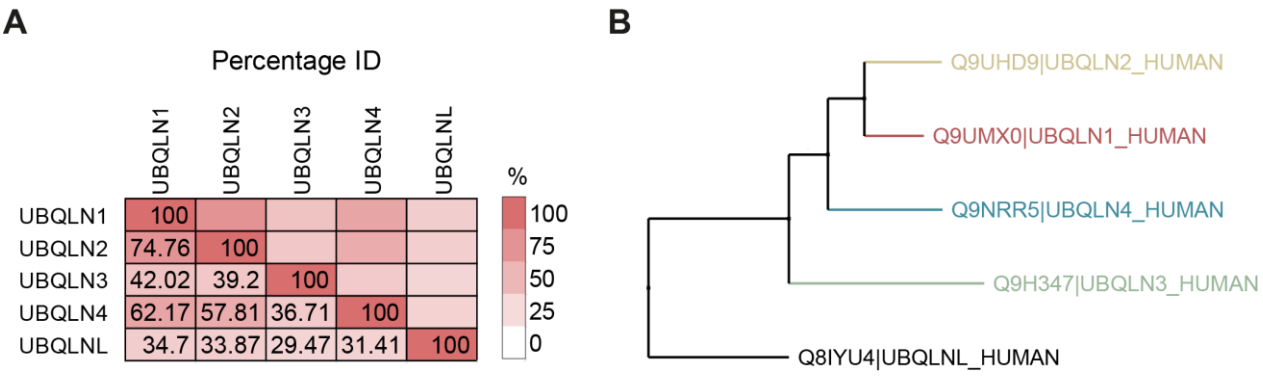


**Figure 1-6: The ubiquilin family.**
**(A)** Pairwise alignment of the UBQLN family members using BLOSUM62 as scoring matrix presenting protein sequence similarities. **(B)** Clustering of the family members in a neighbor joining tree created with Jalview.

UBQLN members also differ in their expression. While UBQLN1, 2 and 4 are ubiquitously expressed, UBQLN3 and UBQLNL are primarily expressed in the testis [143]. Based on the relatively high sequence identity, it is not surprising that the members of the UBQLN family harbor common protein domains. Besides the Ub shuttle signature UBA and UBL domains, UBQLNs have stress-induced protein 1-like (STI1) motifs that mediate chaperone binding. In addition to these domains, UBQLN2, but no other UBQLN protein, contains an intrinsically disordered proline-rich repeat domain containing 12 PXX repeats with unknown function (Figure 1-7) [35, 144].

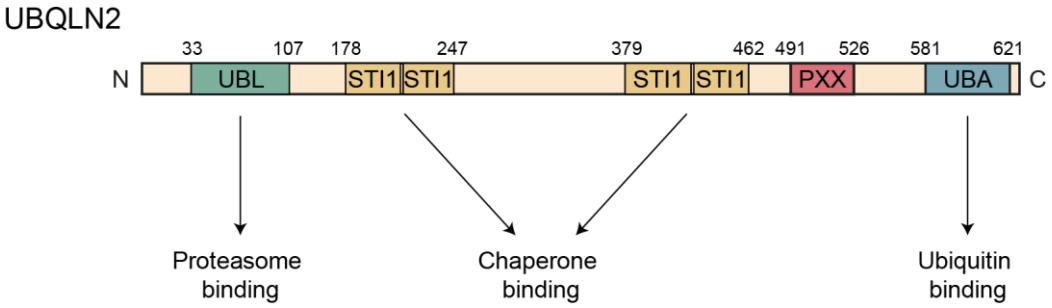


**Figure 1-7: Schematic representation of the UBQLN2 protein structure.**
On the N-terminal UBQLN2 harbors a ubiquitin-like (UBL; green) domain which interacts with the proteasome, whereas the ubiquitin-associated (UBA; blue) domain on the C-terminal allows binding to ubiquitinated substrates. Stress-induced protein 1-like motifs (STI-1; yellow) are implicated in chaperone binding. The function of the UBQLN2-specific PXX region (red) remains elusive. Arabic numbers indicate amino acid position of the motifs.

#### 1.1.2.1 Physiological functions of UBQLN2

In 1999, UBQLN2 was identified as a protein which mediates the interaction between integrin-associated protein (IAP, also CD47) and vimentin-containing intermediate filaments [145]. Therefore, it was originally named protein linking IAP with cytoskeleton 2 (PLIC2). Due to the UBA and UBL domains of UBQLN2, its function as a Ub-shuttle factor is the most intensely studied one.

UBQLN2's roles in protein degradation

UBQLN2's role as a Ub-shuttle factor was already described in the early 2000s [146-149]. Besides the UBA and UBL domains, the STI1 regions were also reported to contribute to UBQLN2's function in the UPS. The STI1 regions are required for binding of heat shock protein 70 (HSP70) [150]. During non-stress conditions, UBQLN2 mainly forms homomers or heteromers with UBQLN1 or 4 and the binding to ubiquitinated proteins is negligible. However, under stress conditions, HSP70 associates with ubiquitinated proteins and binds to UBQLN2, thereby promoting UBQLN2's interaction with ubiquitinated proteins and their shuttling to the proteasome (Figure 1-8A) [151]. Intriguingly, recent evidence suggests that HSP70 is also able to transfer non-ubiquitinated substrates to UBQLN2 and thereby supports the formation of an Ub-independent substrate-shuttle-complex [152]

Misfolded proteins in the endoplasmic reticulum (ER) are eliminated by ER-associated degradation (ERAD). In this pathway, misfolded ER proteins need to be recognized and transported to the dislocation machineries, the so called dislocons. Following the dislocation from the ER, substrates are polyubiquitinated by E3 ligases and finally degraded by the proteasome [153]. UBQLNs, including UBQLN2, are part of several ERAD complexes and function in the ERAD pathway. They were shown to interact with several ERAD components, for example the homocysteine-induced ER protein HERP, UBX domain-containing protein 4

and FAS-associated factor 2 [154-156]. UBQLNs are suggested to bring together components of the ERAD machinery, ubiquitinated substrates and proteasomes at the cytosolic face of ER membranes (Figure 1-8B). The importance of UBQLN2 in the ERAD pathway is stressed by the accumulation of ERAD substrates after UBQLN2 knockdown [156].

Interestingly, in addition to its function as an Ub-shuttle factor in the UPS, UBQLN2 is also implicated in autophagy. While typical autophagy receptors bind via a conserved LIR motif to LC3/GABARAP proteins on the forming autophagosome, UBQLN2 is capable of binding to LC3 via its UBA domain [141, 157]. Thus, it has been proposed that UBQLN2 is able to shuttle ubiquitinated substrates to both, the UPS and the autophagosome (Figure 1-8C) [158]. Noteworthy, UBQLN2 overexpression results in an increased number of autophagosomes [141, 157]. Other evidence indicates a role of UBQLN2 in autophagy via its interaction with the serine-threonine kinase TBK1 which is known to phosphorylate SQSTM1, OPTN, LC3C and GABARAPL2 [159]. In addition, emerging evidence showed that UBQLN2 is involved in the regulation of autophagosome acidification. First insights in this direction were found in a *Drosophila* ubiquilin (dUbqn) knockout model [160]. In this model, impairment of mammalian target of rapamycin complex 1 (mTORC1), the master regulator of cells that also regulates autophagy activity, was detected. mTORC1 is a negative autophagy regulator and hence an induction of autophagy was observed in dUbqn ablated *Drosophila*. Additionally, this study showed that dUbqn interacts with the v-ATPase proton pump subunit Vha100-1, modulates v-ATPase activity and thereby lysosome function. However, flies have only one ubiquilin gene wherefore these findings may not be transferred to human UBQLN2 functions. Nonetheless, similar observations were made in a UBQLN2 knockout (KO) HeLa cell line, which has decreased autophagic flux, altered acidification of autophagosomes and reduced levels of the V-ATPase subunit ATP6v1g1 [161]. Thus, UBQLN2 seems to be implicated in autophagosome maturation and might also regulate autophagy induction.

UBQLN2 is necessary for mitochondrial function

In addition to their role in protein degradation pathways, UBQLN proteins are involved in maintaining mitochondrial health. Mitochondria are crucial for eukaryotic cells especially because they provide ATP via oxidative phosphorylation (OXPHOS). Mitochondria have their own mitochondrial genome that, however, only encodes for a small set of proteins. The majority of mitochondrial proteins, which are encoded by nuclear genes, need to be targeted to mitochondria following their translation in the cytosol [162]. UBQLNs were shown to chaperone transmembrane domain containing proteins, such as the outer mitochondrial membrane protein Omp25 and thus prevent them from aggregation during their targeting to mitochondria (Figure 1-8D) [163]. If these clients fail to successfully insert into mitochondria, UBQLNs facilitate their proteasomal degradation through recruitment of an E3 ligase. Consistent with

these observations, knockout of UBQLN1 or UBQLN2 caused abundance alterations of mitochondrial proteins [164, 165]. Recently it was reported that UBQLN2 KO results in depletion of OXPHOS units, disturbed mitochondrial respiration and ATP production [166]. The reason therefore was an impaired import of mitochondrial proteins. Taken together, UBQLN2 presumably plays a role in mitochondrial protein quality control and is necessary for mitochondrial function.

UBQLN2 and stress granules

Aside from RNA and RBP, stress granules also contain components of the protein quality control (PQC) systems such as heat shock protein 90 (HSP90), Ub and UBQLN2 [97, 167-170]. UBQLN2 was found to locate to stress granules under different cellular stress conditions, such as oxidative, heat and osmotic stress [169]. However, interactome analysis of a stable 293T cell line with an integrated tetracycline-inducible *FLAG-UBQLN2* construct indicate that UBQLN2 associates with stress granule components also under non-stress conditions and negatively regulates stress granule size [170]. Typically, intrinsically disordered low-complexity domains, as they are found in FUS and TDP-43, mediate LLPS and the formation of stress granules. UBQLN2 also contains disordered low-complexity segments, mainly at the C-terminus. Those promote UBQLN2 oligomerization and LLPS of UBQLN2 at physiological temperatures and salt concentrations *in vitro* [169]. While the PXX, the UBL and the UBA-domain contribute to the LLPS behavior of UBQLN2, the second STI1 region is crucial to drive LLPS [169, 170]. Remarkably, addition of purified Ub to UBQLN2 droplets *in vitro* resulted in disassembly of these droplets. This process is depended on an interaction between Ub and UBQLN2's UBA domain. Thus, it is proposed that UBQLN2 traffics ubiquitinated proteins out of stress granules (Figure 1-8E). However, the exact role of UBQLN2 in stress granules is still obscure.

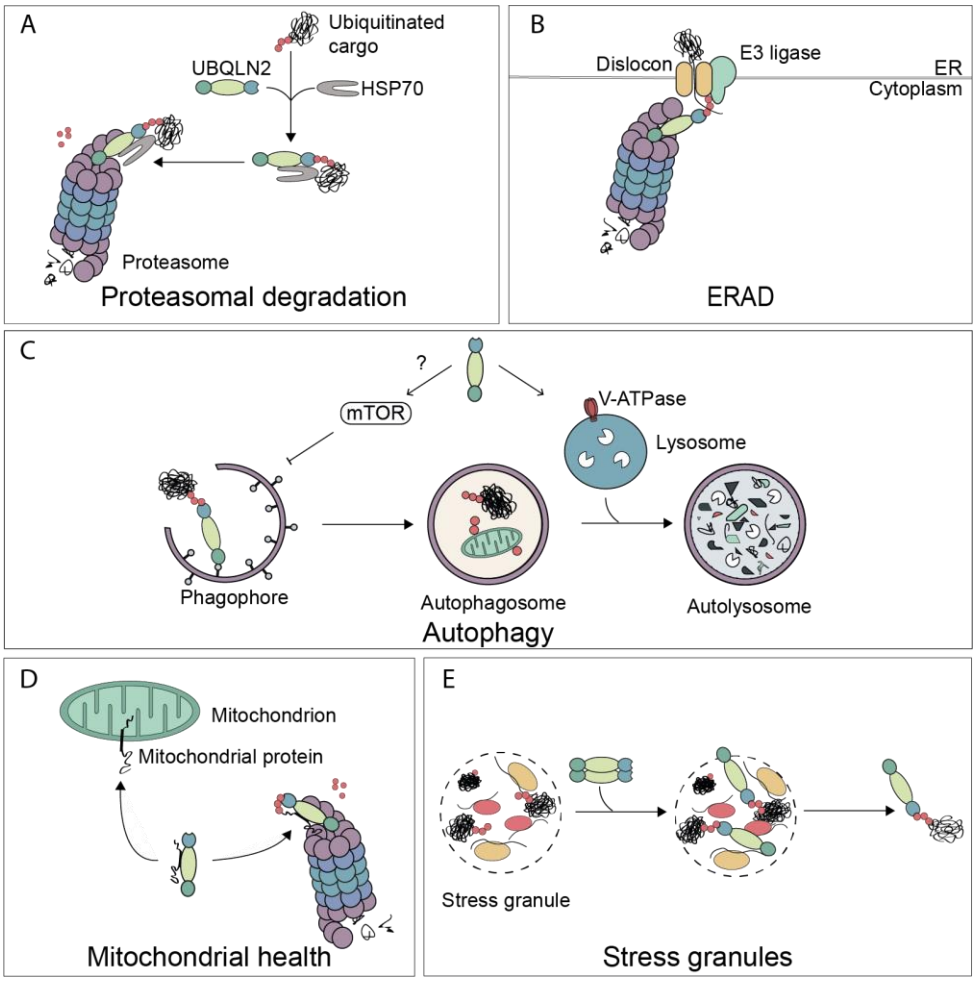


**Figure 1-8: The multifaceted cellular roles of UBQLN2.**
UBQLN2 targets ubiquitinated **(A)** cytosolic substrates as well as **(B)** ERAD substrates to the proteasome for degradation via UBA-Ub and UBL-proteasome interactions. **(C)** The UBA domain of UBQLN2 is also able to bind to LC3 and thus can act as an autophagy receptor. Furthermore, UBQLN2 regulates autophagy and ensures lysosome acidification by stabilizing V-ATPases. **(D)** UBQLN2 can prevent aggregation of mitochondrial proteins, safeguard their cytosolic traffic or facilitate their proteasomal degradation. **(E)** UBQLN2 LLPS promotes its localization to stress granules where it might extract ubiquitinated proteins.

#### 1.1.2.2 UBQLN2 in ALS/FTD

*UBQLN2* is a single-exon gene located on the X-chromosome [35, 171] and mutations are dominantly inherited with reduced penetrance in females [35]. Interestingly, many of the known sporadic and familial ALS/FTD-linked mutations in UBQLN2 are located in the PXX repeat region (P494L, P497H, P497S, P497L, p.Gly502_Ile504del, P500S, P506A, P506T, P506S, P509S and P525S) [35, 172-175]. Other reported ALS/FTD-linked variants are in a STI1 motif (P189T, M392I, M392V, S400G, Q425R, P440L and M446R) or outside of an annotated region (S155N, A282V, A283T, S346C, T487I, N439I, A488T, P533L and V538L) [173, 174, 176-181]. With the discovery of the first ALS-linked UBQLN2 mutations, the subsequent questions on how they affect UBQLN2 functions and how they contribute to disease pathology was the focus of many researchers. Even though the exact mechanism remains elusive, multiple

studies contributed to elucidate these questions, providing indications for both loss- and gain-of-function of UBQLN2. In addition to the genetical linkage of UBQLN2 to ALS/FTD, the presence of UBQLN2 in abnormal cytoplasmic inclusions in neurons of ALS/FTD patients also disclosed a pathological role of UBQLN2. UBQLN2 was found mainly in Ub-positive inclusions but also a colocalization with TDP-43- and FUS-positive inclusions was reported [35, 172, 182].

UBQLN2 mutations impede client delivery for proteasomal degradation

ALS/FTD-linked UBQLN2 mutations are located at several positions, however, so far, no mutations in the UBA or UBL domain were reported. Nevertheless, since shuttling ubiquitinated proteins to the proteasome is one of the main functions of UBQLN2, first investigations concerning functional changes focused on the UPS. Usage of the $Ub^{G76V}$–GFP reporter system, which cannot be deubiquitinated in cells, revealed an accumulation of the reporter in N2a and SH-SY5Y cells expressing mutant UBQLN2, suggesting impaired proteasomal degradation [35]. Concordantly, slower degradation of Myc, a protein rapidly degraded by the proteasome, was reported in HeLa cells overexpressing mutant UBQLN2 compared to non-transfected cells [183]. Interestingly, it appears that UBQLN2 proteins with mutations in the PXX region are still able to bind ubiquitinated proteins but are defective to bind the S5a subunit of the proteasome [183, 184]. The impaired delivery of clients to the proteasome would also explain the accumulation of Ub-positive UBQLN2 inclusions observed in ALS/FTD patients. Even though mutations in the PXX region do not seem to influence the direct binding of UBQLN2 to ubiquitinated proteins, they disturb the binding to HSP70 [151, 152, 174]. The reduced binding to HSP70 impairs clearing of poly-GA dipeptide repeat protein depositions as well as heat shock induced protein aggregates [151, 152]. Besides disturbed delivery of cytosolic substrates, mutations in UBQLN2 also impair delivery of ERAD substrates to the UPS. For example, expression of the P497H mutation in the PXX region of UBQLN2 disturbs the interaction between UBQLN2 and FAS-associated factor 2 and causes an accumulation of ERAD substrates [156]. UBQLN2 mutations may also interfere with the UPS through sequestration of proteasomal subunits into UBQLN2-positive aggregates, possibly causing proteasome disassembly [185-187].

Autophagy impairment caused by UBQLN2 mutations

Accumulating evidence describes an impact of ALS/FTD-associated mutations in UBQLN2 on autophagy. Immunoreactivity of UBQLN2-positive inclusions with the autophagic receptor SQSTM1/p62 in UBQLN2-associated ALS/FTD cases was the first link between UBQLN2 mutations and autophagy [35]. The colocalization of SQSTM1 with UBQLN2 inclusions as well as an increase in SQSTM1 protein levels was also observed in several rodent models with ALS/FTD-linked UBQLN2 mutations [151, 161, 188]. Intriguingly, mutations in UBQLN2 resulted in decreased autophagosome acidification, which is crucial for the activity of the

lysosomal hydrolases and thus digestion of the engulfed autophagy cargo [160, 161]. It has been suggested that UBQLN2 acts as a chaperone for the ATP6v1g1 subunit of the V-ATPase proton pump and that mutated UBQLN2 is unable to bind and facilitate ATP6v1g1 biogenesis [161]. Other data suggest that UBQLN2 mutations affect the interaction between TBK1 and UBQLN2 by increasing their binding affinity. Consequently, TBK1 binding to its substrates is disrupted possibly leading to impaired autophagy [189].

Mutations in UBQLN2 disturb mitochondrial functions

Recently, mitochondrial health has been proposed as another mechanism how UBQLN2 mutations contribute to the ALS/FTD pathology. First evidence emerged from whole proteomic analysis of isolated hippocampus and spinal cord from transgenic mice overexpressing human UBQLN2 variants [165]. In mice expressing P497S mutant UBQLN2 (hUBQLN2$^{P497S}$) a down-regulation of mitochondria-associated pathways was observed. Indeed, mitochondria of motor neurons in the lumbar spinal cord of hUBQLN2$^{P497S}$ mice were shorter and displayed mitochondria cristae deformities [166]. Shorter mitochondria are possibly a result of deregulated levels of mitochondrial fission and fusion. Furthermore, mitochondria from aged hUBQLN2$^{P497S}$ mice showed a decline in several steps of OXPHOS. Ultimately, mislocalization of the mitochondrial import factor TIMM44 (translocase of inner mitochondrial membrane 44) in UBQLN2 knockout HeLa cells was reversible by the re-expression of wild-type (WT) UBQLN2 but not P497S mutated UBQLN2. Since mutated UBQLN2 binds weaker to TIMM44 than WT UBQLN2, it is suggested that mutations in UBQLN2 may result in altered delivery of TIMM44 to mitochondria [166].

UBQLN2 mutations alter self-assembly stress granule dynamics

Since stress granules are dysregulated in ALS/FTD and UBQLN2 can undergo LLPS, it seems likely that mutations in UBQLN2 might impair UBQLN2 LLPS and stress granule dynamics. Interestingly, ALS-linked mutations in UBQLN2 reduce its interaction with RBPs such as hnRNPA1 and FUS, that are known components of stress granules [170, 190, 191]. Consistently, UBQLN2 has been shown to regulate FUS-RNA interaction and stress granule formation. This regulation is impaired in mutated UBQLN2, possibly hindering the capacity of UBQLN2 to negatively regulate stress granule formation [170]. *In vitro* purified UBQLN2 PXX mutants have an increased propensity to oligomerize, promote LLPS and form non-liquid like amorphous droplets or aggregates. Importantly, this modulation is strongly depended on the position of the mutation and only applies for hydrophobic but not for polar residues [192]. Consistent with this biochemical data, UBQLN2 carrying a P497H mutation forms intense cytosolic puncta while UBQLN2 WT is mainly diffusely localized throughout the cytoplasm in *Drosophila* neuronal cells [193]. Similarly, primary rodent cortical neurons expressing UBQLN2 carrying a P506T mutation are more prone to form puncta compared to those expressing WT

UBQLN2 [186]. However, contradictory evidence suggests that ALS/FTD-linked mutations in UBQLN2 might perturb the ability of UBQLN2 to assemble into biomolecular condensates in cells under stress [194].

Having introduced ALS/FTD, its pathological pathways as well as UBQLN2 and its role in the disease, in the following the current scientific knowledge of MAP1B, a protein of interest in this thesis is summarized.

## 1.2 MAP1B

Microtubule-associated proteins (MAPs) were initially discovered as proteins that co-purify with tubulin from brain extracts [111, 195]. While the first identified MAPs were classified based on their capacity to bind and stabilize microtubules, today a large variety of MAPs with various functions are known. MAPs bind to microtubules in several ways and can influence microtubule structure, function or dynamics. Classical, also called structural, MAPs include members of the MAP1, MAP2, MAP4 and tau family and are non-enzymatic proteins which bind along the microtubule lattice [196]. In general, they can promote microtubule polymerization, stabilization and microtubule bundling, though some of them also regulate the dynamic fraction of microtubules [197, 198]. Several MAPs also have the capability to bind other cytoskeletal components beside microtubules such as intermediate and actin filaments and thus can act as cytoskeletal crosslinkers [199, 200]. Some MAPs were even shown to protect microtubules against severing enzymes or modulate the movement of motor proteins [201-203]. Furthermore, evidence suggests that a subset of MAPs acts in various neuronal signaling networks [204]. Since MAPs are crucial for microtubule dynamics and consequently to neuronal health, it is not surprising that various MAPs are linked to neurological diseases. Due to its association with several neurodegenerative diseases including AD, Pick's disease and FTD, the best known and most intensively studied MAP is tau [205].

### 1.2.1 Structure and expression of the MAP1 family member MAP1B

Along with tau, proteins of the MAP1 and the MAP2 family are the major structural MAPs in neurons. In mammals, the MAP1 family consists of three members, MAP1A, MAP1B and MAP1S [206]. While MAP1S is ubiquitously expressed, MAP1A and MAP1B are primarily expressed in the nervous system [207]. After translation, all three members are proteolytically cleaved near the carboxyl terminus into a larger heavy chain (HC; 100-350 kDa) and a smaller light chain (LC; 26-32 kDa) [207-209]. In addition, all LCs harbor an actin-binding domain (ABD) and a microtubule-binding domain (MBD), while the HCs have one or two MBD [210]. Intriguingly, the MAP1B HC harbors an ABD as well. The MAP1B HC was reported to bind the

MAP1A LC (LC2), the MAP1B LC (LC1), as well as the autophagy-associated LC3, which is expressed by the hATG8 genes LC3A-C (Figure 1-9) [211].

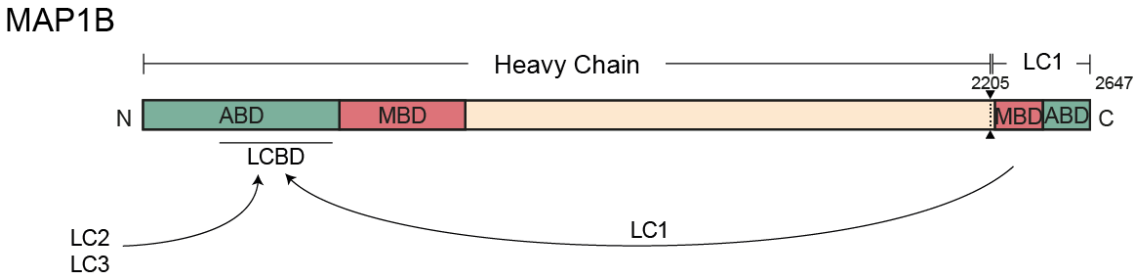


**Figure 1-9: Schematic representation of the MAP1B protein structure.**
The MAP1B protein is proteolytically cleaved into a heavy chain and a light chain (LC1). Both chains contain a microtubule-binding domain (MBD; red) and an actin-binding domain (ABD; green). The MAP1A LC (LC2), the MAP1B LC (LC1), as well as the autophagy-associated LC3 were reported to bind to the heavy chain at the light chain binding domain (LCBD). Arabic numbers indicate amino acid position of the cleavage site.

Originally discovered in the 1980s, MAP1B was also known as MAP1.2, MAP1x, or MAP5 [212-215]. MAP1B is among the first structural MAPs expressed in developing neurons [216]. It was suggested to be especially important in early embryonic development, since its expression levels are highest in newborn rats and decrease postnatally [211]. In developing neurons, MAP1B is enriched in the distal region of the growing axons indicating a role in axonal growth [214, 217]. Accordingly, suppression of MAP1B with antisense oligonucleotides in cultured rat cerebellar neurons inhibits laminin-enhanced axonal elongation [218]. Consistently, cultured neurons from MAP1B-deficient mice display a delay in axonal outgrowth and a reduced rate of elongation [219]. Although MAP1B expression is highest at birth, it continues to be expressed in the mature brain, especially in areas with high synaptic plasticity such as the hippocampus, the olfactory bulb or the cerebellum [211, 216, 220]. Furthermore, after lesions of motor neurons in cats and after brain injury in rats, an increase in MAP1B was observed, suggesting a role of MAP1B in the regeneration of neurons [221, 222].

### 1.2.2 MAP1B phosphorylation determines its localization and function

Interestingly, MAP1B's role in axonogenesis as well as other functions depend on MAP1B phosphorylation. MAP1B contains several potential phosphorylation sites. A proteomic analysis of *in vivo* phosphorylated murine synaptic proteins revealed 33 phosphorylated sites (phosphosites) [223]. However, protein databases (PhosphoSitePlus and Uniprot) list more than 90 phosphosites for MAP1B [224]. So far, two types of MAP1B phosphorylation can be functionally distinguished: mode I or proline-dependent kinase phosphorylation and mode II phosphorylation catalyzed by casein kinase II [225, 226]. While mode I phosphorylated MAP1B is mainly present in the distal part of axons, mode II phosphorylated MAP1B is present in all subcellular domains of the neuron [227]. Mode I phosphorylation decreases with development

and is suggested to control the dynamic properties of neuronal microtubules which is especially important in developing neurons [219]. On the contrary, MAP1B mode II phosphorylation is proposed to promote the assembly and stabilization of microtubules [228, 229]. While mode I and mode II phosphorylation were extensively studied in the last decades, the multiplicity of annotated MAP1B phosphosites and their potential regulation by several other kinases raise the question whether additional phosphorylation modes linked to distinct MAP1B functions may exist.

### 1.2.3 MAP1B and the regulation of microtubule dynamics

Since MAP1B co-purifies with microtubules, extensive research concentrated on its microtubule polymerization properties. Overexpressed MAP1B was observed to stabilize microtubules against depolymerizing reagents in fibroblasts [113]. In general, acetylation and detyrosination are considered to be enriched in mature/stable microtubules, whereas tyrosination is associated with more labile/dynamic microtubule regions [230]. In mouse Map1b knockout neurons a reduced number of acetylated microtubules in growth cones was detected, substantiating a stabilizing effect of MAP1B. However, compared to other MAPs, MAP1B is unable to induce microtubule bundle formation and does not suppress microtubule dynamic instability [113, 231, 232]. Yet, other groups reported increased microtubule dynamics upon MAP1B expression, a reduction of stable microtubules in MAP1B-deficient neurons and exclusive binding of MAP1B to tyrosinated tubulins [219, 233]. Moreover, recent evidence showed an increase of acetylated tubulin in the presence of MAP1B, but a negative regulation of this effect through phosphorylation of MAP1B by glycogen synthase kinase-3 (GSK3) [234]. Overall, this data supports the notion that MAP1B regulates the balance of acetylated, detyrosinated and tyrosinated microtubules based on its phosphorylation status. In addition, MAP1B is also able to influence microtubule dynamics indirectly. For example, it can interact with the microtubule plus-end tracking proteins EB1 and EB3 and thereby sequester these factors in the cytosol. MAP1B deficiency leads to increased binding of EB1 and EB3 to microtubule plus-ends, microtubule overstabilization and looping [235]. Furthermore, MAP1B interacts with tubulin tyrosine ligase (TTL), promoting its activity and the formation of tyrosinated tubulins [197].

### 1.2.4 MAP1B functions beyond regulation of microtubule dynamics

MAP1B and its LC1 were reported to be involved in multiple processes which are unrelated to microtubule stabilizing functions. Among other proteins, MAP1B chains associate with ion channels, neurotransmitter receptor and receptor regulatory proteins, such as metabotropic glutamate receptor sub-group II members, gamma-aminobutyric acid C receptor, calcium channel $Ca_V2.2$, the N-methyl-d-aspartate receptor (NMDAR) subunit NR3A, the glycine

receptor alpha subunit and the serotonin receptors 5-$HT_6$ and 5-$HT_{3A}$ as well as with glutamate receptor interacting protein 1 (GRIP1) [236-244]. These interactors suggest a role of MAP1B in regulating the localization, trafficking and activity of surface receptors possibly by anchoring these proteins to microtubules [238].

The hypothesis that MAP1B might play a role in autophagy emerges from the ability of MAP1B to associate with LC3 [245]. Furthermore, evidence suggests that binding of MAP1B to the death-associated protein kinase-1 (DAPK-1) is necessary for DAPK-1-stimulated autophagy [246]. In addition, LC1 interacts with the autophagic receptor NBR1 and might target it to the microtubule network allowing NBR1 to recruit cargo to autophagosomes [247]. In contrary, recent findings propose that LC1 links syntaxin 17, a protein implicated in autophagosome-lysosome fusion, to microtubules, resulting in a blockage of autophagosome formation [248].

MAP1B seems also to be implicated in neuronal mRNA trafficking. LC1 binds to nuclear export factor proteins (NXFs), their cofactor U2AF as well as to the mRNA-binding protein Staufen 1 (STAU1) and the WD-repeat protein UNRIP. Thus, MAP1B seems to be involved in nuclear export and cytoplasmic trafficking of NXF-containing mRNPs, possibly by tethering the complex to microtubules [249]. In addition, LC1 directly interacts with neuronal Hu proteins, which are RBP that stabilize and transport AU-rich elements (ARE)-containing mRNAs [250, 251]. Since Hu proteins simultaneously bind RNA and LC1, it is suggested that LC1 associates the Hu-mRNA complex to microtubules and thus participates in mRNA expression.

### 1.2.5 MAP1B is implicated in several neurological disorders

MAP1B also emerges in the context of neurodegenerative diseases, such as Parkinson's Disease (PD), AD and ALS/FTD. For example, MAP1B is a component of Lewy bodies, a neuropathological hallmark of PD. MAP1B has the ability to bind monomeric and filamentous α-synuclein and hence might be involved in the formation of Lewy bodies [252]. Interestingly, loss-of-function mutations in DJ-1 (also Parkinson disease protein 7) cause an accumulation and aggregation of LC1 possibly leading to ER stress-induced apoptosis [253]. However, also a neuroprotective role of LC1 was suggested in PD. Indeed, LC1 rescues leucine-rich repeat kinase 2 (LRRK2) mutant-mediated cytotoxicity, probably by inhibiting LRRK2 activity [254]. Fragments of phosphorylated MAP1B are also found in neurofibrillary tangles, aggregates of hyperphosphorylated tau, a hallmark of AD [255, 256]. In addition, MAP1B plays a role in giant axonal neuropathy (GAN). GAN is a rare disorder affecting both the central and peripheral nervous system and is caused by mutations in the gigaxonin gene (*GAN*) and characterized by neurons with giant axons [257]. Gigaxonin binds directly to LC1 and controls its degradation [258, 259]. Ablation of gigaxonin in mice causes an accumulation of LC1, neurodegeneration and cell death, all of which can be rescued by Map1b reduction [259]. Hence, LC1

accumulation contributes directly to the neurodegeneration in GAN. In the last years, MAP1B was reported to be dysregulated in ALS/FTD. TDP-43 was shown to interact with the mRNA of the MAP1B fly homolog *futsch* and regulates its localization and expression [260, 261]. However, it is not completely clear which effect this binding has on MAP1B expression and translation. Some evidence points towards a positive modulation of *futsch* mRNA translation by TDP-43 through its interaction with a UG-rich sequence within the 5′UTR of *futsch* mRNA [260]. Other evidence suggests that TDP-43 inhibits *futsch* expression post-transcriptionally [261]. Interestingly, overexpression of futsch can be neuroprotective in flies overexpressing TDP-43 since this reduced TDP-43 aggregation and suppressed ALS-like locomotor dysfunction [261]. A translation-repressing activity of TDP-43 is substantiated by its association with the known MAP1B repressor FMRP [262]. It is hypothesized that TDP-43 helps to recruit FMRP to the vicinity of mRNAs, including *MAP1B* mRNA [96]. Importantly, MAP1B accumulation in spinal cord motor neuron cell bodies was seen in some ALS patients [261]. Besides TDP-43, FUS seems to be involved in the regulation of *MAP1B* mRNA. Expression of mutated FUS (R521C) causes an increase in synaptic MAP1B levels in zebrafish embryos [92]. It was hypothesized that the cytosolic increase of mutated FUS enhances binding between FUS and FMRP, thus preventing FMRP to repress MAP1B translation. The observation that FUS is capable to bind the same G quadruplex structure of *MAP1B* mRNA as FMRP, supports a directional competition between FUS and FMRP for *MAP1B* binding [263].

## 1.3 Aim of the study

The ubiquitin-binding protein UBQLN2 is among others implicated in the main protein degradation pathways autophagy and the UPS. Mutations in UBQLN2 are genetically and pathologically linked to ALS/FTD. Although multiple functions of UBQLN2 and their impairment in ALS/FTD were reported since the first discovery of ALS/FTD-linked UBQLN2 mutations, the specific pathomechanism remains elusive.

The aim of my thesis project was to further elucidate the role of UBQLN2 in the disease context of ALS/FTD. We sought to pursue this aim with the hypothesis that UBQLN2 deficiency leads to alterations of cellular components regulated by UBQLN2. To test this notion, we combined different omics screening approaches. In detail, we employed protein expression profiling, transcriptomic analysis, interaction proteomics and phosphoproteomics to further understand the impact of ALS/FTD-linked mutations in UBQLN2. In addition to CRISPR/Cas9 gene-edited HeLa cells, patient-derived cells carrying ALS/FTD-causing mutations were used to mimic cellular disturbances present in patients. Further on, we sought to dissect the most prominent candidates and unravel a possible linkage between those. To strengthen the relevance of the new findings, primary rat neurons were studied for validation in a neuronal context.

# 2 Materials and Methods

## 2.1 Materials

### 2.1.1 General chemicals and reagents

| Name | Company | |
|---|---|---|
| 1kb DNA Ladder | NEB | N3232 |
| 2-Propanol | Merck | 109634 |
| Acetic acid | Merck | 100063 |
| Acetic acid (eluent additive for LC-MS) | Honeywell Fluka | 49199-50ML |
| Acetone | Merck | 100014 |
| Acetonitrile (ACN) | Roth | AE70 |
| Acrylamide 4K Solution (30%) | PanReac AppliChem | A0951 |
| Ammonium bicarbonate (ABC) | Sigma-Aldrich | 09830 |
| Ammonium peroxydisulphate (APS) | Roth | 9592 |
| Ampicillin sodium salt | Roth | K029 |
| Anti-HA agarose | Thermo Scientific | 88836 |
| BamHI | New England Biolabs | R0136 |
| BbsI | New England Biolabs | R0539 |
| BC Assay Reagent A | Interchim | UP95424A |
| BC Assay Reagent B | Interchim | UP95425A |
| Benzonase Nuclease HC | Millipore | 71205 |
| Betaine | Sigma-Aldrich | 61962 |
| Bovine Serum Albumin (BSA) | Sigma-Aldrich | A8022 |
| Bromophenol blue | Thermo Fisher | 32712 |
| BsmBI | New England BioLabs | R0739 |
| Carbenicillin disodium salt | PanReac AppliChem | A1491 |
| Chloramphenicol | Sigma-Aldrich | C0378 |
| cOmplete EDTA-free Protease Inhibitor Cocktail | Roche | 04693132001 |
| Dithiothreitol (DTT) | Biomol | 04010 |
| DNA Gel Loading Dye (6x) | Thermo Scientific | R0611 |
| DpnI | New England BioLabs | R0176S |
| Ethanol (EtOH) | Roth | 9065 |
| Formic acid (FA) | Merck | 100264 |

| | | |
|---|---|---|
| Gateway™ BP ClonaseTM II Enzyme mix | Thermo Fisher | 11789100 |
| Gateway™ LR ClonaseTM II Enzyme mix | Thermo Fisher | 11791020 |
| GeneRuler 100bp DNA Ladder | Thermo Scientific | SM0241 |
| Glycerol | Roth | 3783 |
| HA-Peptide | Sigma-Aldrich | I2149 |
| Hard-Shell® 96-Well PCR Plates | Biorad | HSP9601 |
| Hydrochloric acid 32% | Merck | 100319 |
| IGEPAL CA-630 (NP-40) | Sigma-Aldrich | I8896 |
| Influenza Hemagglutinin (HA) Peptide | Sigma-Aldrich | I2149 |
| Iodoacetamide (IAA) | Sigma-Aldrich | I1149 |
| Kanamycin sulphate | Roth | T832 |
| KOD Hot Start DNA Polymerase | Sigma-Aldrich | 71086 |
| Lumigeb ECL Ultra (TMA-6) | Lumigen | TMA-100 |
| Lysyl Endopeptidase® (Lys-C) | FUJIFILM | |
| Methanol | Merck | 106009 |
| Methanol | Roth | AE71 |
| MIDORI Green Advance | Genetics | MG04 |
| Monoclonal Anti-HA-Agarose | Millipore | A2095 |
| Distilled water DNase/RNase free | Gibco | 10977-035 |
| OneTaq DNA Polymerase | New England BioLabs | M0480S |
| One-Taq DNA Polymerase | New England BioLabs | M0480 |
| Paraformaldehyde (PFA) solution 4% in PBS | Chemcruz | sc-281692 |
| PhosSTOP | Roche | 04906837001 |
| Ponceau S | Sigma-Aldrich | P3504 |
| Powdered milk | Roth | T145 |
| ProLong™ Gold Eindeckmittel mit DAPI | Invitrogen | P36931 |
| ProSieve QuadColor Protein Marker, 4.6-300 kDa | Biozym | 830537 |
| Protein Marker VI (10-245) prestained | PanReac AppliChem | A8889 |
| Q5 Hot Start High-Fidelity DNA Polymerase | New England BioLabs | M0493 |
| ReproSil-Pur 120 C18-AQ 1.9µm | Dr. Maisch | r119.aq. |
| SacI | New England Biolabs | R0156 |
| SeaKem LE Agarose | Lonza | 50004 |

| | | |
|---|---|---|
| Sequencing Grade Modified Trypsin | Promega | V5113 |
| Sodium acetate trihydrate | Roth | Roth |
| Sodium chloride | Roth | 3957 |
| Sodium deoxycholate | Sigma-Aldrich | D6750 |
| Sodium dodecyl sulfate (SDS) | Serva | 20765 |
| Spectinomycin dihydrochloride pentahydrate | Sigma-Aldrich | S4014 |
| SsoAdvanced Universal SYBR Green Supermix | Biorad | 1725270 |
| T4 DNA Ligase | New England BioLabs | M020 |
| Tetramethylethylenediamine (TEMED) | Roth | 2367 |
| Thiourea | Sigma-Aldrich | T7875 |
| Trichloroacetic acid solution (TCA) | Sigma-Aldrich | T0699 |
| Trifluoroacetic acid (TFA) | Sigma-Aldrich | 302031 |
| Tris ultrapure | PanReac AppliChem | A1086 |
| Tris-EDTA buffer solution | Sigma-Aldrich | 93302 |
| Triton X-100 | Millipore | 108603 |
| Tropix I-BLOCK | Invitrogen | T2015 |
| Tween-20 | Sigma-Aldrich | 822184 |
| Urea | Serva | 24524 |
| Water LC-MS Grade | Roth | AE72 |
| Western Lightning Plus-ECL/ | Perkin Elmer | NEL105001EA |

### 2.1.2 Cell culture chemicals and reagents

| Name | Company | Identifier |
|---|---|---|
| 0.25% Trypsin-ETDA (1x) | Gibco | 25200056 |
| Bafilomycin A1 (BafA) | Biomol | Cay11038 |
| Blasticidine | InvivoGen | ant-bl-1 |
| Bortezomib (Btz) | LC laboratories | B-1408 |
| Dimethyl sulfoxide (DMSO) Cell culture grade | PanReac AppliChem | A3672 |
| Dulbecco`s modified Eagles`s Medium (DMEM) (1x) + GlutaMAX-I | Gibco | 61965026 |

| | | |
|---|---|---|
| Dulbecco's Phosphate buffered Saline (PBS) | Gibco | 14190144 |
| Fetal Bovine Serum (FBS) | Gibco | 10270106 |
| Fetal Bovine Serum, dialyzed | Gibco | 26400044 |
| L-Arginine | Sigma-Aldrich | A8094 |
| L-Arginine:HCL (13C6, 99%; 15N4, 99%) | Cambridge Isotope Laboratories | CNLM-539-H-PK |
| L-Glutamine 200mM | Gibco | 25030024 |
| Lipofectamine 2000 | Invitrogen | 11668019 |
| Lipofectamine RNAiMAX | Invitrogen | 13778100 |
| L-Lysine monohydrochloride | Sigma-Aldrich | L8662 |
| L-Lysine:2HCL (13C6, 99%; 15N2, 99%)/ | Cambridge Isotope Laboratories | CNLM-291-H-PK |
| Optimal modified Eagle`s Medium (Opti-MEM) I + GlutMAX-I | Gibco | 51985026 |
| Puromycin dihydrochloride | Sigma-Aldrich | P8833 |
| RPMI 1640 Medium for SILAC | Thermo Scientific™ | 88365 |
| Sodium pyruvate 100mM | Gibco | 11360039 |

### 2.1.3 Consumables

| Name | Company | Identifier |
|---|---|---|
| 1.5 ml, polypropylene tube | Beckman coulter | 357448 |
| 2 ml crimp top caps | Agilent | 5181-1211 |
| 2 ml crimp top vials | Agilent | 5181-3375 |
| 4-10% Mini-PROTEAN TGX gels | Bio-Rad | 456-1094 |
| Blotting paper | Macherey-Nagel | MN742112 |
| Capillar tips, 0.5-10 µl | Biozym | 729008 |
| Clear flat-bottom 96-well plates | Thermo Scientific | 442404 |
| Countess cell counting chamber slides | Invitrogen | C10228 |

| | | |
|---|---|---|
| CryoTubes | VWR | 479-1261 |
| Empore SPE disks C18 | Sigma | 66883-U |
| Empore SPE disks cation exchange | Sigma | 66889-U |
| Epredia X50 Microscope Slide | Fisher Scientific | 15998086 |
| Microscope cover glasses | Marienfeld | 0111550 |
| Mini-PROTEAN short plates | Bio-Rad | 1653308 |
| Mini-PROTEAN spacer plates | Bio-Rad | 1653311 |
| Mr. Frosty cryo box | Thermo Scientific | 5100-0001 |
| Multiflex tips 100 µl | Sorenson | 28480 |
| Nitrocellulose blotting membranes, pore size 0.45 µm | GE Healthcare Life science | 10600002 |
| Nunc™ cell culture petri dishes 100x15 | Thermo Scientific | 150350 |
| Nunc™ cell culture petri dishes 150x21 | Thermo Scientific | 168381 |
| Nunc™ cell-culture treated 12-well plates | Thermo Scientific | 150628 |
| Nunc™ cell-culture treated 48-well plates | Thermo Scientific | 142475 |
| Nunc™ cell-culture treated 6-well plates | Thermo Scientific | 140675 |
| Nunc™ MicroWell™ 96-well | Thermo Scientific | 167008 |
| pH test strips | Macherey-Nagel | 92110 |
| Super RX-N | Fujifilm | 47410 19289 |
| Syringe filter, 0.45 µm | VWR | 514-0075 |
| Vial inserts, 250 µl | Agilent | 5181-8872 |

### 2.1.4 Kits

| Name | Source | Identifier |
|---|---|---|
| High pure RNA isolation kit | Roche | 11828665001 |

| | | |
|---|---|---|
| PureLink™ Genomic DNA Mini Kit | Thermo Scientific | K182002 |
| QIAprep Spin Miniprep Kit | Qiagen | 27106 |
| QIAquick Gel Extraction Kit | Qiagen | 28706 |
| QIAquick PCR Purification Kit | Qiagen | 28106 |
| Transcriptor First Strand cDNA Synthesis Kit | Roche | 4897030001 |

### 2.1.5 Oligonucleotides and other sequence-based reagents

| Name | Nucleotide Sequence (5' to 3') or Identifier | Source | Usage |
|---|---|---|---|
| GW_UBQLN2_Ntap_forward | GGGGACAACTTTGTACAAAAAAGTTGGCGCTGAGAATGGCGAGAGCAG | This work | Gateway PCR |
| GW_UBQLN2_Ntap_reverse | GGGGACAACTTTGTACAAGAAAGTTGGGTATTACGATGGCTGGGAGCCC | This work | Gateway PCR |
| hMAP1B GW N-term forward | GGGGACAACTTTGTACAAAAAAGTTGGCGCGACCGTGGTGGTG | This work | Gateway PCR |
| hMAP1b GW N-term reverse | GGGGACAACTTTGTACAAGAAAGTTGGGTACTACAGTTCAATCTTGCATGCA | This work | Gateway PCR |
| UBQLN2 gRNA1 forward | CACCGCCTACTTCCCTCACTCCCTT | This work | gRNA |
| UBQLN2 gRNA1 reverse | AAACAAGGGAGTGAGGGAAGTAGGC | This work | gRNA |
| UBQLN2 knockout gRNA 1 forward | CACCGTTTCGAATCCCGATCTGATG | This work | gRNA |
| UBQLN2 knockout gRNA 1 reverse | AAACCATCAGATCGGGATTCGAAAC | This work | gRNA |
| UBQLN2 knockout gRNA 2 forward | CACCGACGCAGCCTAGCAATGCCGC | This work | gRNA |
| UBQLN2 knockout gRNA 2 reverse | AAACGCGGCATTGCTAGGCTGCGTC | This work | gRNA |

| | | | |
|---|---|---|---|
| UBQLN2 knockout gRNA 3 forward | CACCGACCCCCAAACTGCTCTTGTG | This work | gRNA |
| UBQLN2 knockout gRNA 3 reverse | AAACCACAAGAGCAGTTTGGGGGTC | This work | gRNA |
| UBQLN2 T487I forward | GTGGGGGTGCTGGGAATCGCTATAGGC | This work | Mutagenesis |
| UBQLN2 T487I reverse | GCCTATAGCGATTCCCAGCACCCCCAC | This work | Mutagenesis |
| UBQLN2_P497S forward | GGCCCAGTCACCTCCATAGGCCCCA | This work | Mutagenesis |
| UBQLN2 P497S reverse | GGGGCCTATGGAGGTGACTGGGCCT | This work | Mutagenesis |
| UBQLN2 SacI left homology arm_forward | GCGCCATTCAAGAGCTCATGCTGAATG | This work | PCR |
| UBQLN2 BamHI left homology arm reverse | GCGCGACAGATTTAAAAGGATCCAAATGAAAGTAAAG | This work | PCR |
| TBP PrimePCR™ | qHsaCID0007122 | Bio-Rad | RT-qPCR |
| ACTB PrimePCR™ | qHsaCED0036269 | Bio-Rad | RT-qPCR |
| GAPDH PrimePCR™ | qHsaCED0038674 | Bio-Rad | RT-qPCR |
| MAP1B PrimePCR™ | qHsaCID0012114 | Bio-Rad | RT-qPCR |
| UBQLN2 forward | CCTGCAGCAGATGCAGAATCCAG | This work | Sequencing |
| UBQLN2 reverse | CAACACTTGTTCACCCAACTGTGAAGG | This work | Sequencing |
| U6 forward | GAGGGCCTATTTCCCATGATTCC | GATC/ eurofins Genomics | Sequencing |
| Flag forward | CAAGGATGACGATGACAAGC | This work | Sequencing |
| CMV forward | CGCAAATGGGCGGTAGGCGTG | GATC/ eurofins Genomics | Sequencing |
| rat Ubqln2 shRNA | GCTTCAAATCGCAAACCGA | This work | shRNA |

| | | | |
|---|---|---|---|
| ON-TARGETplus siRNA FUS | J-009497-09-0005 J-009497-10-0005 | Dharmacon | siRNA |
| ON-TARGETplus Non-targeting Control siRNA | D-001810-01-20 | Dharmacon | siRNA Control |

### 2.1.6 Antibodies

| Name | Source | Identifier | Application |
|---|---|---|---|
| Rabbit anti-MAP1B | Sigma | HPA022275 | IF (1:100) |
| Rabbit anti-MAP1B | Proteintech | 21633-1-AP | WB (1:500) |
| Guinea Pig anti-MAP1B-LC1 | SYSY | 410 005 | WB (1:1000) |
| Mouse anti-GAPDH | Thermo Scientific | AM4300 | WB (1:4000) |
| Rabbit anti-Calnexin | Abcam | ab22595 | WB (1:1000) |
| Rabbit anti-UBQLN2 | Cell Signaling | 85509S | WB (1:1000); IF (1:300) |
| Mouse anti-UBQLN2 | Sigma | WH0029978M3-100UG | WB (1:1000); IF (1:300) |
| Mouse anti-FUS | Santa Cruz | sc-47711 | WB (1:5000) |
| Rabbit anti-HA | Cell Signaling | 3724S | WB (1:1000) |
| Rabbit anti-Acetyl-a-Tubulin (Lys40) | Cell Signaling | 5335 | IF (1:800) |
| FITC Anti-alpha Tubulin antibody | Abcam | ab64503 | IF (1:300) |
| Donkey anti-rb-555 | Invitrogen | A31572 | IF (1:500) |
| Goat anti-rabbit-488 | Invitrogen | A11034, | IF (1:500) |
| Goat anti-mouse-555 | Invitrogen | A21424 | IF (1:500) |
| Goat anti-mouse-488 | Invitrogen | A11001, | IF (1:500) |
| anti-rabbit-HRP | Promega | W401B | WB (1:1000) |
| anti-mouse-HRP | Promega | W402B | WB (1:1000) |
| Goat Anti-Guinea Pig IgG Antibody, F(ab') 2, HRP | Sigma-Aldrich | AQ108P | WB (1:1000) |

### 2.1.7 Recombinant DNA reagent

| Name | Reference or Source | Identifier |
|---|---|---|
| MGC Human UBQLN2 Sequence-Verified cDNA (CloneId:4543266) | Dharmacon | MHS6278-202831640 |
| ORFeome Collab. Human MAP1B ORF w/ Stop Codon | Horizon | OHS5893-202503825 |
| Cas9 expressing plasmid pX330 | Addgene (Gift from Feng Zhang) | 42230 |
| pLentiCRISPR-HF1 Puro plasmid | Addgene (Gift from Lukas Dow) | 110850 |
| pAAV-SEPT plasmid | Addgene (Gift from Todd Waldman) | 25648 |
| FU3a tagRFP plasmid | Dieter Edbauer; DZNE Munich | N/A |
| pcDNA3.1-VSVG | Dieter Edbauer; DZNE Munich | N/A |
| psPAX2 | Addgene (Gift from Didier Trono) | 12260 |
| pMD.2 | Addgene (Gift from Didier Trono) | 12259 |
| pDONR223 | Wade Harper; Harvard Medical School | N/A |
| pHAGE-N Tap (Flag-HA) | Wade Harper; Harvard Medical School | N/A |

### 2.1.8 Mammalian and bacterial cells

| Cells | Reference or Source | Identifier |
|---|---|---|
| HeLa (Human) | ATCC | Cat#CCL-2 |
| HEK293T | ATCC | Cat#CRL-3216 |
| LCL UBQLN2 T487I | Jochen Weishaupt; MCTN Heidelberg | N/A |
| LCL UBQLN2 P497S | Jochen Weishaupt; MCTN Heidelberg | N/A |
| LCL UBQLN2 WT (Control for T487I) | Jochen Weishaupt; MCTN Heidelberg | N/A |

| | | |
|---|---|---|
| LCL UBQLN2 WT (Control for P497S) | Jochen Weishaupt; MCTN Heidelberg | N/A |

### 2.1.9 Equipment

| Name | Source | Identifier |
|---|---|---|
| Automatic cell counter | Invitrogen | Countess II |
| Bacteria incubator | New Brunswick Scientific | innova42 |
| Benchtop centrifuge | Eppendorf | 5424 |
| Cell incubator | Thermo Scientific | HERACELL 150i |
| Confocal laser scanning microscope | Zeiss | Zeiss LSM800 with oil-immersion 60x objective |
| Cooled benchtop centifuge | Eppendorf | 5810R / 5424R |
| Digital Rotary Mixer | LABINCO | LD76 |
| Gel Documentation System | Bio-Rad | Gel Doc XR+ |
| Laminar flow hood | Thermo Scientific | Safe 2020 |
| Light microscope | hund WETZLAR | WilovertS Mikro |
| Mass spectrometer | Thermo Scientific | QExactive$^{HF}$ |
| Microcentrifuge | VWR | MiniStar silverline |
| Microplate Reader | BioTEK | PowerWave XS |
| Multichannel pipette (300 µl) | Eppendorf | Research plus |
| Nano-flow UHPLC | Thermo Scientific | EASY-nLC 1200 |
| Pipet-Lite XLS (10 µl, 200 µl, 1000 µl) | Mettler Toledo | 17014388, 17014391, 17014382 |
| Pipette controller | BRAND | Accu-jet® pro |
| Pipettes (2 µl, 10 µl, 200 µl, 1000 µl) | Pipetman | MA52721, EE53946, ML52581, M52184, EJ91013 |
| Power Supply | Biorad | PowerPac$^{TM}$ PowerPac$^{TM}$HC |
| Power-Pac Basic | Bio-Rad | 1645050 |
| Power-Pac HC | Bio-Rad | 1645052 |
| Real-Time PCR Detection System | Biorad | CFX96 |
| Scale | Denver Instruments | MXX-2001 |

| | | |
|---|---|---|
| Sonifier | Branson Ultrasonics™ | W-250D |
| Spectrophotometer | Thermo Scientific | NanoDrop™ 2000c |
| Thermal Cycler | Bio-Rad | T100 |
| Thermo Mixer | Eppendorf | F1.5 |
| Ultrasonic baths | BANDELIN | SONOREX |
| Vacuum concentrator | Eppendorf | Concentrator plus™ |
| Vortex mixer | Scientific Industries | Vortex-Genie™ 2 |
| X-Ray cassette 20x25 cm | Kisker Biotech GmbH | ZV0025 |
| X-Ray developer machine | Cawo | Cawomat 2000 IR |

### 2.1.10 Buffers and solutions

General buffers

PBS [pH 7.4]: 0.6 mM Na2HPO4 x 2H2O, 0.018 mM KH2PO4, 0.27 mM KCl, 1.36 M NaCl
TAE [pH 8.3]: 40 mM Tris-HCl, 1 mM EDTA, 20 mM acetic acid (AcOH)
LB [pH 7.0]: 10 g/l bacto trypton, 5 g/l bacto yeast extract, 5 g/l NaCl
LB-Plates: 12 0g/l bacto agar in LB-medium

Immunoblotting and mass spectrometry buffers

Laemmli SDS-PAGE loading dye (3x): 200 mM Tris-HCl [pH 6.8], 20% glycerol, 10% DTT (m/v), 6%SDS, Bromphenol Blue

Urea buffer: 9 M urea, 50 mM Tris [pH 8], 150 mM NaCl, 1x protease inhibitor

RIPA-lysis buffer: 50 mM Tris [pH 7.4], 150 mM NaCl, 0.1% SDS, 0.5% sodium deoxycholate, 1% NP-40, 1x protease inhibitor, 1x PhosSTOP

MCLB buffer: 50 mM Tris-, 150 mM NaCl. 0.5% NP40, 1x protease inhibitor

Urea buffer: 2 M / 3 M Urea in 50 mM ABC

Denaturation buffer: 6 M Urea, 2 M Thiourea, 10 mM Tris-HCl [pH 8.0]

Urea lysis buffer: 9 M Urea, 50 mM Tris [pH 8], 150 mM NaCl, 1x protease inhibitor

SDS-PAGE Laemmli running buffer: 25 mM Tris-Base, 200 mM glycine, 1 g/l SDS

SDS-PAGE transfer buffer: 25 mM Tris-HCl, 190 mM glycine

Phos-Tag transfer buffer: 0.1%SDS, 25 mM Tris-Base, 200 mM glycine, 5% v/v MeOH, (+1 mM EDTA)

TBS [pH 7.6]: 20 mM Tris-HCl, 150 mM NaCl

TBS-T: TBS + 0.1% Tween-20

Stop and go extraction (stage) tipping buffers

Loading buffer (Buffer A): 0.1% FA

Elution buffer (Buffer B): 80% ACN, 0.1% FA

Equilibration buffer (Buffer C): 5% ACN, 1 % TFA

Pre-fractioning stage tipping buffers

Reversed-phase ion exchange (ReX)-Buffer 1: 0.5% AcOH

ReX-Buffer 2: 0.5% AcOH, 80% ACN

ReX-Buffer 3: 20mM NH4AcO, 0.5%AcOH

ReX-Buffer 4: 40mM NH4AcO, 0.5%AcOH, 20%ACN

ReX-Buffer 5: 100mM NH4AcO, 0.5%AcOH, 20%ACN

ReX-Buffer 6: 500mM NH4AcO, 0.5%AcOH, 20%ACN

## 2.2 Methods

### 2.2.1 Molecular biology

DNA and RNA isolation

Genomic DNA and total RNA were isolated from cell pellets with the PureLink™ Genomic DNA kit and the High Pure RNA isolation kit according to the manufacturer's protocol, respectively. Concentrations were measured by determining the absorption at 260 nm using a NanoDrop™ 2000c. While RNA was frozen in liquid nitrogen and stored at -80°C, genomic DNA was stored at 4°C. Isolated RNA was used for cDNA generation or for RNA sequencing performed in collaboration with Elisabeth Graf from the Helmholtz Zentrum München, Munich, Germany.

Generation of cDNA and RT qPCRs

Reverse transcription of RNA to cDNA was conducted with the Transcriptor First Strand cDNA kit according to the manufacturer's instructions. For real time quantitative PCRs (RT-qPCR) performed in 96-well plates with cycling conditions shown in table Table 2-1, 1 µl of 20xPrimePCR Assay, 10µl SsoAdvanced™ universal supermix, 2 µl cDNA sample and 7 µl $H_2O$ were pipetted in each well.

Table 2-1: Cycling conditions for RT-qPCRs.

| **Step** | **Temperature** | **Time** | **Number of cycles** |
|---|---|---|---|
| Activation | 95°C | 2 min | 1 |
| Denaturation | 95°C | 5 sec | 40 |
| Annealing | 60°C | 30 sec | |
| Melt curve | 65-95°C (+0.5°C per step) | 5 sec/step | 1 |

PCRs and gel electrophoresis

Polymerase chain reactions (PCR) were performed to amplify full genes as well as gene fragments using plasmids, purchased open reading frames (ORF) or genomic DNA as templates. Either KOD-Hot Start or OneTaq DNA polymerase kits were used in combination with respective primers in a thermal cycler.

To separate DNA fragments such as PCR products according to their size, gel electrophoresis was performed in agarose gels. For these gels, 1-2% agarose (m/v in 1xTAE) was melted in a microwave, mixed with the DNA dye Midori Green and poured in a gel tray. After gels had completely solidified, samples were mixed with loading buffer and were loaded together with a molecular weight ladder into the gel. Agarose gels were run between 80 and 120 V up to 1.5 hours. DNA fragments were visualized with a GelDocTM XR+.

Bacterial transformation and plasmid preparation

To introduce plasmids for multiplication into bacteria, an aliquot of the plasmid was mixed with 30 µl of freshly thawed competent cells in a 1.5 ml tube. This mix was incubated on ice for 30 minutes before performing a one-minute-long heat shock at 42°C. The bacteria were then placed for 10 minutes on ice and 100 µl lysogeny broth (LB) medium was added. The tube was moved into a 37°C preheated, 300 rpm shaking heat block for 1 hour. Afterwards, the bacteria were plated onto a LB plate with the appropriate antibiotics. Bacteria were allowed to grow overnight at 37°C. The next day, isolated colonies were picked and transferred to a bacterial culture tube containing 5 ml LB medium and appropriate antibiotics. Bacteria were incubated overnight at 37°C shaking at 200 rpm. For harvesting, pipette tips were removed and bacteria were centrifuged at 3500 g for 10 minutes. Subsequently, plasmids were purified using the QIAprep Spin Miniprep Kit according to the manufacturer's instructions and concentrations were measured with a Nanodrop$^{TM}$ 2000c at 260 nm. Finally, a portion of the extracted plasmid was sent for sequencing.

Gateway® cloning

The Gateway® cloning system was used to clone ORFs of the genes of interest into multiple vector systems. For this purpose, special Gateway primers were designed, which contain next to the template specific sequence attB sites (see chapter 2.1.5). The template specific primers were chosen by applying the cloning tool of Primer3Plus (https://www.bioinformatics.nl/cgi-bin/primer3plus/primer3plus.cgi). These Gateway® primers were used in a KOD Hot Start PCR to attach the attB sites to the ORF of the gene of interest. The PCR products were run on a 1% agarose gel containing Midori Green to check for correct product size. Subsequently, 1 µl of the PCR product was used for a BP reaction including 1 µl BP clonase II and 0.5 µl of pDONR223 to introduce the ORF of interest in the donor vector pDONR223. The reagents were mixed and incubated overnight at room temperature. The plasmids were then transformed into *E.coli* Top10 competent cells and then validated by sequencing. Correct pENTR223 vectors were then used to generate destination vectors containing the ORF. Therefore, LR reagents (1 µl pNTRY223, 0.5 µl destination vector, 1 µl LR clonase II and 2 µl $H_2O$) were mixed and incubated for 4 hours at room temperature. Again, plasmids were transformed in *E.coli* Top10 cells and validated by sequencing.

Small guide RNAs (gRNAs) design and cloning

For the generation of knockout or mutation cell lines, gRNAs were designed with the Broad Institute web gRNA designer (https://portals.broadinstitute.org/gppx/crispick/public) and ordered together with the complementary strand as oligonucleotides. Those gRNAs were cloned into the pLentiCRISPR-HF1 Puro vector or the pX330 vector, respectively. Therefore, complementary diluted gRNAs (10 µM) were heated for 5 minutes at 95°C and annealed for 10 minutes at room temperature. Then they were introduced into the digested backbone vector (Table 2-2) by a ten-minute long incubation with a T4 DNA ligase (Table 2-3). Vectors were then transformed into XL1-Blue competent cells for multiplication and checked for correct insertion by sequencing.

Table 2-2: Digestion conditions of backbone vectors.

| **Vector** | pLenti | pX330 |
|---|---|---|
| **Restriction enzyme** | BsmBI | BbsI |
| **Buffer** | 1x NEB Buffer 3.1 | 1x NEB Buffer 2.1 |
| **Incubation temperature** | 55°C | 37°C |
| **Incubation time** | 1 hour | 1 hour |

Table 2-3: Ligation reaction components.

| **Component** | **Amount [µl]** |
|---|---|
| Digested backbone vector | 1 |
| Annealed gRNA mix (0.5µl) | 1 |
| T4 ligase buffer (5x) | 2 |
| T4 ligase | 0.5 |
| $H_2O$ | 5.5 |

Cloning of homology arms

To generate homology-directed repair (HDR) templates, UBQLN2 homology arms were cloned into a pAAV SEPT DTA BSD 2A Tag vector by traditional cloning. For this purpose, homology arms were amplified from genomic HeLa DNA by PCR. Therefore, primers were used which simultaneously introduce restriction enzyme binding sites, if such were not already present. PCR products were separated on a 1% agarose gel and DNA was extracted from the correct PCR bands with the QIAquick Gel Extraction Kit according to the manufacturer's protocol. The homology arm inserts as well as the backbone vector were digested with the same restriction enzymes and then mixed for ligation as described for the insertion of gRNAs into a backbone vector. Sequencing was used to check for correct insertion.

Mutagenesis

Site-directed mutagenesis was used to introduce specific nucleotide substitutions. Therefore, primers were used, which were designed with the QuickChange Primer Design tool (https://www.agilent.com/store/primerDesignProgram.jsp) and harbored the mutation(s) of interest. Two subsequent KOD Hot Start PCR reactions were performed. Firstly, two short PCRs were conducted, separately for the forward and the reverse primer (Table 2-4). Then, the two products were mixed and a final PCR was run after addition of 0.7 µl fresh KOD Hot Start Polymerase (Table 2-5). Afterwards, a DpnI digest was used to eliminate the wild-type DNA, recognized by its methylation. For this purpose, 1 µl DpnI was added to the completed PCR reaction and incubated for 2 hours at 37°C. The mutated vectors were transformed into *E.coli* Top10 cells and sequencing was used to check for correct mutagenesis.

Table 2-4: PCR cycling conditions for the first part of the site-directed mutagenesis

| **Step** | **Temperature** | **Time** | **Number of cycles** |
|---|---|---|---|
| Activation | 95°C | 2 min | 8 cycles |
| Denaturation | 95°C | 20 sec | |
| Annealing | 60°C | 10 sec | |
| Extension | 70°C | 25 sec/kb | |
| Cool down | 10°C | infinite | |

Table 2-5: PCR cycling conditions for the second part of the site-directed mutagenesis

| **Step** | **Temperature** | **Time** | **Number of cycles** |
|---|---|---|---|
| Activation | 95°C | 2 min | |
| Denaturation | 95°C | 20 sec | 18 cycles |
| Annealing | 60°C | 10 sec | |
| Extension | 70°C | 25 sec/kb | |
| Cool down | 10°C | infinite | |

### 2.2.2 Cellular biology

Maintenance of immortal cell lines

293T and HeLa cell lines were maintained in Dulbecco's Modified Eagle's Medium (DMEM) GlutMax supplemented with 10% fetal bovine serum (FBS), 1% sodium pyruvate and antibiotics if needed. Lymphoblast cell lines (LCLs) were maintained using Roswell Park Memorial Institute (RPMI) 1640 supplemented with 20% or 10% FBS. All cells were cultured at 37°C with 5% $CO_2$ and were passaged after reaching 80-90% confluency. Adherent cells were detached with 0.25% trypsin/EDTA before passaging. For storage, cell pellets were suspended in FBS containing 10% DMSO, expect for LCLs which were suspended in RPMI 1640 medium containing 30% FBS and 5% DMSO. Cells were slowly frozen at -80°C using a freezing container filled with isopropyl alcohol.

Cultivation of primary rat neurons

Primary hippocampal and cortical rat neurons were cultured from embryonic day 19 Sprague-Dawley rats. They were plated on poly-D-lysine coated plastic dishes or cover slip containing plastic dishes that were treated beforehand with 65% nitric acid and sterilized at 200°C for 6 hours. Neurons were maintained in Neurobasal medium supplement with 2% B27, 1% Pen/Strep and 0.25% glutamine or 0.125% glutamate for cortical neurons and hippocampal neurons, respectively, at 37°C and 5% $CO_2$.

Generation of stable cell lines

Stable cell lines were generated either in the S1 laboratory or in the S2 laboratory via lentiviral transfection. For the latter, 293T cells were used for virus production. 293T cells were transfected with Lipofectamine 2000 together with plasmids for viral packaging (psPAX2), envelop proteins (pMD2.G) and either a pHAGE plasmid for overexpression cell lines or a pLentiCRISPR-HF1 vector for the generation of knockout cell lines. The two following days, virus containing medium was collected and filtered (0.45 µm). The filtered medium was complemented with 8 µg/ml polybrene and recipient cells were transduced through replacement of the culture medium with the virus containing medium. One day after transduction, the medium was replaced with virus-free medium and two days after transduction selection was started by adding selection medium. After three passages cells were moved to the S1 cell culture laboratory. Endogenous mutant cell lines were generated in the S1 cell culture laboratory by transfection. HeLa cells were transfected with Lipofectamine 2000 together with the vector containing the gRNA and the pAAV SEPT DTA BSD 2A Tag with the homology sites with either the wild-type sequence or the sequence with point mutations. After 5 h medium was changed to full growth medium.

Transient transfection of cells

Transient transfections were conducted to achieve transient overexpression of proteins or to transiently knockdown a protein of interest.

To introduce foreign DNA into HeLa cells, HeLa cells were seeded usually into a 6-well dish one day before transfection. For transfection of plasmid DNA Lipofectamin 2000 was used. In detail, 250 µl of OptiMEM were mixed with 10 µl of Lipofectamine 2000 and simultaneously the 0.5 µg plasmid DNA was added to the same amount of OptiMEM, followed by a merge of both mixtures. The final mixture was incubated for 20 minutes at room temperature and dropwise added to the cells. Cells were harvest 1 to 2 days after transfection.

To carry out a transient knockdown of a protein of interest, siRNAs were transfected using Lipofectamine RNAiMax. Also, for this experiment, cells were seeded usually into a 6-well dish one day before transfection but were harvested 72 hours post-transfection. Before transfection, 500 µl OptiMEM were mixed with 5 µl Lipofectamine RNAiMax and 4.5 µl siRNA (20 µM stock) and incubated for 20 minutes. The mixture was drop-wise added to the cells and medium was replaced with full growth medium 24 hours after transfection.

Treatments

Some experiments required different treatments to trigger or impair specific cellular pathways. In general, treatments were performed when cells reached a confluency of 80-90%. Autophagy

was inhibited with bafilomycin A1, which targets the v-ATPase proton pump, at a concentration of 200 nM for 2 hours. Proteasomal degradation was inhibited by treatment of the cell with a 1 µM bortezomib for 8 hours.

Virus production and transduction of primary rat neurons

Lentiviruses with high titer for transduction of primary rat neurons were generated by transfecting three 10 cm dishes 293T with constructs for lentivirus generation and packaging: the envelope protein VSV-G plasmid, the packaging plasmid psPAX2 containing Gag-Pol-Rev for virus formation and the lentiviral transfer plasmid encoding the insert of interest (Table 2-6).

Table 2-6: Components of the transfection mix used to induce lentivirus production.

| **Component** | **Amount** |
|---|---|
| LTR vector | 18.6 µg |
| psPAX2 | 11.0 µg |
| pVSV-G | 6.4 µg |
| OptiMEM | 4.5 ml |
| Combined with: | |
| Lipofecamine 2000 | 108 µl |
| OpiMEM | 4.5 |

Components were mixed and incubated for 20 minutes prior to addition of 3 ml transfection mix per 10 cm dish of 293T cells in OptiMEM supplemented with 10% FBS. After 24 hours medium was exchanged to DMEM GlutMax (Gibco$^{TM}$) supplemented with 10% FBS,1% NEAA and 1.3% bovine serum albumin (BSA). 48 hours after transfection the medium was collected, filtered through a 0.45 µl membrane and centrifuged at 66,000 g for 2 hours at 4°C. The virus-containing pellet was resuspended in 120 µl Neurobasal medium, aliquoted and stored at -80°C.

For transduction 2 µl of this virus preparation was added to a 6-well dish of rat primary neurons three days after their preparation. Five days after transduction, primary neurons were either fixed in PFA for immunofluorescence or harvested in 3x loading buffer for immunoblotting.

Stable isotope labeling by/with amino acids in cell culture (SILAC) for phosphoproteomics

For the phosphoproteomic experiment, LCLs from healthy donors were SILAC labeled. For this purpose, LCLs were passaged for at least 5 times in heavy (R10/K8) RPMI medium containing beside 10% dialyzed FBS also isotopically labeled analogs of the amino acids lysine (L-lysine; K8) and arginine (L-arginine; R10). Successful incorporation of labeled amino acids was assessed by mass spectrometry. The other cell population, more specifically LCLs from patients harboring UBQLN2 mutations, were labeled with light lysine and arginine residues (K0

and R0). Cells were counted, mixed on a 1:1 ratio and phosphoproteomics were performed in collaboration with Jörn Dengjels group (Department of Biology, University of Fribourg, Switzerland).

### 2.2.3 Biochemistry

Cell lysis

Cells were harvested by centrifugation and then washed with PBS. Depended on the cell amount, an appropriate volume of lysis buffer was used to resuspend the cells. RIPA, MCLB, or urea lysis buffer was used as lysis buffer, contingent on the subsequent experiment. Lysis was allowed to proceed for 40-45 minutes on ice. Then cell debris was removed by centrifugation at 20,000 g at 4°C for 5 minutes. The protein concentration of the supernatant was estimated by using a bicinchoninic acid (BCA) protein assay kit in combination with a BSA standard curve following manufacturer's instructions. In general, for western blotting protein concentration was adjusted to a final concentration of 2 µg/µl by addition of lysis and Laemmli buffer. The samples were then denatured by boiling them for 5 minutes at 95°C. Protein samples which were also used to blot for MAP1B were directly boiled in sample buffer after cell number adjustment.

SDS-Page and Immunoblotting

Proteins were separated on SDS-PAGE gels with a percentage suitable for the protein size. Therefore, 6%, 8%, 10%, 12%, or 15% polyacrylamide gels were self-casted using the Biorad Mini-PROTEAN Tetra Cell Casting Stand & Clamps (Table 2-7). Alternatively, precast 4–15% Mini-PROTEAN® TGX™ were used. Normally, 20 µg of protein were loaded together with protein marker VI or ProSieve QuadColor and separated for 1 hour at 100 V in a Mini-PROTEAN Tetra cell. Afterwards, the proteins were transferred to either a nitrocellulose or a polyvinylidene difluoride (PVDF) membrane for 135 minutes at 0.3 mA in Mini Trans-Blot® chamber. Successful protein transfer was verified by a Ponceau S staining. Then, membranes were blocked for 1 hour at room temperature with either 5% milk, 5% BSA or I-Block™ solved in Tris-buffered saline (TBS)-Tween-20 (TBST). The primary antibody was incubated overnight at 4°C. The next day it was washed 3 times with TBST, followed by a 1-hour incubation with the secondary antibody (1:1000) at room temperature. Finally, washed membranes were covered with Western Lightening Plus ECL solution and developed on X-ray films in a dark room. Primary as well as secondary antibodies and used concentrations are listed in 2.1.1.6. Quantification of immunoblot bands of at least 3 independent biological experiments were performed in ImageJ.

Table 2-7: Self-casted gels

| **Component** | **Resolving gel** | **Stacking gel** |
|---|---|---|
| Acrylamide | 6-15% | 4-6% |
| Tris-HCl [pH 6.8] | 375 mM [pH 8.8] | 125 mM [pH 6.8] |
| SDS | 0.1% (m/v) | 0.1% (m/v) |
| APS | 0.1% (m/v) | 0.1% (m/v) |
| TEMED | 0.01% (m/v) | 0.01% (m/v) |

Phos-tag™ assay

For detection of changes in phosphorylation phosphate-affinity electrophoresis technique was performed by using SuperSep™ Phos-tag™ precast gels according to the manufacturer's protocol. Cell pellets were lysed in urea lysis buffer and by performing 3 short sonification steps. Samples were centrifuged at 2500 g, 4°C for 10 minutes and after a BCA assay, protein concentrations were adapted. TCA precipitation was performed by adding TCA to final volume of 20% to remove possible impurities. After an incubation of half an hour on ice, samples were centrifuged at maximal speed at 4°C for 30 minutes. Afterwards, samples were washed 3 times with ice-cold acetone. Finally, the samples were solved in 3x Laemmli buffer with β-mercaptoethanol and loaded on gels for electrophoresis. Afterwards, gels were washed 3 times in transfer buffer containing 10 mM EDTA and were then immersed in transfer buffer without EDTA. Gels were transferred onto a PVDF membrane and further steps (blocking and antibody incubation) were performed as for conventional immunoblots.

Immunofluorescence

HeLa cells were seeded onto uncoated coverslips while LCLs and rat neurons were seeded on poly-L-lysine coated coverslips. They were fixed with cold 4% PFA or methanol for 10 minutes at room temperature as soon as they reached 70-90% confluency. After removing the fixation solution by washing 3 times with PBS, cells were permeabilized with 0.5% Triton-X 100 for 10 minutes at room temperature. Cells were then washed again and blocked for 1 hour with 1% BSA in PBS. Primary and secondary antibodies were incubated for 1 hour in 0.1% BSA at room temperature. For acetylated-tubulin staining of HeLa cells, the antibody was solved in 1%BSA, 10% goat serum and 0.2% Trition-X and primary antibody staining was performed overnight at 4°C. Finally, the coverslips were mounted with ProLong Gold Antifade Mountant with DAPI. Images were acquired with a Zeiss LSM 800 confocal microscope. Mean fluorescence intensity measurement of orthogonal projections (maximum intensity projection) was performed with ImageJ.

Incorporation check

To assess successful incorporation of heavy amino acids in proteins of treated cells, cells were harvested from one 6-well dish and lysed in denaturation buffer supplemented with 0.5 µl Benzonase® nuclease. After 15 minutes incubation at 25°C, lysates were centrifuged at 16,000g for 10 minutes and 20 µl supernatant was transferred to a fresh tube. 80 µl 20mM ABC and 0.4 µl to start the tryptic digest. The next day, 10 µl TFA were added to stop the digest and samples were desalted by stage tipping.

HA-Immunoprecipitation (IP)

For HA-IPs destined for mass spectrometry (MS) analysis, 4x15 cm cell culture plates were harvested and collected by centrifugation. Washed pellets were lysed by addition of 3 ml MCLB lysis buffer, a subsequent incubation of 30 minutes on ice and centrifugation at maximum speed for 10 minutes at 4°C. Lysates were cleared by filtration through a 0.45 µm spin filter and concentrations were adapted after performing a BCA assay. Anti-HA beads were pre-equilibrated and combined with the cleared lysates. After an overnight incubation with rotation at 4°C, beads were washed 5x with MCLB and 5x with PBS. Proteins were eluted by addition of 50 µl HA-peptide in PBS (250 µg/ml) and a subsequent centrifugation step. This elution step was performed 3 times and the supernatants were pooled. TCA was added to a final concentration of 20%, vortex and incubated for 30 minutes on ice to remove contaminants. After centrifugation at maximum speed, the supernatants were aspirated and samples were washed 3 times with ice cold acetone. For the in-solution tryptic digest, tried samples were resuspended in 30 µl 50 mM ABC/10% ACN [pH 8] with 0.5 µl trypsin. After an incubation for 4 hours at 37°C, the digest was stopped with 30 µl 5% formic acid/5% ACN. Samples were dried by vacuum condensation, resuspended in Buffer C and desalted by stage tipping.

Desalting by stage tipping

Stage tips were assembled by embedding two C18 disks in a 200 µl pipette tip. Stage tips were activated with methanol, equilibrated with buffer B and washed two times with buffer A without trying out before sample loading. Then the C18 material was washed with buffer A, followed by the peptide elution using buffer B. Eluted peptides were collected in a fresh tube and buffer B was evaporated in a vacuum condensator. Dried peptides were resuspended in 10 µl buffer A before analysis on the MS.

Whole proteome analysis

Cell pellets were resuspended in Urea lysis buffer, sonicated and cleared by centrifugation at 2,500 g. A BCA assay was performed and protein amounts were adapted. For protein reduction, DTT was added to a final concentration of 5 mM and incubated for 25 minutes at

56°C. Protein alkylation was performed by adding IAA to a final concentration of 14 mM followed by an incubation of 30 minutes in the dark. This reaction was quenched with DTT (5 mM final). To reduce the urea concentration, samples were diluted 1:5 with 1 M Tris [pH 8.2]. Protein digestion was started using 2 µg Lys-C per 100 µg protein. After 3 hours at room temperature, $CaCl_2$ was added (1 mM final) together with trypsin (0.5 µg/100 µg protein)). After an overnight incubation at 37°C, the tryptic digest was stopped by adding 1/10 volume 10% TFA. Peptide samples were pre-fractioned by custom made C18-SCX stage tips according to Rappsilber et al. (2007) [264]. Pre-fractioning stage tips were pre-conditioned with methanol, ReX-Buffer 2, ReX-Buffer 1, ReX-Buffer 6 and again ReX-Buffer 1. Then, peptide samples were loaded onto the pre-fractioning stage tips and once washed with ReX-Buffer 1. ReX-Buffer 2 was used to elute peptides from the C18 disks and allow the transfer to the SCX disks. To obtain four separate fractions, peptides were eluted sequentially by using 20 µl ReX-Buffer 3, 4, 5 and 6. Eluates were collected separately and mixed with 60 µl ReX-Buffer 1. The mixed fractions were desalted on custom-made C18 stage tips before MS analysis.

Recombinant protein expression and electrophoretic mobility shift assay (EMSA)

For expression and purification of recombinant FUS protein variants (WT, S439A and S439E), bacterial expression vectors were introduced into E. coli BL21-DE3-Rosetta LysS and expanded in LB medium. At an optical density (OD) of approximately 0.8, isopropyl-beta-D-thiogalactopyranoside (IPTG) was induced for 22 h. Lysed cells were purified using Ni-NTA Agarose (QIAGEN) and amylose resin (NEB) and washed. Concentrations were measured and 0-10 µM recombinant protein were mixed with 5 nM of a Cy5-labelled SON transcript containing both the stem loop and a downstream GUU (GGAUCUUUAACUACUCAAGAUACUGAACAUGACAUGGUA). After allowing binding for 20 min at room temperature, samples (20 µl) were loaded onto a non-denaturating polyacrylamide gel (6%) in 0.5 x TBE. Gels were rim at 100 V for 40 min at room temperature and imaged with a Bio-Rad ChemiDoc MP Imaging system. Protein purification and EMSA experiments were performed in collaboration with Dorothee Dormann (Institute for Molecular Physiology, Johannes Gutenberg-University Mainz, Germany).

# 3 Results

The purpose of this work was to further elucidate the role of ALS/FTD-associated UBQLN2 mutations using an unbiased multi omics approach. Parts of the results presented hereinafter are based on a previously published article in Life Science Alliance by Strohm et al. (2022) [265].

## 3.1 Patient-derived LCLs and CRISPR/Cas9 engineered HeLa cell lines

Pursuing to further characterize the role of UBQLN2 in the disease context of ALS/FTD, we firstly focused on two cellular models. On the one hand, immortalized lymphoblastoid cell lines (LCLs) from patients with a familial history of ALS were used. Those harbored either the T487I mutation, preceding the PXX region, or the P497S mutation, located in the PXX region of UBQLN2. On the other hand, to complement this cell model, we generated HeLa cells carrying either one of those mutations by CRISPR/Cas9-mediated homology-directed repair (HDR). Since this process is decisive for the valuation of the engineered cell lines, it is shortly described and illustrated below (Figure 3-1). To prepare the donor plasmid template, we isolated two regions flanking the cut site, the left and right homology arm, by PCR amplification from genomic HeLa DNA and cloned them into the vector backbone with a Neomycin (Neo) cassette. Subsequently, a site-directed mutagenesis was performed to introduce the T487I or the P497S mutation in the left homology arm that contains the PXX region.

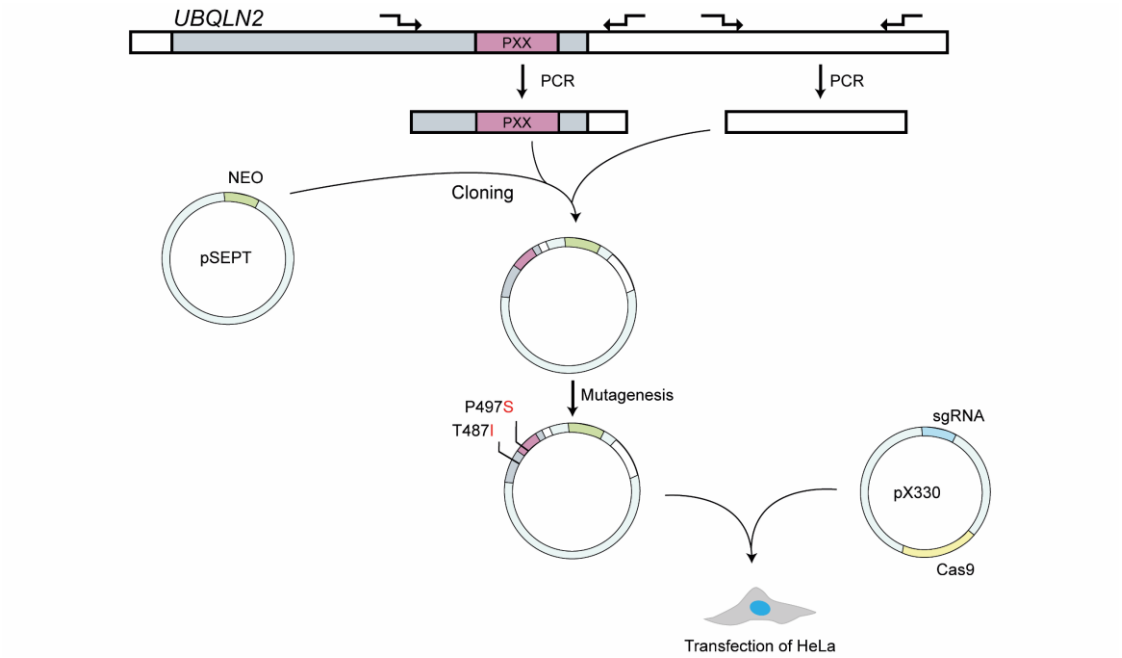


**Figure 3-1: Workflow of introducing UBQLN2 mutations in HeLa cells using CRISPR/Cas9.**
PCR-amplified UBQLN2 from HeLa cells was mutated and cloned into the pSEPT vector backbone to serve as a homology-directed repair (HDR) template. The HDR template was transfected together with a vector co-expressing Cas9 and a gRNA targeting UBQLN2.

After simultaneous transfection with an UBQLN2-specific gRNA and Cas9 expressing vector, we checked Neo-selected, single cell clones for insertion of the Neo-cassette by PCR followed by gel electrophoresis (Figure 3-2A). In addition to the Neo-cassette containing PCR fragments, also a wild-type (WT) UBQLN2 (lower bands) was present, pointing to the heterozygous character of the generated cell lines. DNA was extracted from the lower (WT) and higher bands containing the Neo-cassette and sequence verified for correct introduction of the mutations (Figure 3-2B).

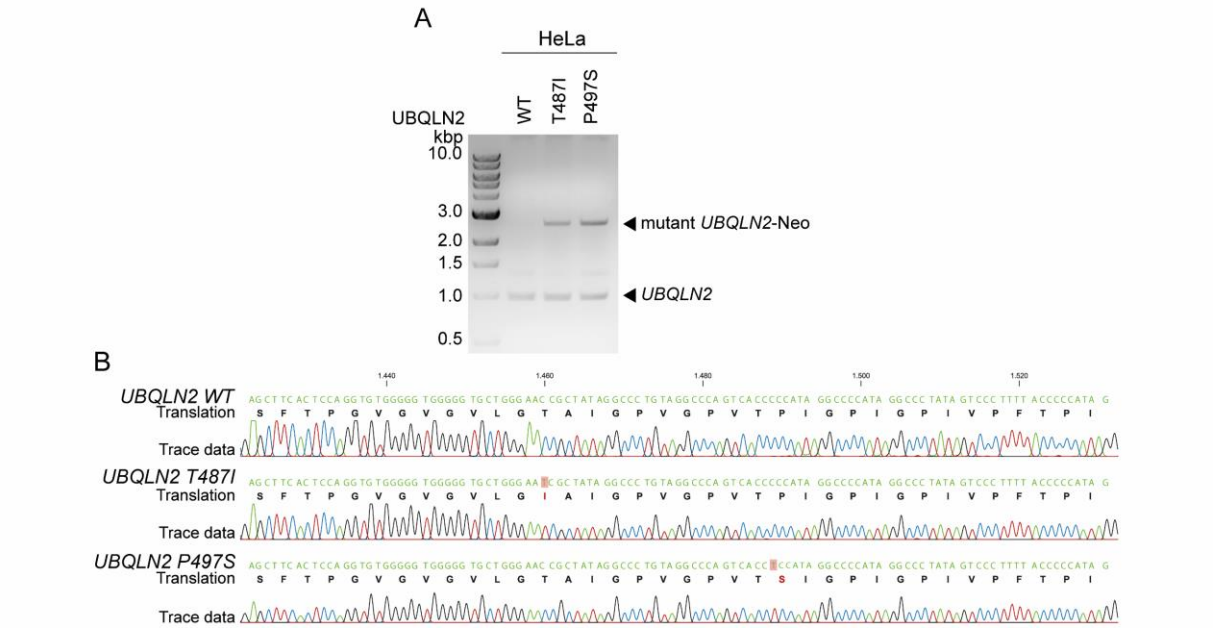


**Figure 3-2: Validation of CRISPR/Cas9 engineered HeLa cells.**
**(A)** Electrophoretic gel preceded by a UBQLN2-specific PCR demonstrating the successful introduction of the Neomycin (Neo) cassette and thereby UBQLN2 mutations. **(B)** Sequencing results of WT and mutated UBQLN2 HeLa cell lines obtained by Sanger sequencing.

Cells are susceptible to changes in UBQLN2 protein levels [165]. Therefore, UBQLN2 protein levels were evaluated by immunoblotting, to confirm that they remained unchanged in UBQLN2 mutant LCL and CRISPR/Cas9 engineered HeLa cells (Figure 3-3).

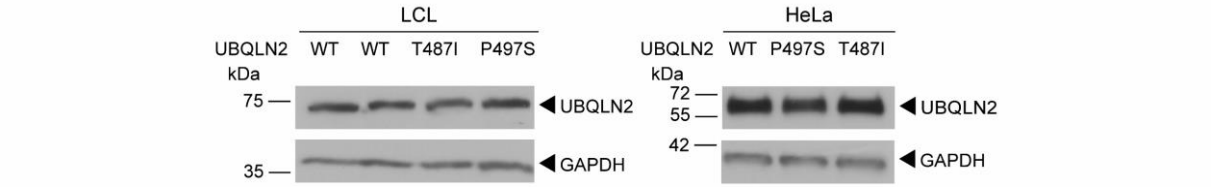


**Figure 3-3: Unchanged UBQLN2 protein levels in patient-derived LCL and CRISPR/Cas9 engineered HeLa cells.**
Protein lysates from LCL and HeLa cells were separated by SDS-PAGE and immunoblotted against UBQLN2 and GAPDH.

After checking for correct introduction of the UBQLN2 ALS/FTD-associated mutations in HeLa cells and the verification of unchanged UBQLN2 protein levels in mutant LCLs and generated HeLa cells, the cellular tools were ready for our multi-omics screening.

## 3.2 Whole proteome analyses of ALS/FTD-linked UBQLN2 mutant lines show alterations in ALS/FTD-associated pathways

Global, label-free quantification-based proteomics of engineered HeLa and patient-derived LCLs were performed to gain broad-scale insights into changes at the protein level in ALS/FTD-associated UBQLN2 mutant variants. For this purpose, digested protein lysates were subjected to a pre-fractionation using cation exchange (SCX) stop-and-go-extraction tip (stage tip) before liquid chromatography with tandem mass spectrometry (LC-MS/MS) analysis (Figure 3-4).

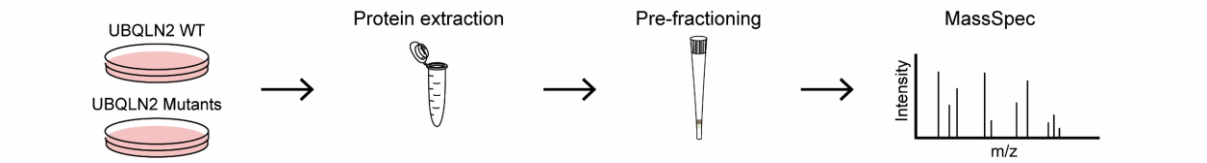


**Figure 3-4: Schematic representation of the global, label-free quantification-based proteomic workflow.**
UBQLN2 WT and mutant cell lines were expanded, protein extracted, digested and then pre-fractioned using a C18-strong cation exchange (SCX) StageTip prior to LC-MS/MS analysis.

More than 4000 proteins were quantified with this approach (Table 3-1). To filter for most prominently changed proteins, a cutoff of a $\log_2$ fold change ($\text{Log}_2\text{FC}$) of ≥ 1 or ≤ -1 and an FDR-corrected p-value (q-value) of ≤ 0.05 was applied. With these threshold parameters on average 123 and 181 proteins significantly increased and decreased in their abundance in UBQLN2 mutant compared to UBQLN2 WT cells, respectively.

**Table 3-1: Total and significantly altered ($\text{Log}_2\text{FC}$ ≥ 1 or ≤ -1 and q-value ≤ 0.05, t-test) proteins in patient-derived LCL and engineered HeLa cells.**

| | | Total | Down | Up |
|---|---|---|---|---|
| LCL | T487I | 4034 | 136 | 96 |
| | P497S | | 146 | 102 |
| HeLa | T487I | 4142 | 318 | 158 |
| | P497S | | 126 | 134 |

In a first analysis, we examined candidate proteins with significant changes for their disease involvement (Figure 3-5). However, none of the candidates that were associated with ALS/FTD was altered in a similar manner across the two different mutants or the two different cell types compared to their respective WT counterpart. Nevertheless, a few ALS/FTD-linked candidates were indeed found in individual cell lines. For example, GRN was significantly decreased in UBQLN2 T487I but increased in P497S mutant LCLs. SOD1 was significantly decreased in P497S mutant LCLs, but not significantly changed in any other mutant line. The same applies for SQSTM1, which was only significantly elevated in UBQLN2 T487I HeLa cells. Thus,

mutations in UBQLN2 did not consistently affect the abundance of proteins genetically linked to ALS/FTD.

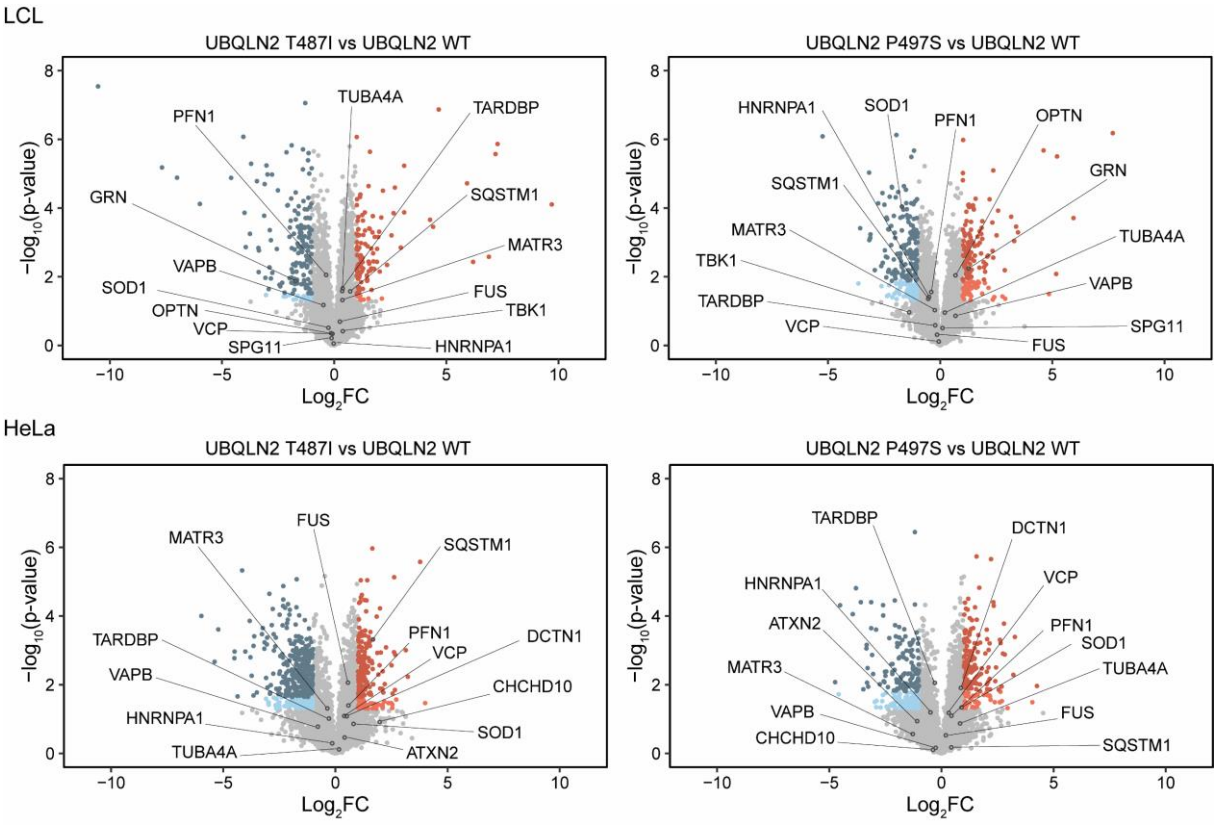


**Figure 3-5: Quantitative proteomic analyses of UBQLN2 mutant patient-derived LCL and engineered HeLa cells.**
Volcano plots showing increased and decreased proteins as $\log_2$ fold change ($Log_2FC$) versus the $-\log_{10}$ of the p-value. Proteins reaching a $Log_2FC \geq 1$ or $\leq -1$ and p-value $\leq 0.05$ are highlighted in light red and blue, respectively. Those with a q-value $\leq 0.05$ are highlighted in a darker shade. Detected ALS/FTD-linked proteins are labelled.

To assess alterations that are mutual within cell types or mutants, we performed an overlap analysis (Figure 3-6). On the proteomic level, most common changes were observed between UBQLN2 mutants in HeLa cells, while only a few proteins were commonly altered between UBQLN2 mutants in LCLs or in HeLa cells and LCLs carrying the same UBQLN2 mutation. The lower number of enriched or reduced proteins shared between the two LCL UBQLN2 mutants were likely due to the fact that they originate from patients of different ethnicity, sex and age. In contrast, UBQLN2 mutants in HeLa cells were engineered from an identical genetic background. No protein was commonly decreased across all mutants and cell types. However, one protein was significantly elevated across all conditions.

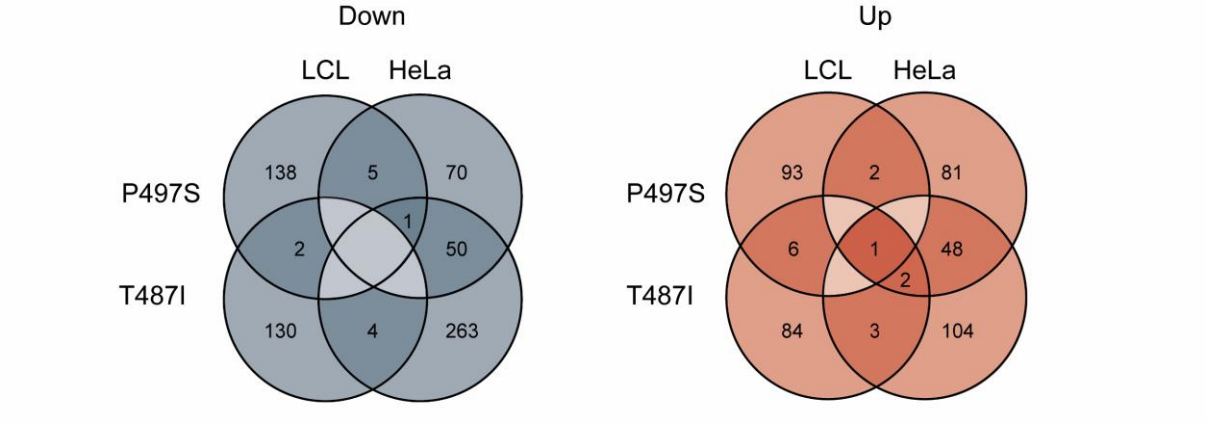


**Figure 3-6: Overlap analyses of enriched or decreased proteins across cell types and mutation types.**
Overlap of proteins between LCLs and HeLa cells, as well as P497S and T487I UBQLN2 mutants, which were significantly decreased or increased ($Log_2FC \geq 1$ or $\leq -1$ and q-value $\leq 0.05$).

Since the number of proteins significantly altered in the same direction was limited, we performed in a next step an unbiased gene ontology (GO) analysis of significantly altered proteins. This analysis allows the identification of biological processes, cellular location and molecular functions mutually impacted across cell types and mutants. The assessment revealed the overrepresentation of several GO terms for each individual data set. To focus on GO terms appearing in more than one data set, GO terms were filtered for emergence in at least two of the four data sets with an FDR ≤ 0.05. Upon this filtering step, besides a number of ALS/FTD-linked terms such as ‘mitochondrion’ and ‘poly(A) RNA binding’, also terms with no or only preliminary association with ALS/FTD such as ‘extracellular exosome’ or ‘cell-cell adherens junctions’ were enriched (Figure 3-7).

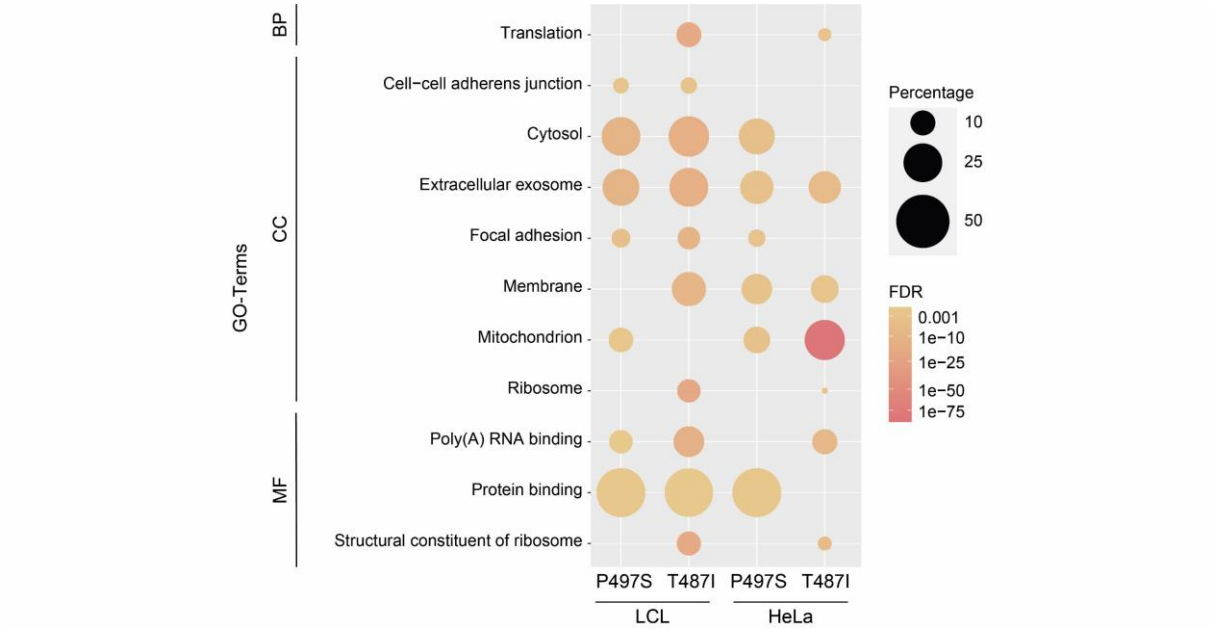


**Figure 3-7: Gene Ontology (GO) enrichment analysis of significantly altered proteins in mutated LCL and engineered HeLa cells.**
False-discovery rate (FDR)-corrected p-values are used as significance levels and represented in the color gradient. The percentage of proteins of the input list associated with the GO term are represented through circle size. BP, biological process; CC, cellular component; MF, molecular function.

## 3.3 The levels of multiple mRNA are affected by ALS/FTD-linked UBQLN2 mutations but only few are commonly regulated

Concomitantly to the proteomic analyses, we applied a transcriptomic approach to dissect alterations at the mRNA level in response to UBQLN2 mutations. In short, RNA was extracted, and RNA sequencing was performed in collaboration with Elisabeth Graf (Helmholtz Zentrum München, Munich, Germany) (Figure 3-8).

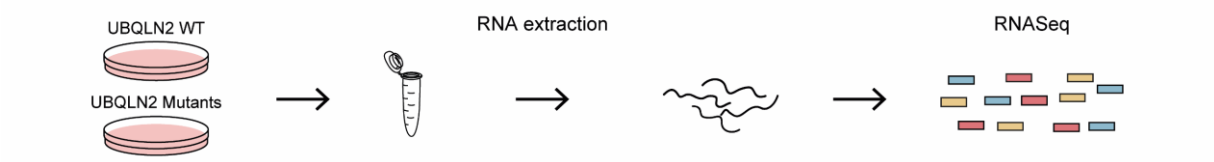


**Figure 3-8: Schematic representation of the transcriptomic workflow.**
UBQLN2 WT and mutant cells were expanded, harvested, RNA extracted and then send for RNA Sequencing (RNASeq).

On the transcriptomic level, more than 20,000 transcripts were detected (Table 3-2). This almost 5-fold higher detection level compared to the proteomic approach was accompanied by a larger number of significantly altered candidates when the same cutoffs, a $Log_2FC$ of ≥ 1 or ≤ -1 and an FDR adjusted p-value (q-value) of 0.05, were applied.

**Table 3-2: Total detected and significantly altered ($Log_2FC \geq 1$ or $\leq -1$ and q-value $\leq 0.05$, t-test) mRNA transcripts in patient-derived LCL and engineered HeLa cells.**

| | | Total | Down | Up |
|---|---|---|---|---|
| LCL | T487I | 22844 | 2020 | 1204 |
| | P497S | 22920 | 1438 | 1756 |
| HeLa | T487I | 20421 | 1300 | 1643 |
| | P497S | 20635 | 574 | 1266 |

As for the proteomic data set, the transcriptomic data set was inspected regarding altered mRNA levels of known ALS/FTD-associated genes (Figure 3-9). The majority of ALS/FTD-associated genes was not significantly affected, with a few exceptions. Of those, the receptor tyrosine-protein kinase erbB-4 (ERBB4) stands out as its mRNA levels were up-regulated in three of the four RNASeq data sets. Interestingly, while SQSTM1 protein levels were elevated in HeLa T487I UBQLN2 mutants, mRNA levels were significantly decreased in both HeLa mutants. Although a few ALS/FTD-associated genes were altered at the mRNA level, none of those were significantly regulated in all UBQLN2 mutants.

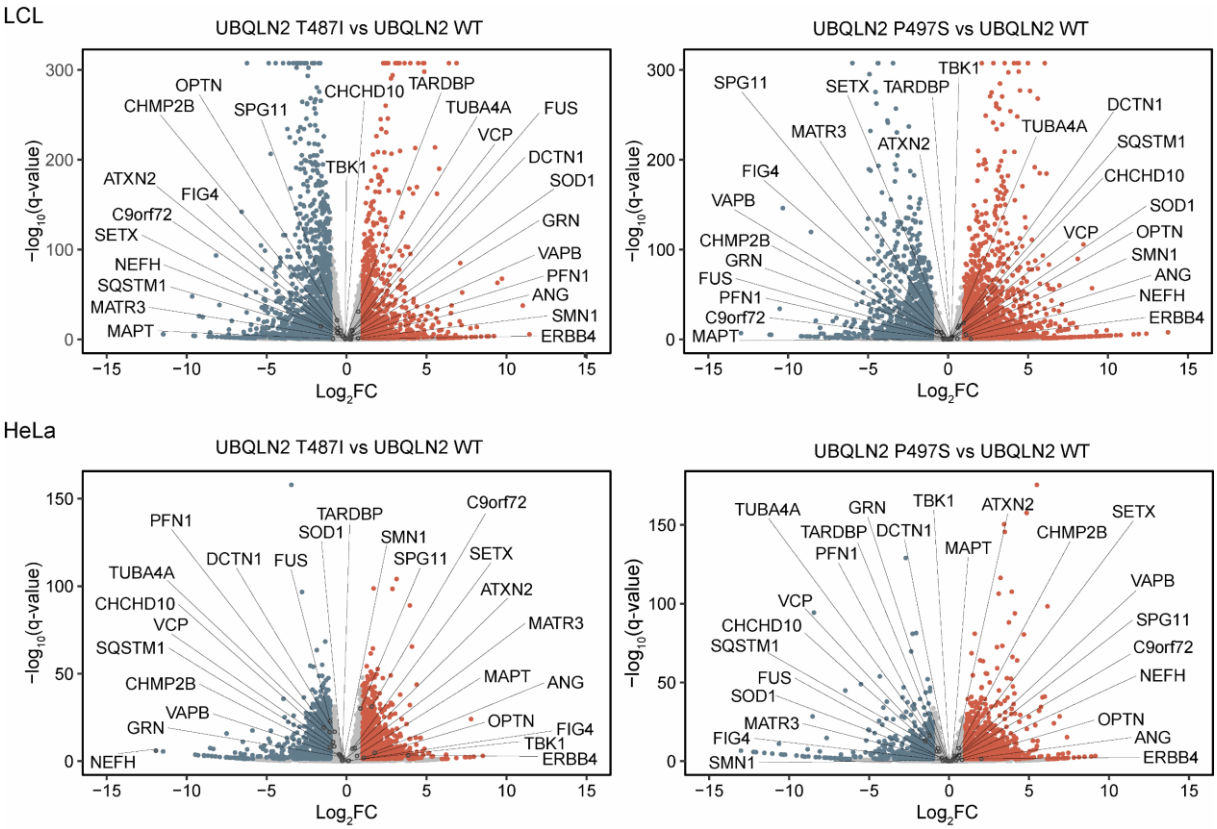


**Figure 3-9: Quantitative transcriptomic analyses of UBQLN2 mutant patient-derived LCL and engineered HeLa cells.**
Volcano plots showing up- and down-regulated transcripts as $log_2$ fold change ($Log_2FC$) versus the $-log_{10}$ of the FDR-corrected p-value (q-value). Transcripts reaching a $Log_2FC \geq 1$ or $\leq -1$ and a q-value $\leq 0.05$ are highlighted in red and blue, respectively. Detected ALS/FTD-linked genes are labelled.

Compared to the proteomics, on an absolute level, more mRNA transcripts were regulated in the same direction in the transcriptomic data set (Figure 3-10). While on a proteomic level, the overlap between the two LCL UBQLN2 mutant lines was considerably smaller than that of the HeLa UBQLN2 mutants, this divergency was not observed at the transcriptomic level. Similar to the proteomics, more candidate mRNAs were commonly affected within two mutants of one cell type than within the same mutation in the two different cell types.

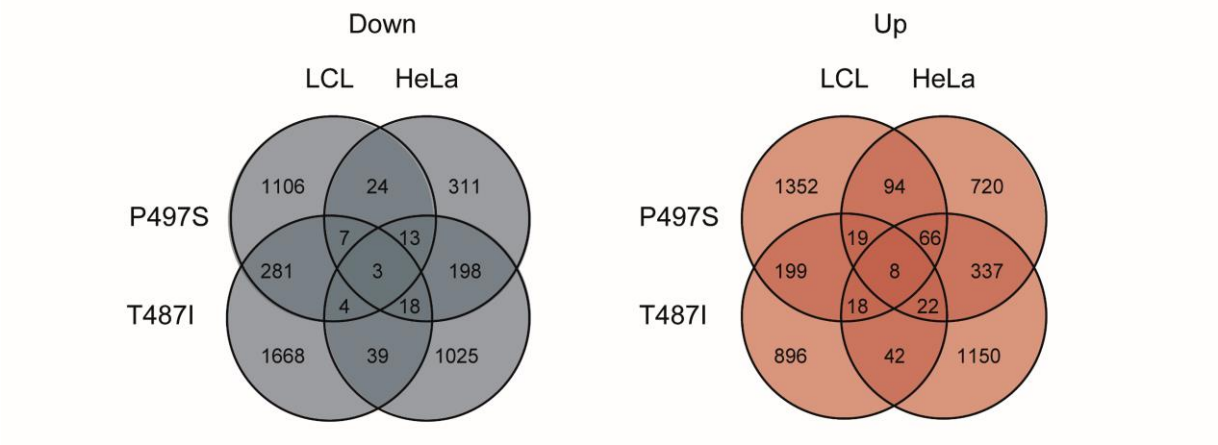


**Figure 3-10: Overlap analyses of enriched and decreased transcripts across cell types and mutation types.**
Overlap of transcripts between LCL and HeLa, as well as P497S and T487I UBQLN2 mutants, which were significantly decreased or increased ($Log_2FC \geq 1$ or $\leq -1$ and q-value $\leq 0.05$).

The majority of terms revealed by GO term analysis of all significantly up- and down-regulated transcripts were known to be affected by ALS/FTD. Amongst others, an overrepresentation of Golgi-associated, mitochondrial-associated as well as transcription- and translation-related terms was observed (Figure 3-11).

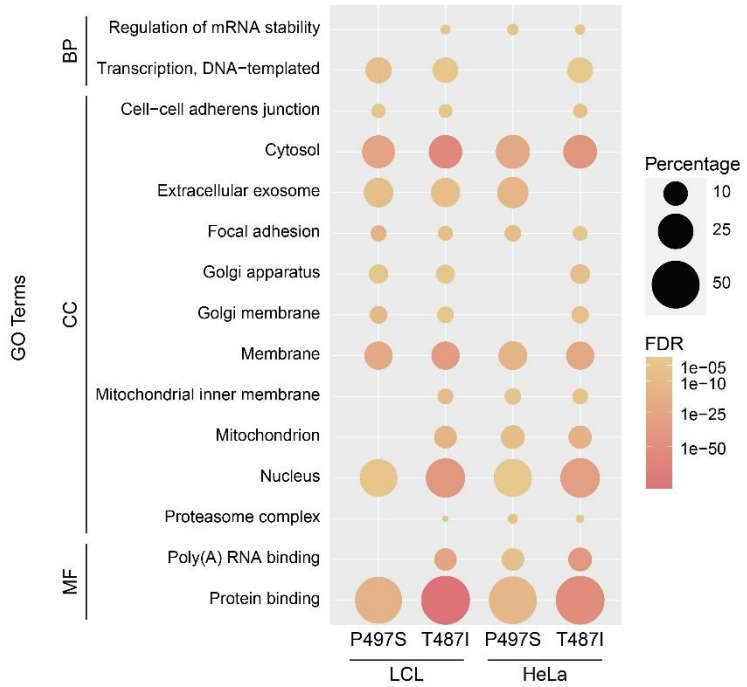


**Figure 3-11: Gene Ontology (GO) enrichment analysis of significantly altered transcripts in mutated LCL and engineered HeLa cells.**
False-discovery rate (FDR)-corrected p-values are used as significance levels and represented in the color gradient. The percentage of proteins of the input list associated with the GO term are represented through circle size. BP, biological process; CC, cellular component; MF, molecular function.

## 3.4 Comparison of proteomic and transcriptomic data sets reveal commonalities but also independent effects

In addition to the separate analysis of the proteomic and transcriptomic data sets, we examined the interrelation of both types of data sets. Thereto, a correlation analysis across candidates that were significantly altered in at least one data set was conducted, revealing a positive correlation (Pearson's correlation coefficient ≥ 0.2 and p-value ≤ 0.05) between both HeLa mutants at the transcriptomic and proteomic level (Figure 3-12). However, no positive correlation was detected between transcriptomics and proteomics within specific HeLa mutants. Contrariwise, transcriptomics of each LCL UBQLN2 mutant positively correlated with the respective proteomics but no positive correlation was present between the LCL mutants.

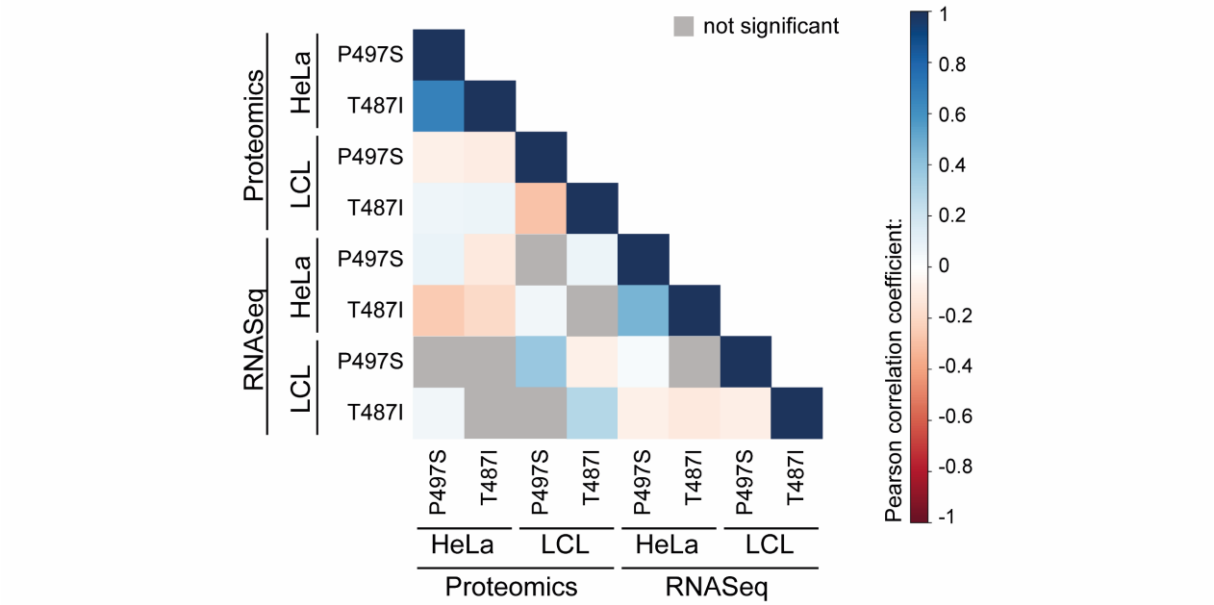


**Figure 3-12: Correlation plot based on hits significantly changed in at least one data set.**
Colors indicate Pearson's correlation coefficient. Blue corresponds to significant positive, red to significant negative correlation (p-values ≤ 0.05; Student's t-test). Non-significant cells are shown in grey.

To address to what extent the observed protein changes can be ascribed to changed mRNA levels, we compared significantly altered candidates of the proteomic and transcriptomic data sets (Figure 3-13). Up to 17.8% of proteins with decreased abundance can at least partially be explained by changes in their transcription while this fraction reached up to 29.4% for proteins whose levels increased. Given these relatively low percentages, the majority of protein abundance changes in the ALS/FTD-associated UBQLN2 mutations seemed likely to be a result of impaired protein translation or degradation.

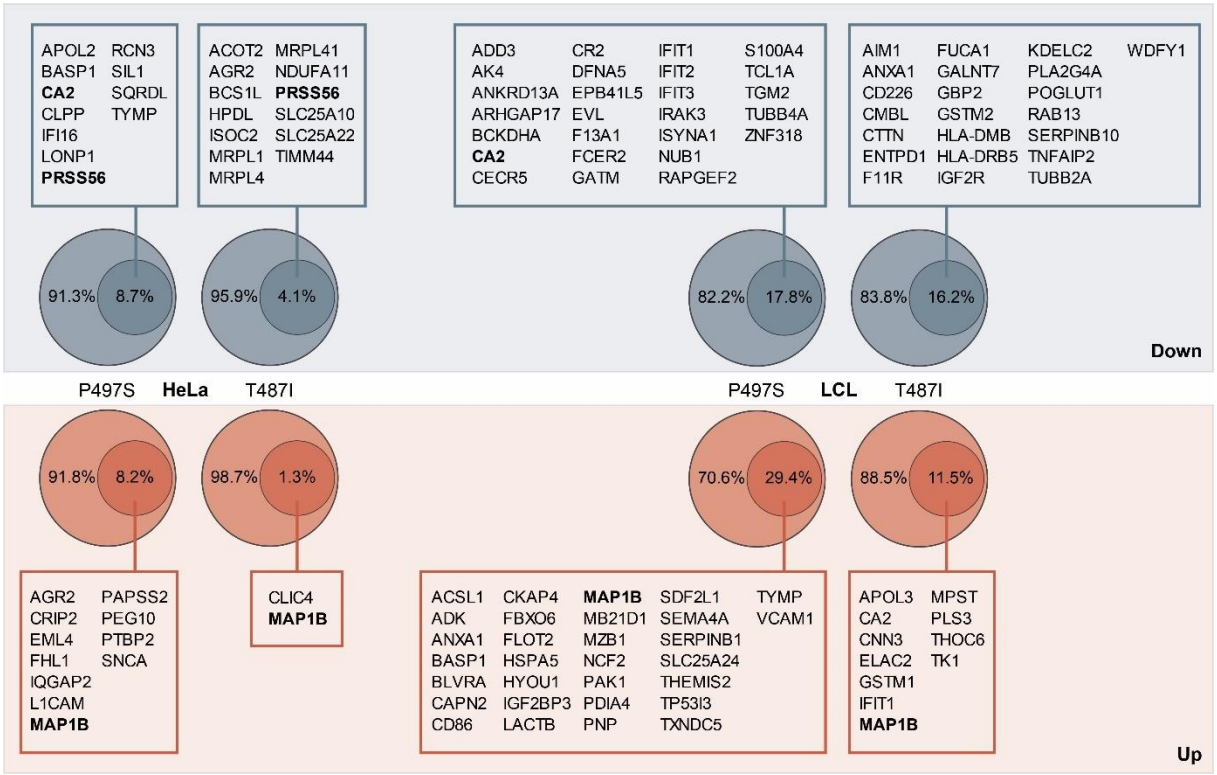


**Figure 3-13: Altered protein levels caused by changes in transcription.**
Inner circles represent altered proteins which are regulated in the same direction on the proteomic level as on the transcriptomic level, while outer circle present significantly altered proteins not mutually regulated as on the transcriptomic level.

## 3.5 Integrated transcriptomic and proteomic analyses of ALS/FTD-linked mutations identify MAP1B as a novel player in ALS/FTD

After examining the correlation and intersection of the proteomic and trancriptomic data sets, in the next step, we insepected the top differentially expressed candidates of both profiling approaches. By focusing only on candidates which were significantly altered in the same direction in at least four of eight data sets one candidate clearly stood out: the microtubule-associated protein 1B (MAP1B). Of the top 18 differentially candidates, MAP1B was the only candidate that significantly changed in the same direction on the transcriptomic and proteomic level in both UBQLN2 mutants in HeLa cells and LCLs (Figure 3-14).

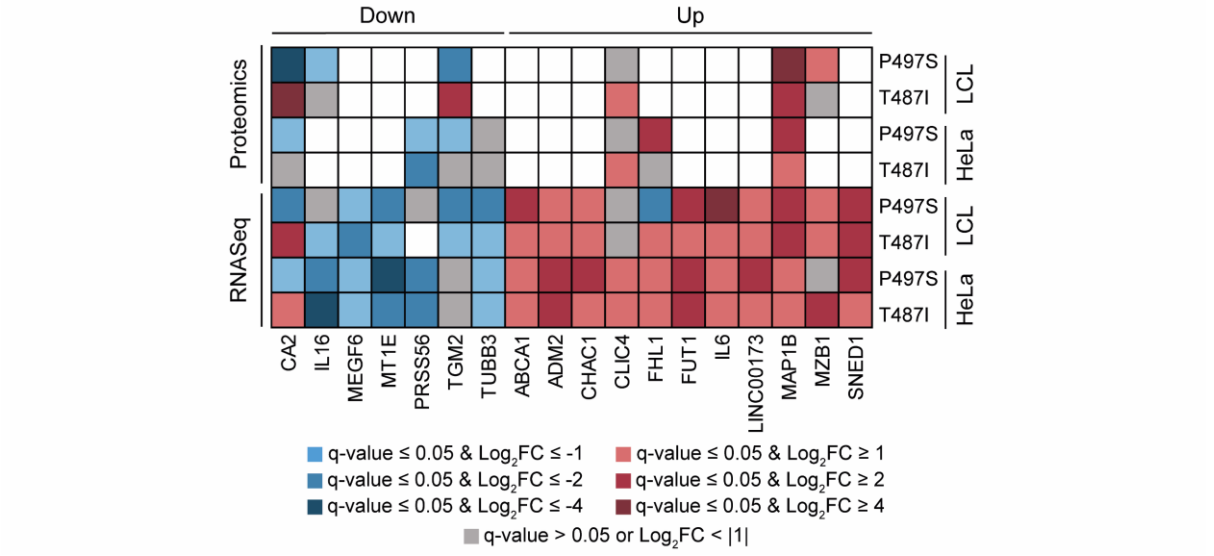


**Figure 3-14: Heat map representing common candidates of the proteomic and transcriptomic analyses.**
Significant (q-value ≤ 0.05) increase and decrease of mRNA and protein abundance are marked in red and blue, respectively. Cells are marked in grey if candidates were quantified but did not reach a $Log_2$ fold change ($Log_2FC$) of |1| or a q-value ≤ 0.05. Cells are marked in white if candidates were not detected in the data set.

Due to the consistent up-regulation of MAP1B, its known function in regulating cytoskeletal dynamics and its important role in neuronal cells, we decided to focus subsequent experiments on this candidate.

To validate this candidate, elevated mRNA and protein levels in the two UBQLN2 mutant cell types were confirmed by RT-qPCR, immunoblotting and -staining. Since MAP1B is post-translationally cleaved into a large heavy (HC) and a smaller light chain (LC1), both proteoforms were analyzed in immunoblotting experiments. In LCLs and HeLa cells, both forms were strongly increased in UBQLN2 mutation carriers compared to the controls (Figure 3-15A and B). Immunofluorescence staining of the patient-derived LCLs showing elevated MAP1B levels in UBQLN2 mutant cells further reinforced this observation (Figure 3-15C).

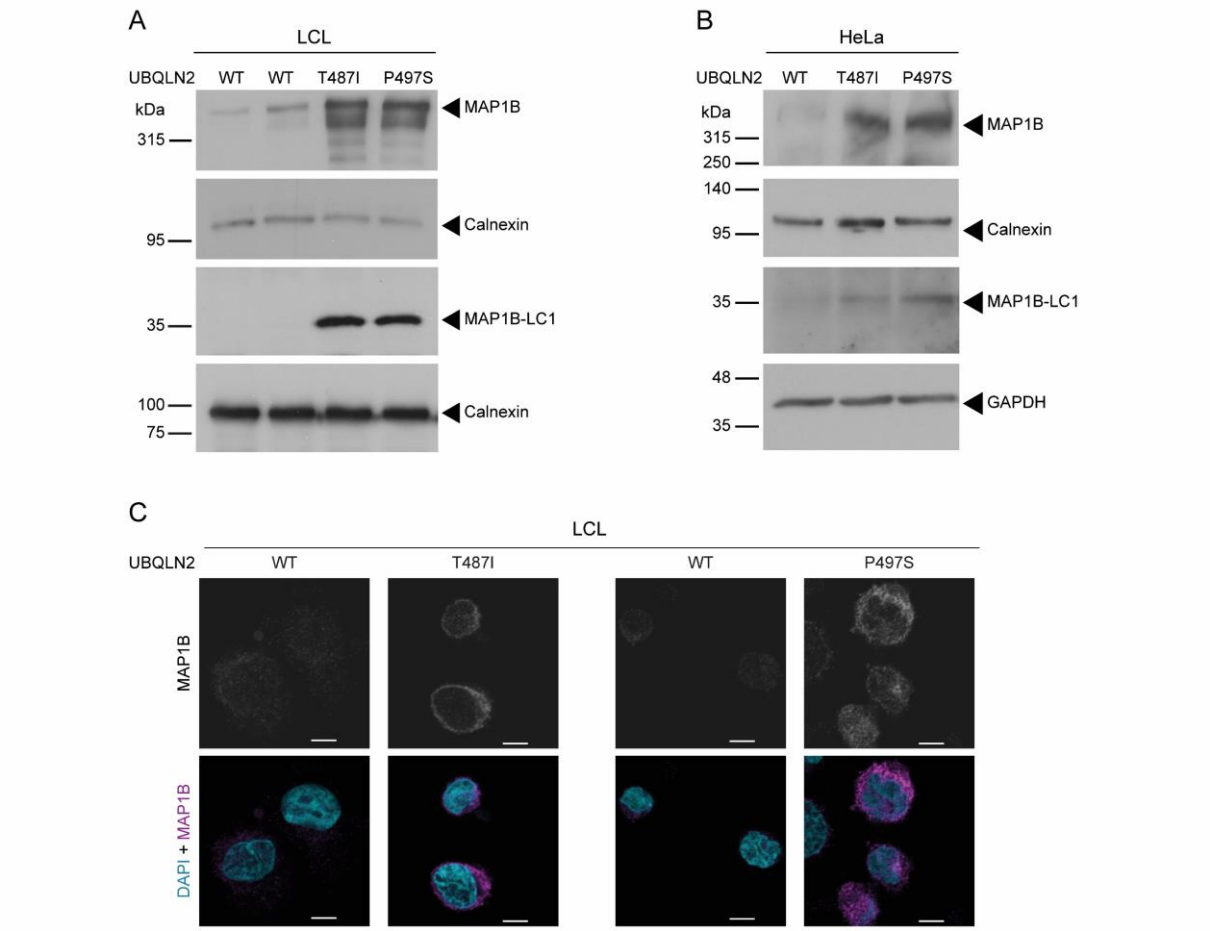


**Figure 3-15: UBQLN2 mutations result in higher MAP1B protein abundance.**
**(A+B)** Immunoblot of UBQLN2 WT and mutant **(A)** LCLs and **(B)** engineered HeLa cells analyzed for full length MAP1B and LC1. **(C)** Single plane images of patient-derived LCLs carrying either WT or mutated UBQLN2, fixed and stained with indicated antibodies, were obtained on a confocal microscope. Elevated levels of MAP1B protein were observed in mutated UBQLN2 cells compared to WT counterparts. Scale bar: 5 µm.

Also, the transcriptomic alterations of MAP1B were validated. Normalized to the expression of the housekeeping genes Glyceraldehyde-3-Phosphate Dehydrogenase *(GAPDH),* TATA-binding protein *(TBP)* and β-actin *(ACTB), MAP1B* mRNA levels were found to be indeed significantly increased (Figure 3-16). They reached up to 3.3-fold higher levels in the UBQLN2 mutants compared to the respective WT controls.

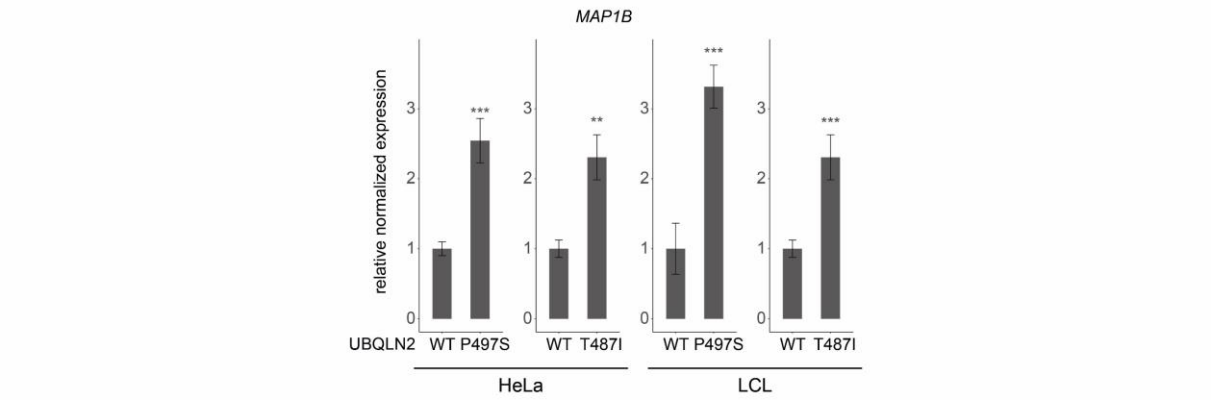


**Figure 3-16: Up-regulated MAP1B mRNA levels in UBQLN2 mutant LCLs and engineered HeLa cells.**
Analyses of quantitative RT-qPCR showing mRNA levels of MAP1B relative to the housekeeping genes *GAPDH*, *TBP* and *ACTB*. Data shown are averages over three biological replicates with three technical replicates each. Error represent ±SE. ***: p-value ≤ 0.001; ** p-value ≤ 0.01; Student's t-test.

To assure that the observed elevation of MAP1B is not caused by disturbed protein degradation, blockage of autophagy and proteasomal degradation was performed. Bafilomycin A1 (BafA) was used to block late-phase autophagy while bortezomib (Btz) was applied as proteasomal inhibitor. Both treatments did not increase MAP1B protein levels (Figure 3-17). Even though most changes in protein abundance in UBQLN2 mutant cells were not caused by changes in transcription, this is clearly the case for MAP1B.

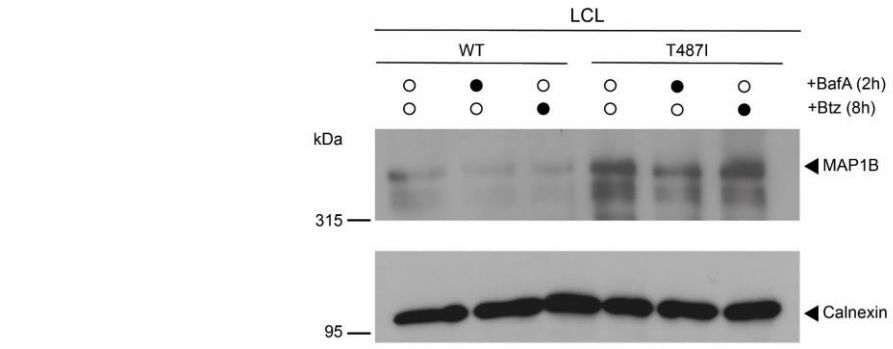


**Figure 3-17: MAP1B elevation is not caused by disturbed protein degradation.**
LCLs carrying WT or T497I UBQLN2 were treated with bafilomycin A1 (BafA, 200 nM) or bortezomib (Btz, 1 µM). Immunoblots of those lysates were exposed to a MAP1B specific antibody.

## 3.6 Elevation of MAP1B–a loss-of-function effect

The robust increase in *MAP1B* mRNA and MAP1B protein levels in cells expressing mutant UBQLN2 triggered the question whether this effect resulted from a loss-of-function or gain-of-function mechanism of UBQLN2. To address this question, we deleted UBQLN2 in HeLa cells using the CRISPR/Cas9 system. Strikingly, in these UBQLN2 knockout (KO) cells, MAP1B protein levels were strongly increased, as shown in Figure 5-18A and B by immunoblotting and immunofluorescence staining.

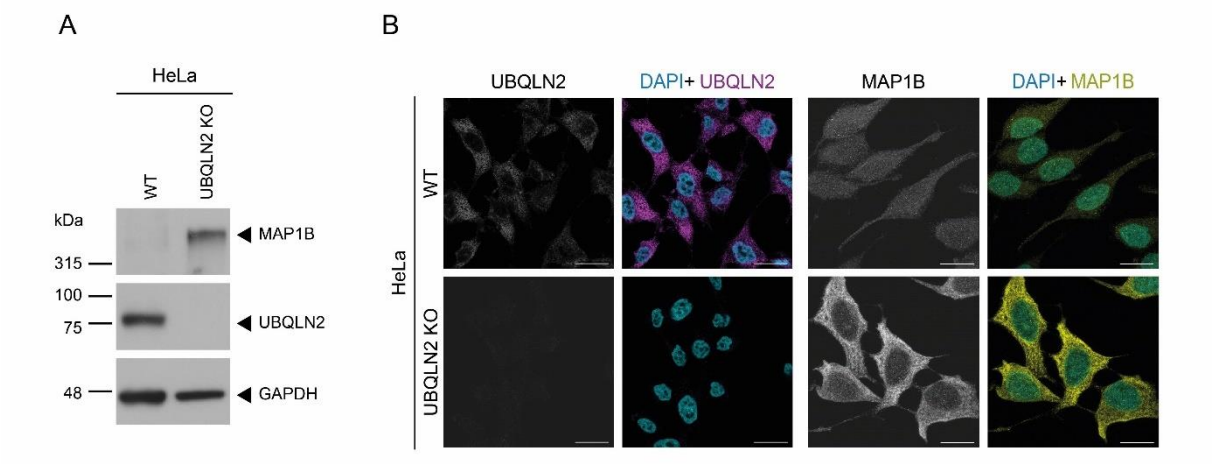


**Figure 3-18: UBQLN2 KO leads to increased MAP1B protein abundance.**
**(A)** Immunoblots of WT and UBQLN2 KO HeLa cell lysates subjected to MAP1B and UBQLN2 specific antibodies. **(B)** HeLa WT and UBQLN2 KO cells were fixed and stained with MAP1B and UBQLN2 antibodies. Scale bar: 20 µm.

To test wether re-introduction of UBQLN2 was able to revert this elevation of MAP1B, we transfected UBQLN2 KO cells with HA-UBQLN2. Indeed, as shown in Figure 5-19A and B, the overexpression of HA-UBQLN2 was sufficient to significantly lower the MAP1B protein levels in UBQLN2 KO cells.

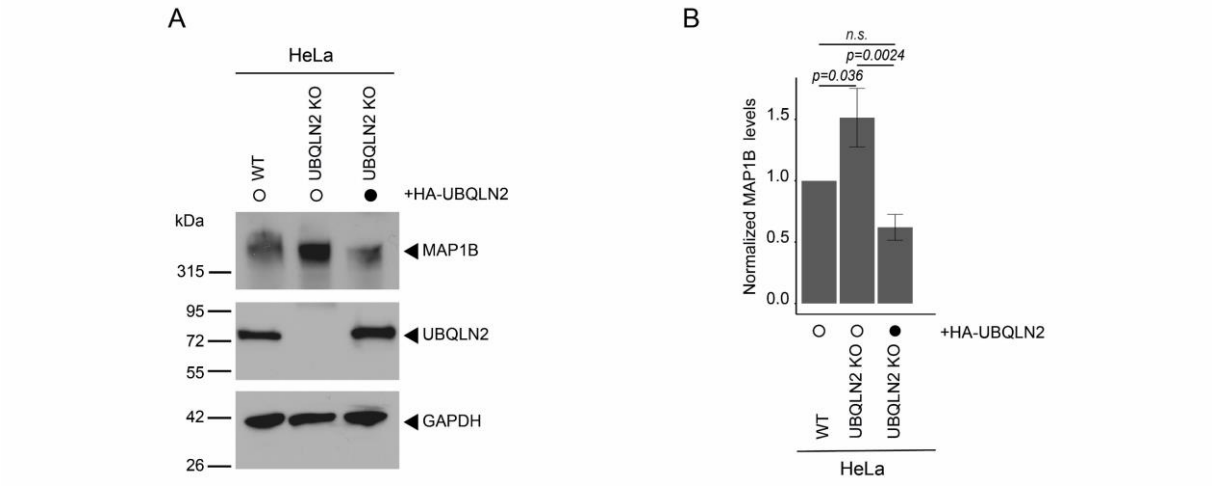


**Figure 3-19: Re-expression of UBQLN2 in UBQLN2 KO HeLa cells rescues MAP1B phenotype**.
**(A)** Immunoblots of WT and UBQLN2 KO HeLa cell lysates transfected with HA-UBQLN2 or left untreated (MOCK). **(B)** Quantification of MAP1B protein levels relative to GAPDH protein levels in (A) performed with ImageJ. Data represent mean (n = 3) ± SD. Statistical analysis was performed using one-way analysis of variance (ANOVA) followed by Tukey's post hoc test. n.s., not significant.

While we used HeLa and patient-derived LCLs for the transcriptomic and proteomic screening, thorough validation of the UBQLN2-depended increase in MAP1B required a neuronal context, especially since ALS and FTD are neurodegenerative disorders. For this purpose, primary rat cortical and hippocampal neurons were used. Short hairpin RNAs (shRNAs) against rat Ubqln2 were designed by Dieter Edbauer (German Center for Neurdegenerative Diseases Munich,

Germany) and tested for efficient Ubqln2 knockdown in 293T cells transiently overexpressing rat GFP-tagged Ubqln2 (Figure 3-20).

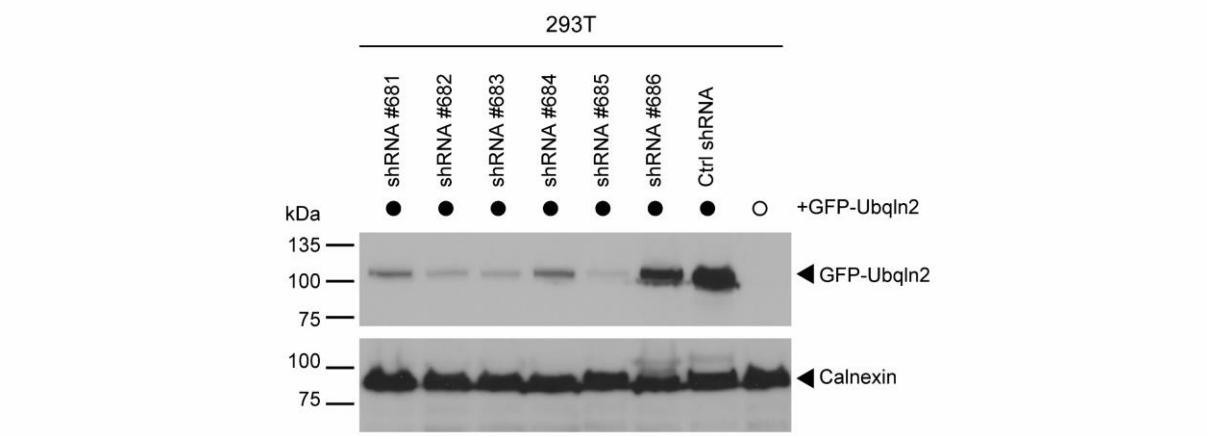


**Figure 3-20: Identification of shRNAs targeting rat Ubqln2.**
Immunoblots of 293T cells overexpressing GFP-Ubqln2 and transfected with multiple shRNAs targeting rat *Ubqln2*.

The most efficient *Ubqln2*-targeting shRNA (#685) was cloned in a FU3a tagRFP vector and used for the production of lentiviral particles. Viral transduction of *Ubqln2* shRNA led to a significant reduction of Ubqln2 levels in primary rat cortical and hippocampal neurons compared to the transduction of control shRNA (shCtrl). Importantly, this decrease in UBQLN2 was accompanied by a significant elevation of MAP1B as already observed in HeLa UBQLN2 KO cells (Figure 3-21A-C). In conclusion, in non-neuronal but also neuronal cells increase of MAP1B is a loss-of-function effect of UBQLN2.

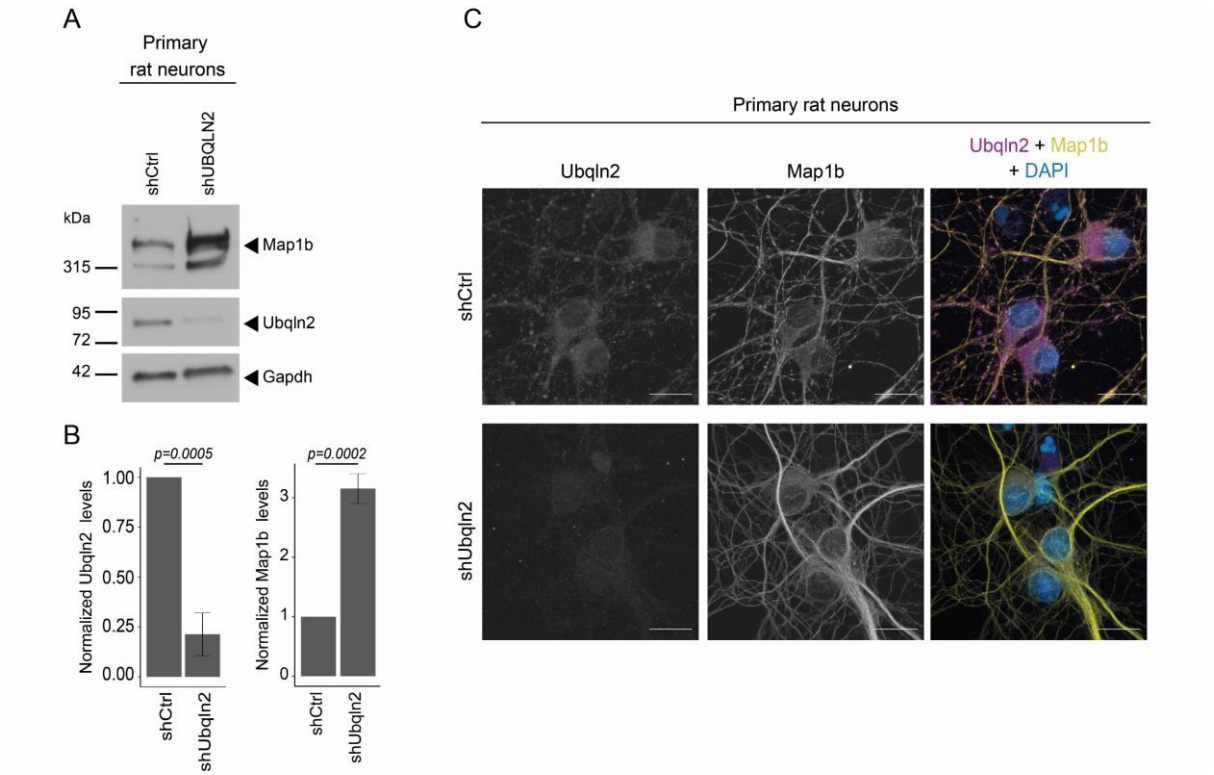


**Figure 3-21: Elevation of Map1b upon Ubqln2 knockdown in primary rat neurons.**
**(A)** Immunoblots of primary rat cortical neurons transduced with lentivirus expressing either Ubqln2 targeting shRNA (shUbqln2) or a control shRNA (shCtrl) and subjected to Map1b and Ubqln2 antibodies. **(B)** Quantification of Ubqln2 and Map1b protein abundance in (A) performed with ImageJ. Data represent mean ± SD (n = 3). Statistical analysis was performed using Student's t-test. **(C)** Maximum intensity projection of z-stack images taken from transduced primary rat hippocampal cells fixed and stained with Map1b and Ubqln2 antibodies. Scale bar: 20 µm.

## 3.7 Cellular consequences of increased MAP1B abundance

The fact that the increase in MAP1B observed in ALS/FTD patient-derived LCLs and mutation engineered HeLa cells was likely caused by a loss-of-UBQLN2 function mechanism conserved in neuronal cells raised the question about the molecular consequences of elevated MAP1B in cells. Given that microtubule binding is a prominent feature of MAP1B, we focused on microtubules for the next experiments. In particular, we examined microtubule mass and microtubule acetylation in the UBQLN2 KO HeLa cells (Figure 3-22).

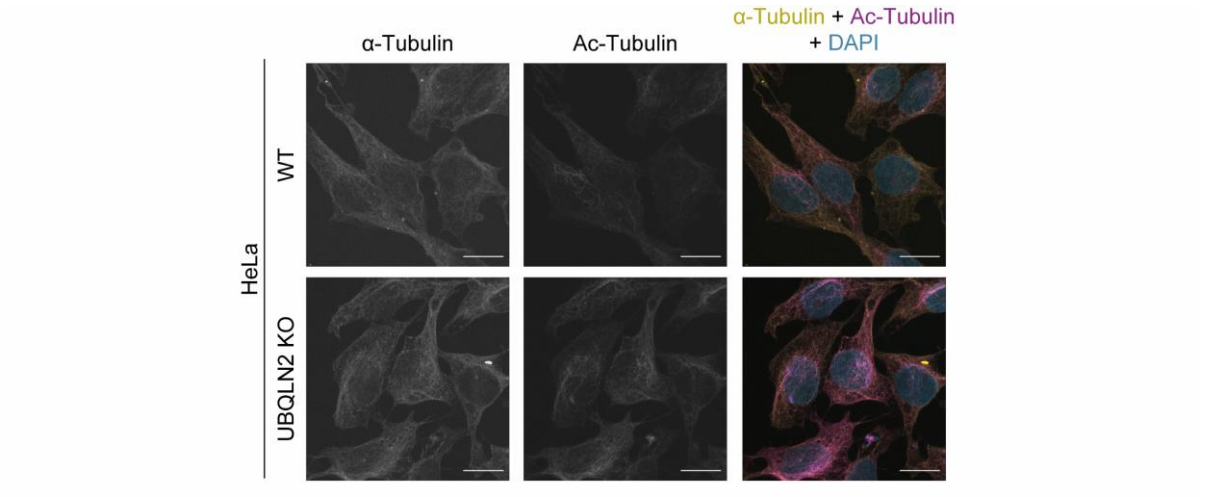


**Figure 3-22: Increased microtubule mass and acetylation in UBQLN2 KO HeLa cells.**
Maximum intensity projection of z-stack images taken from WT and UBQLN2 KO HeLa cells fixed and stained with indicated antibodies. Scale bar: 20 µm.

Since a trend towards increased microtubule mass and microtubule acetylation was observed, the mean intensity levels of five biological replicates stained for α-tubulin and acetylated α-tubulin (Ac-tubulin) were analyzed. For each coverslip the average grey value of 20 cells was measured, resulting in a total of 100 analyzed cells per condition. This quantification revealed a significant increase in both, Ac-tubulin and α-tubulin (Figure 3-23). However, the ratio of Ac-tubulin to total α-tubulin remained unchanged in UBQLN2 KO cells, indicating that the surplus of microtubules is not present in a stabilized condition.

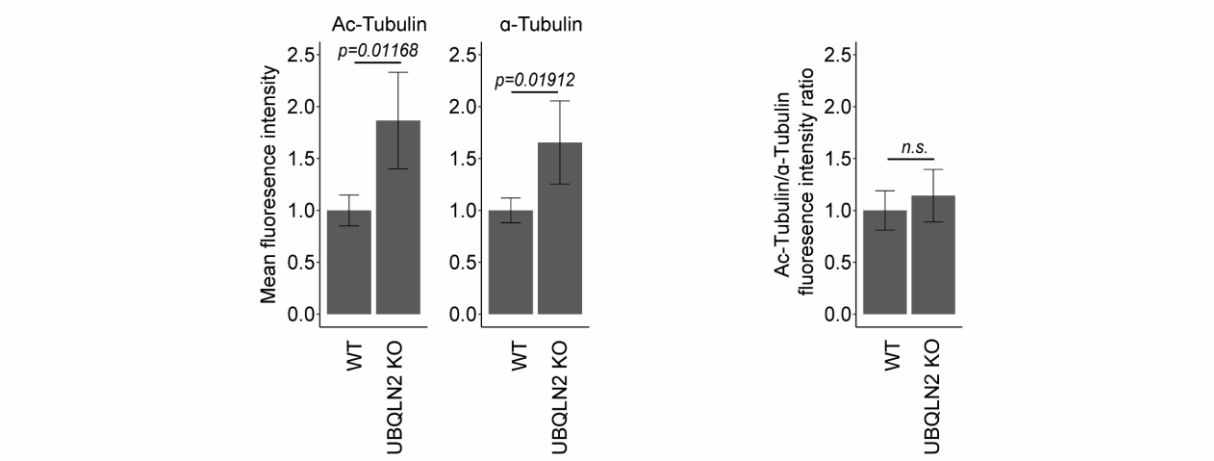


**Figure 3-23: Quantification of total and acetylated α-tubulin levels.**
Quantification of mean grey intensity levels of total and acetylated α-tubulin levels, as well as their ratio were performed with ImageJ. Data represent the mean of 5 biological replicates, each based on the mean of 20 individual cells. Statistical analysis was performed using Student's t-test. Error bar presents ±SD. Ac-Tubulin, acetylated α-tubulin.

Analysis of the interactome of a specific protein can contribute to the understanding of protein functions. Thus, an HA-IP followed by mass spectrometry was conducted in HeLa cells stably overexpressing HA-tagged full length MAP1B (Figure 3-24A and B). Statistical analysis of

quadruplicate HA-MAP1B overexpressing cells compared to parental HeLa cells revealed several MAP1B interactors. Among these MAP1B interactors, three categories were in particularly interesting. In addition to expected cytoskeleton-linked MAP1B interaction candidates (indicated in yellow in Figure 3-24C), the most prominent category is the UPS with several subunits of the proteasome complex, the ubiquitin binding proteins (SQSTM1 and FAF2) and the ubiquitin ligase HUWE1 labelled in purple. An additional category includes multiple chaperones, such as BAG6 and SMAKA1, but also all eight members of the chaperonin containing tailless complex polypeptide 1 (CCT). The accumulation of chaperones and proteins of the UPS points towards an overutilization of the cell's proteostasis network as a consequence of increased MAP1B levels.

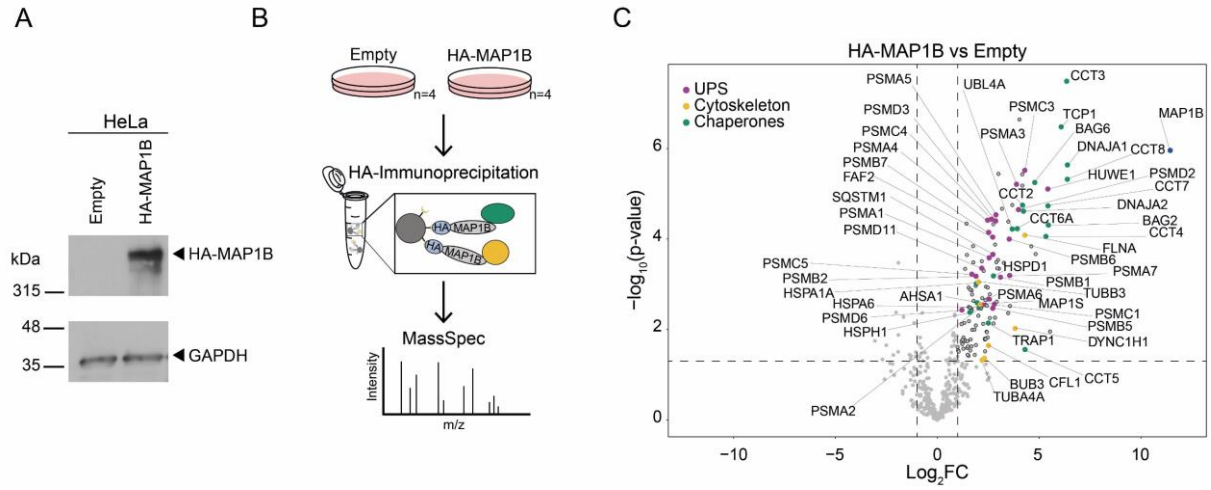


**Figure 3-24: MAP1B predominantly interacts with constituents of the UPS and the cytoskeleton as well as with chaperones.**
**(A)** Immunoblots of empty HeLa cells and HeLa cells stably overexpressing HA-MAP1B. **(B)** Schematic workflow of HA-immunoprecipitation followed by MS-analysis. **(C)** Volcano plot showing the interacting proteins of MAP1B in an overexpressing setup as $\log_2$ fold change ($Log_2FC$) versus the $-\log_{10}$ of the p-value. Dashed lines indicate significance and $Log_2FC$ cutoffs. Proteins belonging to one of the three categories (UPS, cytoskeleton and chaperones) are labelled and highlighted in the specific color. UPS, ubiquitin-proteasome system.

## 3.8 Phosphoproteomics reveal changes in RNA-binding proteins

Since MAP1B is known to be phosphorylated at multiple sites and these posttranslational modifications strongly influence its function, we used patient-derived LCLs to examine the phosphorylation state of mutant UBQLN2-driven MAP1B. Therefore, the LCL panel was subjected to a phosphoproteomic experiment performed in collaboration with Jörn Dengjel (Department of Biology, University of Fribourg, Switzerland). UBQLN2 WT and mutant LCLs were differentially labeled by stable isotope labeling by amino acids in cell culture (SILAC) and phosphopeptides enriched prior to LC-MS/MS analysis (Figure 3-25A). Overall, 41,070 phosphorylation sites (phosphosites) were identified (Figure 3-25B). After filtering for confident

phosphosite localization and quantification in at least two biological replicates, 11,454 and 11,649 phosphosites were normalized to the corresponding protein abundances. Of those, the majority of phosphosites was located to serines (89.8%), less phosphosites were detected on threonines (9.7%) and tyrosines (0.5%) (Figure 3-25C). 101 and 95 phosphosites were significantly reduced and increased, respectively, in both LCLs carrying a UBQLN2 mutation compared to LCLs from healthy individuals.

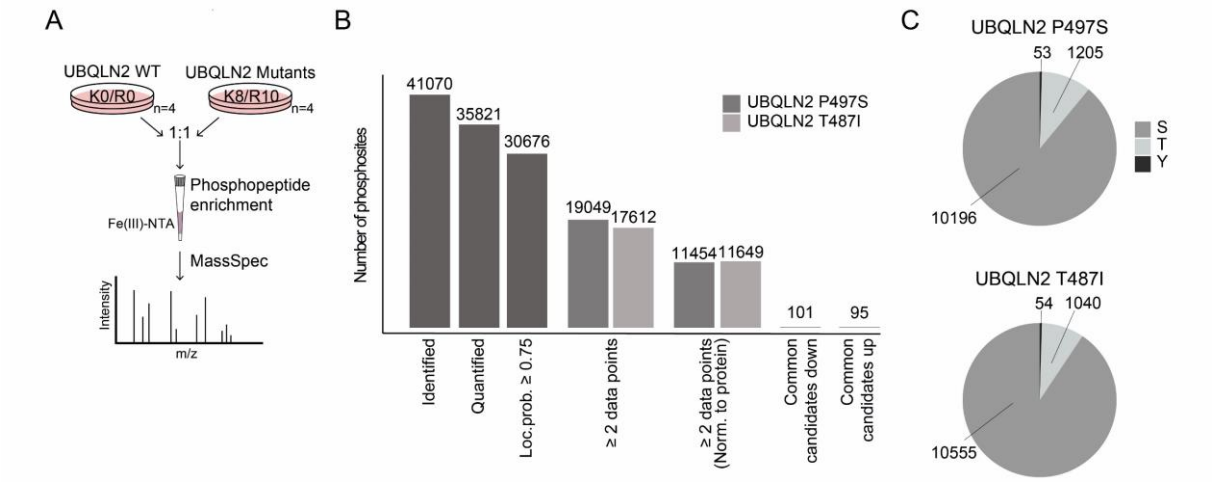


**Figure 3-25: Global phophoproteomic approach to identify phosphoproteomic changes in UBQLN2 mutant LCLs.**
**(A)** Schematic representation of the SILAC-based quantitative MS workflow. **(B)** Data analysis pipeline presenting number of identified and quantified phosphosites as well as sites fulfilling further indicated criteria. **(C)** Distribution of identified phosphorylation sites on the amino acids serine (S), threonine (T) and tyrosine (Y).

Public databases list between 100 (Uniprot) and 250 (PhosphoSitePlus) phosphosites for MAP1B. The phosphoproteomic analysis within this project revealed a total of 124 phosphosites, with 116 quantified and 95 that could be localized with high confidence (Loc. Prob ≥ 0.75) to specific amino acid residues. Of those, 16 phosphosites were significantly altered in at least one of the two LCL cells with UBQLN2 mutations after normalization to MAP1B protein abundance. Interestingly, all these 16 phosphosites were hypophosphorylated in the ALS/FTD UBQLN2 mutant cells, indicating that the surplus of MAP1B in these cells is mostly present in a dephosphorylated form (Figure 3-26). Although 16 phophosites were significantly less phosphorylated in at least one UBQLN2 mutant cell line, only a single MAP1B phosphosite, namely pT1864 was commonly less phosphorylated in both UBQLN2 mutant cell lines. While pT1864 is a known MAP1B phosphosite located outside of any annotated region in the heavy chain of MAP1B, so far, no function has been reported for this phosphosite. Thus, further work is required to clarify the effects of MAP1B dephosphorylation in the context of ALS/FTD-linked mutations in UBQLN2.

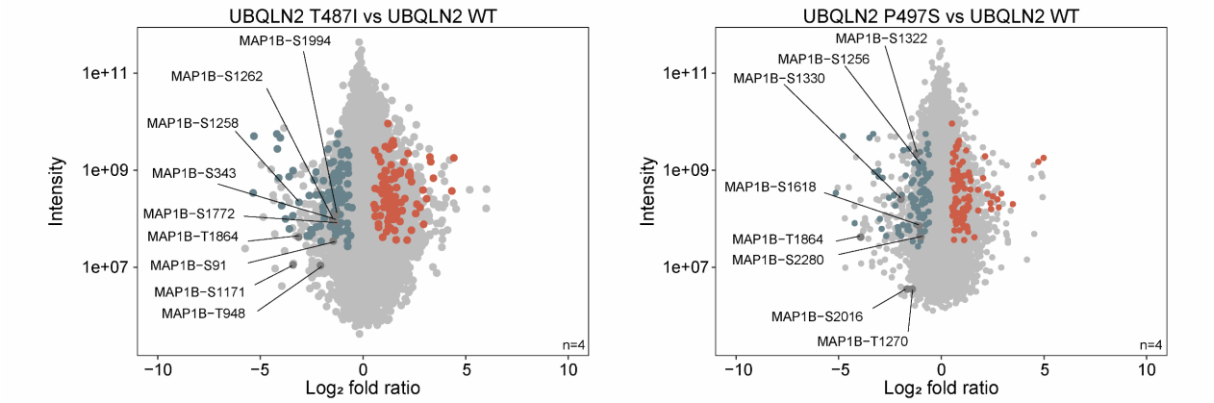


**Figure 3-26: Quantitative proteomic comparison of phosphosites identified in UBQLN2 WT and mutant LCLs.**
Intensities of detection are plotted against the fold change of regulation ($log_2$ SILAC ratio). Common hits that were significantly regulated in both mutants are highlighted in blue and red. Significantly changed MAP1B phosphosites are labelled.

Subsequently, we used the phosphoproteomic data set to mine for proteins that might play an intermediator role in the elevation of MAP1B downstream of UBQLN2. For this purpose, we filtered for phosphosites commonly regulated in both UBQLN2 mutants and for $log_2$ ratio ≥ 1 or ≤ -1 in at least one of the two mutants. 95 up-regulated and 101 down-regulated phosphosites on 165 proteins fulfilled these criterions. Unbiased functional annotation analysis of these proteins revealed a significant (FDR ≤ 0.05) enrichment of 19 GO terms, including several cytoskeleton-associated terms and RNA metabolism-associated terms such as ‘intracellular ribonucleoprotein complex’ or ‘poly(A)RNA binding’ (Figure 3-27).

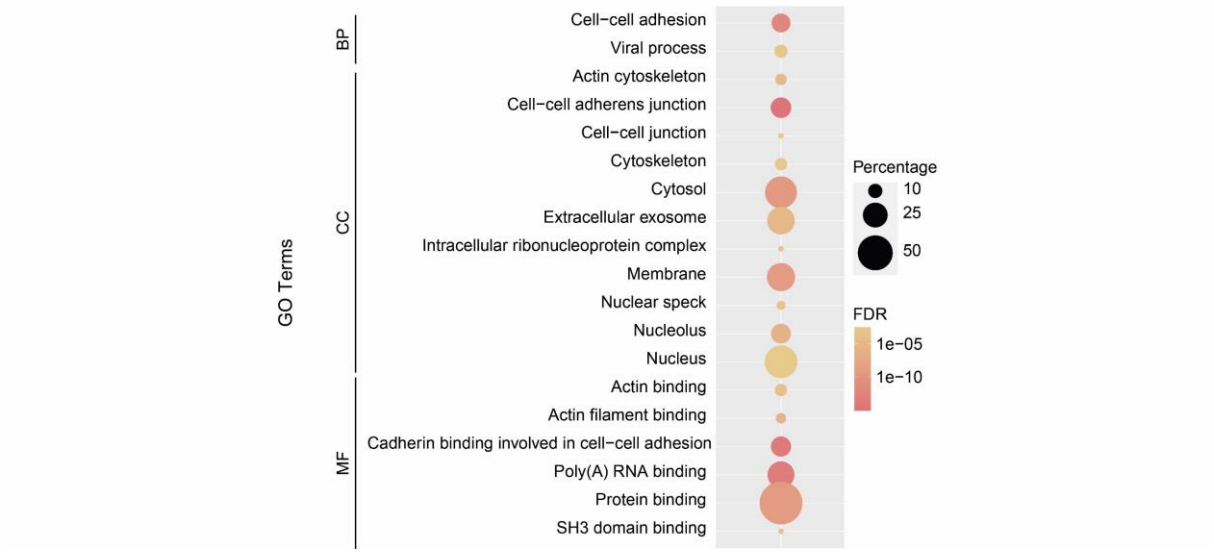


**Figure 3-27: Gene Ontology (GO) enrichment analysis of proteins with altered phosphorylation.**
False-discovery rate (FDR)-corrected p-values are used as significance levels and represented in the color gradient. The percentage of proteins of the input list associated with the GO term are represented through circle size. BP, biological process; CC, cellular component; MF, molecular function.

To analyze the degree of connectivity between proteins found enriched within these GO terms, we used the STRING protein-protein interaction database to detect interaction clusters.

Interestingly, MAP1B was found to be present in a cluster which was dominated by RNA-binding proteins (approximately 78% of all proteins in this cluster), as shown in Figure 3-28. Of those RNA-binding proteins, three are genetically associated with ALS/FTD, namely heterogeneous nuclear ribonucleoprotein A1 (hnRNPA1), heterogeneous nuclear ribonucleoproteins A2/B1 (hnRNPA2B1) and fused in sarcoma (FUS).

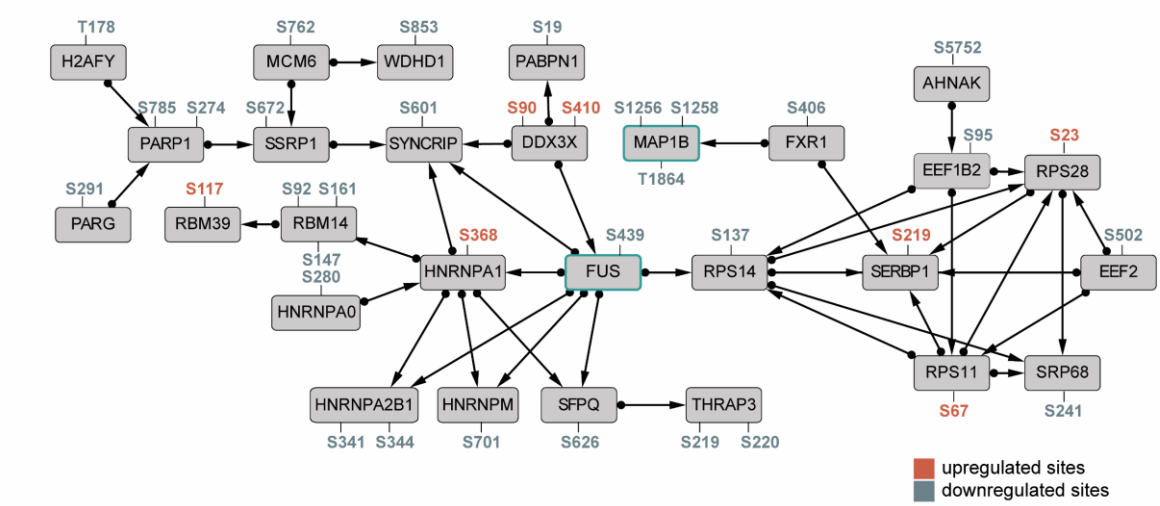


**Figure 3-28: MAP1B connectivity cluster is dominated by RNA-binding proteins.**
The protein–protein interaction network of proteins whose phosphorylation status was significantly changed in both mutants with at least one mutant exceeding a $\log_2$ ratio of ≥ 1 or ≤ -1, containing MAP1B. Significantly up- and down-regulated phosphosites are highlighted in red and blue, respectively. MAP1B and FUS are marked with a turquoise frame.

## 3.9 FUS pS439 is required for RNA-binding

Of the ALS/FTD-linked RNA-binding proteins in the interaction cluster with MAP1B, FUS captured our attention. Mutations in this protein are a relatively frequent cause for ALS/FTD and FUS represents a major aggregating protein in ALS/FTD. Intriguingly, FUS carried one phosphosite that was significantly less phosphorylated in both LCL mutants compared to the respective controls. Although this phosphosite, located at the serine 439 (pS439), was so far not associated with ALS/FTD or any other disease, its location in FUS' zinc finger domain awoke our interest because of two reasons (Figure 3-29): First, the zinc finger domain in FUS participates in FUS-RNA-binding [266]. Second, FUS was reported to bind *MAP1B* mRNA and therewith affecting its translation [79, 92, 263].

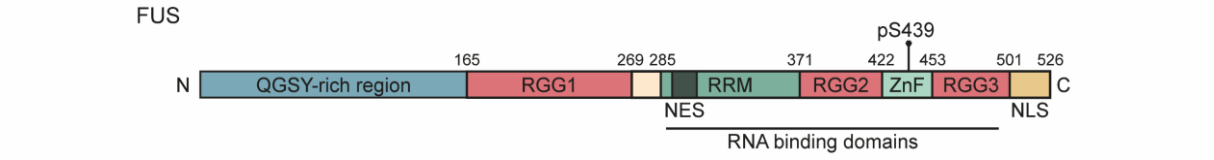


**Figure 3-29: Schematic representation of the location of pS439 in FUS.**
Major motifs of FUS are shown and the location of pS439 in the ZnF motif is indicated. SYGQ-rich, serine, tyrosine, glycine, glutamine-rich domain. RRM, RNA recognition motif. RGG, arginine-glycine-glycine-rich region. NLS, nuclear localization signal. ZnF, zinc finger domain.

Since changes in phosphorylation of FUS pS439 might mediate the elevation of MAP1B observed in UBQLN2 deficient cells, we sought to validate the dephosphorylation of this site in the patient-derived LCLs. Firstly, immunoblot analysis of cell lysates was conducted to confirm that FUS protein abundance did not change in WT and mutant LCLs (Figure 3-30A). Since antibodies against FUS pS439 were not yet available, Phos-tag™ gels were used to separate proteins based on their phosphorylation status. Consistent with the large-scale phosphoproteomic results, immunoblotting following Phos-tag™ electrophoresis revealed a prominent, higher phosphorylated band which was less abundant in both UBQLN2 mutant cells compared to respective control cells (Figure 3-30B).

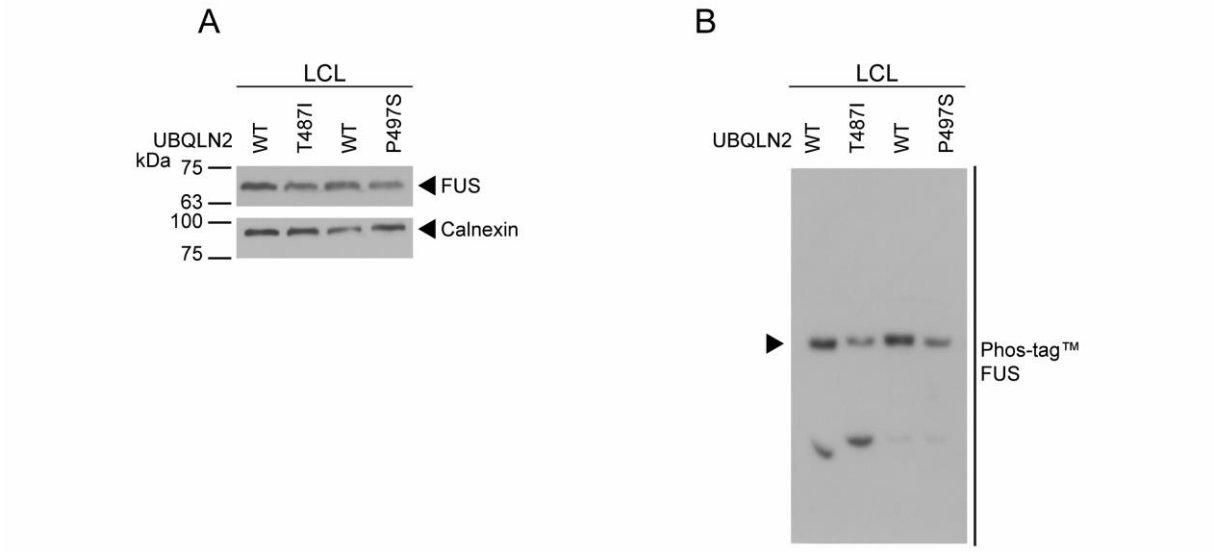


**Figure 3-30: Reduced levels of phosphorylated FUS in UBQLN2 LCL mutants.**
**(A)** Immunoblots of lysates from LCLs subjected to FUS antibody show unchanged FUS protein abundance. **(B)** Analysis of same lysates from (A) separated on a Phos-tag™ gel present lower abundance of a phosphorylated form of FUS in UBQLN2 mutant LCLs compared to respective controls.

To address whether FUS was in fact involved in the elevation of MAP1B upon depletion of UBQLN2, FUS was depleted using siRNAs in UBQLN2 KO HeLa cells. Notably, efficient depletion of FUS in these cells resulted in a significant reduction of MAP1B protein levels (Figure 3-31).

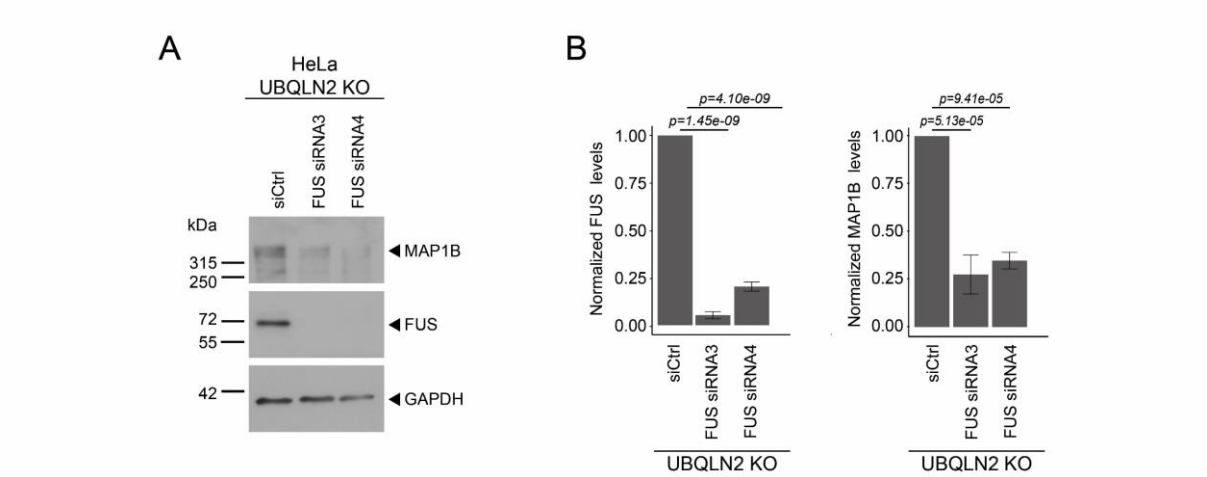


**Figure 3-31: FUS knockdown results in lower MAP1B abundance in UBQLN2 KO HeLa cells.**
**(A)** Immunoblots of UBQLN2 KO cell transfected with FUS siRNA or MOCK control, lysed and subjected to MAP1B and FUS specific antibodies. **(B)** Quantification of protein abundance levels from (A) performed with ImageJ. Data show the mean ± SD (n=3). Statistical analysis was performed using one-way analysis of variance (ANOVA) followed by Dunnett's post hoc test.

The findings that FUS pS439 is dephosphorylated in UBQLN2 mutants and that MAP1B protein levels are reduced in response to siRNA-mediated knockdown of FUS led us to the hypothesis that the RNA-binding capacity of FUS might be regulated by pS439. To test this notion, we introduced phospho-mimetic and phospho-deficient mutations at S439 of FUS. The mutation of serine to glutamic acid mimics the negative charge of a phosphorylated serine residue while the mutation of serine to alanine prevents potential phosphorylation. FUS WT, FUS S439A and FUS S439E variants were purified and electrophoretic mobility shift assays (EMSA) were conducted in collaboration with Dorothee Dormann (Institute for Molecular Physiology, Johannes Gutenberg-University Mainz, Germany). In these experiments, varying amounts of synthetic SON pre-mRNA containing the stem loop and a downstream GUU sequence [266] known to bind to the RRM and ZnF domain of FUS were mixed with purified maltose binding protein (MBP)-FUS-$His_6$ variants (WT, S439A and S439E). Strikingly, while WT and the S439A variants, both present in a non-phosphorylated form in this *in vitro* reaction, were able to bind the RNA probe, RNA-binding was completely abolished when FUS S439E was used (Figure 3-32A and B).

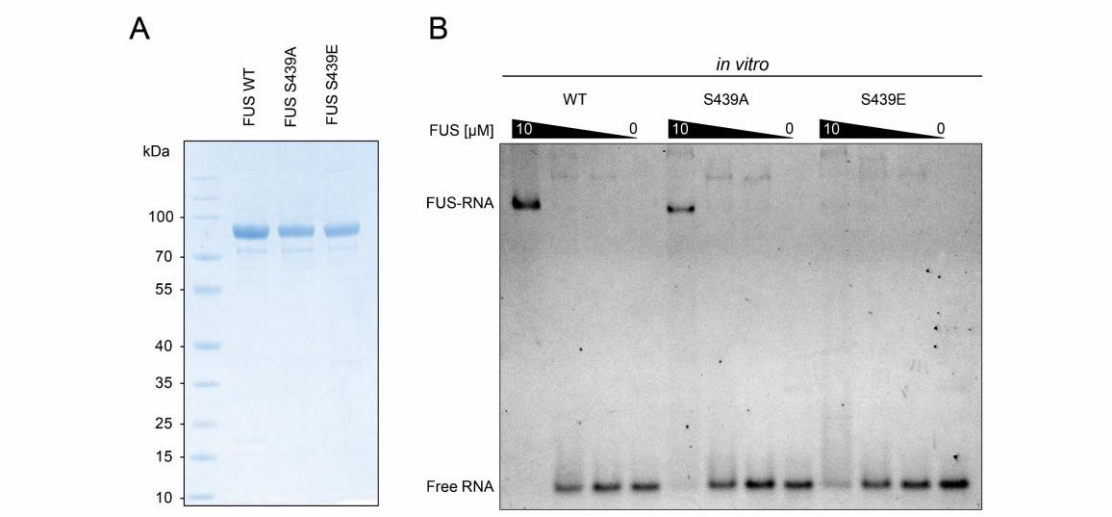


**Figure 3-32: The phospho-mimetic mutation FUS S439E hinders the formation of the FUS-RNA-complex.**
**(A)** Coomassie blue staining of SDS-PAGE from recombinant FUS variants (WT, S439A, S439E). **(B)** Electrophoretic mobility shift assay (EMSA) of MBP-FUS-His6 variants (WT, S439A, S439E) and the SON transcript template containing the stem loop and a downstream GUU (5 nM). 3 biological replicates were performed.

Lastly, it remained to be examined whether the phospho-deficient FUS S439A variant influences MAP1B levels in HeLa cells. For this purpose, we generated FUS knockdown (KD) cells using CRISPR/Cas9 and reconstituted them with either HA-tagged FUS WT or S439A. Immunoblotting against MAP1B revealed a significant elevation of MAP1B protein levels in cells re-expressing HA-FUS S439A compared to those expressing HA-FUS WT (Figure 3-33A-C).

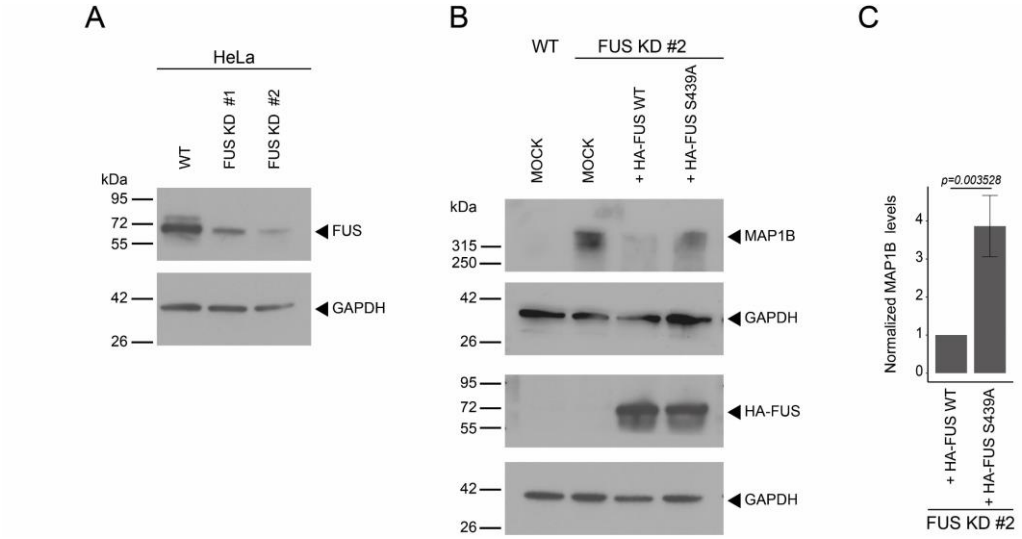


**Figure 3-33: Phospho-deficient FUS induces MAP1B protein elevation in a UBQLN2 knockdown background.**
**(A)** Immunoblots showing reduced FUS levels in CRISPR/Cas9 engineered FUS knockdown (KD) HeLa cells. **(B)** HeLa WT and FUS KD cells were transfected with HA-FUS variants (WT or S439A) or MOCK, lysed and stained with antibodies specific for FUS and HA. **(C)** Quantified MAP1B protein levels from (B) received by ImageJ analysis. Data present means ±SD (n=3). Statistical analysis was performed using Student's t-test.

Taken together, this work provides evidence that loss of UBQLN2 function in cells relevant for ALS/FTD causes an increase in *MAP1B* mRNA and MAP1B protein levels which is likely mediated by dephosphorylation of the RNA-binding protein FUS at S439. Hence, FUS might act as an intermediator between mutated UBQLN2 and elevated MAP1B.

.

# 4 Discussion

ALS and FTD are two entangled diseases. Although this disease continuum is extensively studied and several pathways suspected to play a role in the disease development are known, the exact disease mechanism remains unclear. In this project we applied a systematic, unbiased proteomic and transcriptomic approach to identify molecular alterations in response to ALS/FTD-linked UBQLN2 mutations. Since UBQLN2 acts mainly in protein degradation pathways, it was expected that these pathways are predominantly affected by UBQLN2 mutations. Yet, our gene ontology (GO) analyses revealed multiple terms associated with RNA metabolism to be affected in UBQLN2 mutant cells. Unexpectedly, one specific candidate, which was so far scarcely associated with ALS/FTD, the microtubule-associated protein MAP1B, was significantly elevated both at the transcriptomic and proteomic level in UBQLN2 mutant cells. Although changes in this protein cannot be directly linked to UBQLN2 mutations, its major role in the cytoskeletal organization in neurons match anticipated alterations in ALS/FTD. Accordingly, MAP1B elevation was accompanied with increased levels of acetylated and total α-tubulin. However, it remains unclear what specific consequences MAP1B elevation causes in the ALS/FTD-disease setting. Increased MAP1B levels were also detected in UBQLN2 knockout cells, ascribing this effect to a loss-of-function mechanism of UBQLN2. Besides the discovery of MAP1B as a new player in ALS/FTD, this work provided first evidence for FUS S439 dephosphorylation in ALS/FTD. We hypothesize that this change in FUS phosphorylation possibly mediates the up-regulation of MAP1B, since the overexpression of phospho-deficient FUS variant S439A led to MAP1B elevation in FUS depleted cells. Finally, we suggest that FUS pS439, which so far was not associated with ALS/FTD, is a critical factor in FUS' RNA-binding capacity due to disturbed binding of the FUS S439E phospho-mimicking variant to a known FUS RNA target.

## 4.1 SQSTM1 in UBQLN2-linked ALS/FTD

In this work, only a few ALS/FTD-linked proteins were found to be affected in UBQLN2 mutants on a transcriptomic or proteomic level and none was commonly changed across multiple cell lines. The autophagy receptor SQSTM1 was only found to be significantly increased in UBQLN2 T487I HeLa cells. Interestingly, SQSTM1 is known to be present in UBQLN2-positive inclusions in ALS/FTD patients [35]. In addition, this phenotype was also detected in a variety of ALS/FTD-linked UBQLN2 animal models; in rat, mouse and drosophila disease models an accumulation of SQSTM1 and its colocalization with UBQLN2 was reported [151, 160, 161, 188, 193, 267, 268]. Thus, the question arises whether the unchanged SQSTM1 levels in most of our data sets are unexpected. However, available literature is conflicting concerning whether SQSTM1 accumulation is accompanied by an increase in abundance or might results from

changes in subcellular distribution. Whereas some studies in fact observed an increase in SQSTM1 [160, 161, 267], others did not detect abundance changes [151, 188, 268]. In a study that used overexpression of mutant UBQLN2 P497H in spinal motor neurons of mice, SQSTM1 was found to be elevated at 1 month but not at 6 and 12 months [188]. In this particular study, also a weaker diffuse cytoplasmic presence of SQSTM1 was seen in UBQLN2 mutant mice, pointing to an impaired subcellular distribution rather than a change in total protein abundance. In addition, most of the existing studies are based on an overexpression of human WT and mutant UBQLN2 in transgenic animals and should therefore be treated with caution, especially since cells react very susceptible to changes in UBQLN2 protein levels [165]. One exception is the study by Kurz and colleagues, in which the authors knocked-in the equivalent human P506T mutation (mP520T) by homologues repair. These mice demonstrated cognitive and pathological features, including SQSTM1 inclusion pathology, but no changes in SQSTM1 protein levels were detected [151]. In a proteomic study by Whiteley et al. which also used an overexpression of human UBQLN2 variants (WT and P497S), an increase of SQSTM1 was observed in hippocampal and spinal cord tissue [165]. A significant increase in SQSTM1 was also reported in lymphoblasts of patients carrying the P497S, P494L and P506A mutations compared to healthy controls in a study by Teyssou and colleagues [174]. The question arises, why we detected an increase in UBQLN2 T487I HeLa but not in UBQLN2 P497S cells, as the latter carry the identical mutations as the model used in Whiteley et al. The main difference between our and Whiteley and colleagues' study is the disease model. While here human non-neuronal cell lines with mutations on endogenous UBQLN2 were used, Whiteley et al. performed whole proteomics from murine brain tissues overexpressing WT and mutant human UBQLN2. Furthermore, in the present study a relatively strict cutoff of a $Log_2FC$ of ≤-1 or ≥1 was applied. In Whiteley et al., on the other hand, a cutoff of a $Log_2FC$ of |0.5| was applied. Such a cutoff results in a significant (q-value: 0.04, $Log_2FC$: 0.7) increase of SQSTM1 in UBQLN2 T487I LCLs, but not in the P497S mutant cells. In addition to the transgenic overexpression model, Whiteley et al. also examined a knock-in mouse model with a P520T mutation. In this model, SQSTM1 was not elevated. However, this does not explain the varying results between our and Teyssou and colleagues' study. Possibly, this variation originated from other patient-dependent features. For example, LCLs carrying the P497S mutation used in our study originated from a male patient, while LCLs with the P497S mutation from Teyssou and colleagues' study were received from a female donor.

Our whole proteomic data set revealed the significant ($Log_2FC \geq 1$) increase of SQSTM1 in one UBQLN2 mutant cell line. In cells carrying endogenous P497S mutations, no increase was observed. In accordance with the available data reporting only in certain cases an elevation of SQSTM1, the increase of SQSTM1 appears not to be a persistent consequence of UBQLN2 mutations. Since P497S mutations in other disease models result in SQSTM1 elevation, the

disease model including species, cell type and expression method but possibly also gender, age and other factors seem to influence SQSTM1 levels. Further work is required, examining changes in SQSTM1 upon mutations in UBQLN2 in detail to further evaluate the relevance of SQSTM1. For this purpose, the identical $Log_2FC$ and significance cutoffs should be applied in omics screenings and in addition to changes in abundance, also changes in distribution considered.

Disregarding changes in SQSTM1, proteins from the autophagic pathway were not prominently deregulated in the proteomic or transcriptomic data sets, as revealed by GO analyses of those.

## 4.2 Multiple cellular processes are associated with UBQLN2 disturbances and ALS/FTD

Enrichment analyses of the proteomic and transcriptomic data sets were performed to discover which GO terms are affected in UBQLN2 mutant cells. Based on UBQLN2's main role as a Ub-shuttle factor in the UPS, occurring terms such as 'protein binding' and 'proteasome complex' were not surprising and in line with the literature. However, further categories emerged, which are to a variable extend associated with mutations in UBQLN2 or at least with ALS/FTD in general.

On both, the proteomic and the transcriptomic level, proteins assigned to the cellular compartment 'mitochondrion' were afflicted by UBQLN2 mutations. Mitochondria are in many ways connected to ALS/FTD. Multiple identified ALS/FTD genes were shown to be relevant for mitochondrial function [48]. A good example are mutations in the coiled-coil-helix-coiled-coil-helix domain containing 10 (*CHCHD10*) gene, found in ALS and FTD patients [269, 270]. The CHCHD10 protein is a mitochondrial protein located in the mitochondrial intermembrane space with unknown function. The ALS/FTD-associated mutations were reported to disturb the mitochondrial architecture and result in respiratory chain deficiency [269, 271]. In general, independent of the disease cause, neurons of individuals affected with ALS/FTD show morphologic altered and aggregated mitochondria [272]. In accordance with those patients, disease models carrying mutations in *C9orf72*, *SOD1*, *TDP-43* or *FUS* were reported to have mitochondrial defects, ranging from fragmented, vacuolated, swollen or aggregated morphology to abnormal mitochondrial transport [273-275, 276 ]. Also, first connections between disturbed UBQLN2 and mitochondrial function were demonstrated. For instance, in ubiquilin depletion and UBQLN2 ALS/FTD mutation models an accumulation of mitochondrial precursor proteins, changes in mitochondrial morphology and impaired mitochondrial fusion were described, possibly resulting from a disturbed mitochondrial protein quality control [163, 166]. In addition, whole proteomics of Ubqln2 knockout and transgenic mice revealed changes in mitochondrial proteins [165]. Thus, the observed alterations of mitochondrial protein

abundance in this work are conform with known disturbances in ALS/FTD as well as with literature providing a link between UBQLN2 and mitochondrial dysfunction. Furthermore, our findings reinforce the proposed linkage.

RNA metabolism-related GO terms, such as ‘poly(A) RNA binding’ or ‘regulation of mRNA stability’ were widely present in the enrichment analyses of the proteomic and transcriptomic data sets. While a disturbed RNA metabolism is an established pathomechanism in ALS/FTD, only in recent years evidence accumulated that suggest a role of UBQLN2 in RNA metabolism, in particular in stress granules [169, 170, 192]. In addition to the observation that UBQLN2 itself undergoes liquid-liquid phase separation (LLPS), it was also reported that it interacts with multiple RNA-binding proteins, such as FUS or members of the hnRNP family and modulates early-stage LLPS dynamics and stress granule formation [169, 170, 190, 192]. Even though UBQLN2 was in the past primarily associated with a role in protein quality control, our data is in line with recent studies, supporting a key role of UBQLN2 in RNA homeostasis.

Finally, Golgi-related GO terms turned up in the proteomic data set and the GO term ‘extracellular exosome’ in both, the proteomic and transcriptomic data sets. Golgi alterations fit to previous research showing defects in ER to Golgi transport and Golgi fragmentation in UBQLN2 mutants [277]. However, extracellular exosome effects were so far not studied extensively in ALS/FTD. Nevertheless, key ALS proteins, including SOD1, FUS or TDP-43, were found in extracellular exosomes which contribute to the transport of RNA and proteins from one cell to another [278-280].

Since motor neurons are the cells primarily affected in ALS, the use of HeLa cells, an immortal epithelial cell line, and LCLs, originating from patient-derived B-lymphocytes, are a major shortcoming of this work. To overcome this drawback, at least partially, we validated some of our findings in primary rat neurons. However, GO term analyses of proteomic and transcriptomic data in this study were limited on data from non-neuronal cells. Thus, an expansion of our screening approaches to more advanced cell models, such as induced pluripotent stem cell (iPSC)-derived motor neurons, would be beneficial. Nevertheless, comparison of GO terms enriched in our proteomic and transcriptomic data sets with the literature disclosed a high consensus. Importantly, besides the verification of established ALS/FTD-associated categories, our data also further substantiates recently emerging disease mechanisms.

## 4.3 Possible consequences of MAP1B up-regulation in ALS/FTD

Following the gene enrichment analyses, we compared proteins affected in the same direction in multiple data sets. In doing so, the microtubule-associated protein MAP1B caught our

attention, especially since it was the only candidate up-regulated in the proteomic and transcriptomic data sets of all examined cell lines. After validating these effects in ALS/FTD-associated mutants, the elevation was also confirmed in HeLa cells and primary rat neurons with depleted UBQLN2 levels. As a component of the cytoskeleton and its primarily expression in neurons [216], changes in MAP1B abundance harmonize with the cytoskeletal defects reported in ALS/FTD-linked mammalian cell models [281]. Yet, MAP1B hardly received any attention in the ALS/FTD field. So far, it was reported to be a translational target of TDP-43 and suggested to have a neuroprotective effect in drosophila [261]. Conversely to this proposed neuroprotective effect in flies, zebrafish embryos expressing an ALS-associated FUS mutant showed increased synaptic expression of the MAP1B homolog futsch [92]. Overexpression of futsch, in turn, was reported to induce neuromuscular junction abnormalities and defects in neurotransmission [282]. While such a striking elevation in MAP1B, as we observed it here, was not reported in ALS/FTD-associated cells before, similarly alterations in MAP1B were recently described in a spinal muscular atrophy (SMA) model [283]. Since SMA and ALS are both motor neuron disorders with common pathological hallmarks [284], the elevation of MAP1B might also be a shared feature between these diseases.

The remarkable increase in MAP1B abundance results inevitably in the question, what consequences it entails in cells. Based on MAP1B's ability to bind microtubules and influence microtubule stability, we examined microtubule mass and α-tubulin acetylation. For both parameters, a significant increase was observed, however, the ratio of acetylated α-tubulin to total α-tubulin remained unchanged. Thus, the surplus of tubulin was neither present in an over- nor under-acetylated state. As acetylation is predominantly found on stable microtubules, it can be deduced that the elevation of MAP1B does not result in a higher proportion of stable microtubules. Proposed effects of MAP1B on microtubule stability in the literature are multifaced. Takemura et al. and Barnat et al., for example, reported enriched acetylation in MAP1B-transfected cells [113, 234]. Concordantly, futsch deficient drosophila larvae were shown to have reduced levels of acetylated tubulin [285]. Controversially, overexpression of futsch in drosophila did not induce a statistically significant difference in the actylated-tubulin to tubulin ratio [285]. Likewise, other authors, such as Tortosa et al., did not observe a significant increase in acetylated tubulin upon MAP1B overexpression [235]. Besides acetylation, also detyrosination is associated with stable microtubules while tyrosination is associated with dynamic microtubules [286]. Interestingly, previous research has demonstrated that MAP1B associates with tyrosinated, dynamic microtubules as well [197, 235]. Summing up, MAP1B was occasionally shown to bind to stable microtubules, other times association with dynamic microtubules was evidenced. This controversiality was suggested to originate from the multiple phosphorylation states MAP1B can be present in [234]. Indeed, promotion of MAP1B phosphorylation by the glycogen synthase kinase GSK3β led to

association of MAP1B with tyrosinated microtubules and a decrease in detyrosinated microtubules. Inhibition of GSK3β on the other hand increased the portion of stable, detyrosinated microtubules [233].

In our phosphoproteomic analysis, 16 of 95 phosphosites localized to a specific site in MAP1B were significantly altered upon normalization to MAP1B protein abundance in at least one of the UBQLN2 mutant lines. All of those were found to be less phosphorylated in the mutant line. However, only one phosphosite (pT1864) was significantly dephosphorylated ($Log_2$ ratio < -1) in both mutants. Since this phosphosite is neither located in any annotated motif nor was investigated before, no consequence of its hypophosphorylation can be deduced.

Defects in axonal transport and ALS/FTD-associated mutations in microtubule proteins imply microtubule impairments in the disease [119]. However, investigations of microtubule dynamics *in vivo* are limited and the microtubule interference in ALS/FTD is not fully understood. Revealing insights came from ALS-linked SOD1 mutant mice, in which an increased microtubule dynamic was demonstrated [287]. Importantly, administration of a microtubule stabilizing agent delayed symptoms and increased lifespan of these mice [287]. Since MAP1B was among others reported to bind to dynamic microtubules, it is possible that an elevation of MAP1B could likewise increase microtubule dynamics.

Here we present strong evidence that MAP1B abundance is increased in ALS/FTD-associated UBQLN2 mutants as well as in UBQLN2 deficient cell models. Furthermore, we provided first indication for an increased microtubule mass in UBQLN2 deficient cells. However, a systematic analysis of other UBQLN2 mutants as well as different ALS/FTD-disease models, dissecting changes in MAP1B abundance, phosphorylation and microtubule organization including posttranslational modifications and stability, is needed. It also remains to be uncovered if the surplus of MAP1B is associated with stable or dynamic microtubules or if it is free in the cytosol (Figure 4-1). Such investigations could further clarify the relevance of MAP1B impairment and possible consequences for ALS/FTD pathogenesis. Further research should also focus on rescue experiments by reducing MAP1B in UBQLN2 mutant or UBQLN2 KO cells, to substantiate that indeed the elevation in MAP1B is responsible for the observed effects.

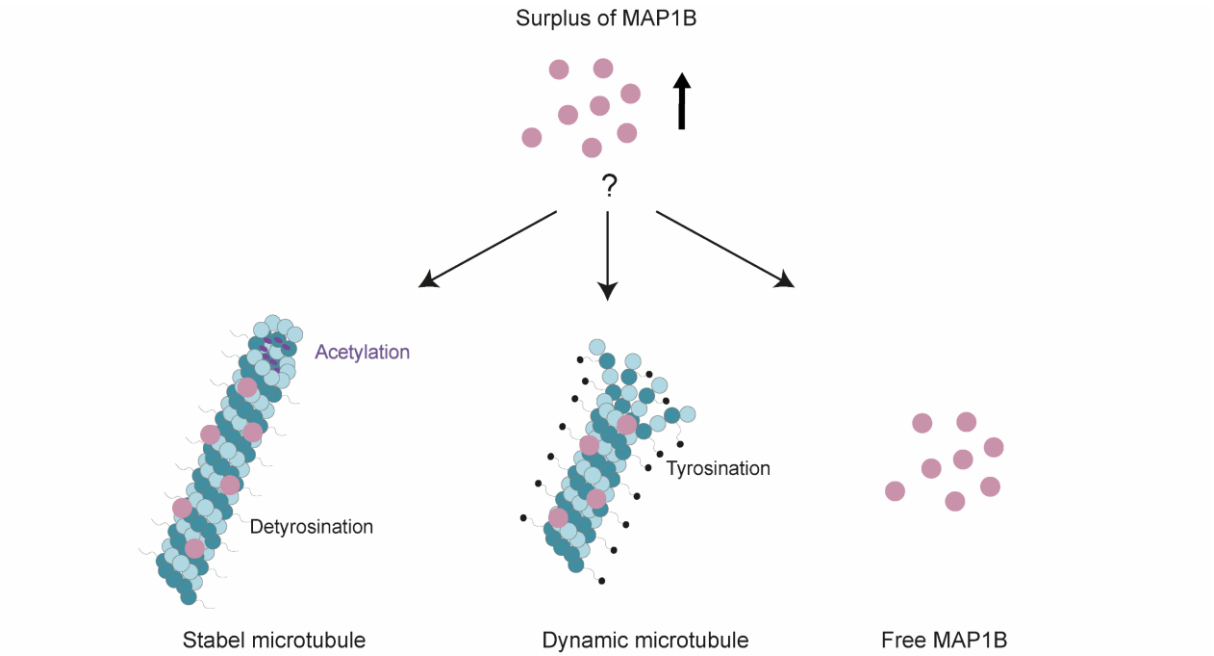


**Figure 4-1: Possible subcellular localization of a MAP1B surplus.**
The surplus of MAP1B might bind to stable or dynamic microtubules or to both. Also, a non-microtubular localization is possible.

MAP1B is primarily known for its function as a microtubule stabilizer. However, in the last two decades evidence accumulated, stating new roles of MAP1B independent of its microtubule stabilizing effects. Most of them are based on new identified interaction partners of MAP1B. These studies indicate roles of MAP1B as a regulator of mitochondrial transport, neurotransmitter trafficking and autophagy [288]. While these areas were not studied in this work, there is abundant room for further examination of possible consequences of elevated MAP1B levels aside microtubule stabilizing effects.

## 4.4 Mutations in UBQLN2 cause ALS/FTD via loss- and gain-of-functions

In this work, the phenotype of elevated MAP1B levels observed in UBQLN2 mutant cells, was also seen in cells lacking UBQLN2, indicating a loss-of-function mechanism. To evaluate to what extent this observation integrates to the current knowledge, in the following, present evidence pointing for and against a loss-of-function mechanism of UBQLN2 mutations are summarized. Multiple mutations in UBQLN2 were found to have a lower penetrance or a later disease onset in female compared to male mutation carriers [35, 172, 174]. The low penetrance in females point to a loss-of-function mechanism of pathogenic UBQLN2 mutations because of the X-chromosomal location of UBQLN2. In this case, the retention of the WT *UBQLN2* allele could compensate for the mutant *UBQLN2* allele in females. On the other side, due to potential X-inactivation, as detected by Carrel and Willard, it seems also possible that the mutated *UBQLN2* allele is less expressed in females [289]. Such a case would suggest a gain-of-function of pathogenic UBQLN2. Importantly, this topic remains controversial although

various studies aimed to answer the question whether pathogenic UBQLN2 mutations result in a loss- or gain-of-function. A strong indication for a loss-of-function mechanism is the demonstration of reduced neuropathology in P497S UBQLN2 mice upon overexpression of the close family member UBQLN1 [290]. In accordance with this finding, mitochondrial dysfunction and disturbed autophagosome acidification observed in UBQLN2 mutant mice were shown to be reduced by re-expression WT UBQLN2 and thus were ascribed to a loss of normal function [161, 166]. In addition, several studies reported impaired binding of mutant UBQLN2 to normal binding partner, further supporting a loss-of-function mechanism [151, 156, 170, 190]. These findings accord with our observed loss-of-function phenotype. However, depletion of UBQLN2 in animal models led, if at all, to mild motor impairment and no neuronal loss was observed [165, 267]. In the contrary, rats expressing human or rat WT UBQLN2 showed neuronal death and special learning deficits indistinguishable from rats expressing mutant UBQLN2, suggesting a toxic gain-of-function [291]. Yet, animal models overexpressing WT UBQLN2 demonstrate variable phenotypes. For example, two mouse models expressing WT UBQLN2 had normal life spans, no accumulation of UBQLN2 inclusions and presented no or only mild signs of motor neuron disease [292]. In another mouse model overexpressing human WT UBQLN2 reduced levels of HSP70 and profound retinal degradation, but no signs of neurodegenerative or behavioral changes were detected [268]. Importantly, one study examining Ubqln2 KO and P497S overexpressing rats discovered cognitive deficits and neuronal loss in mutant Ubqln2 rats, but no abnormalities in Ubqln2 KO rats [267]. Taken together, the data from these studies provide both evidence for a loss-of-function and a toxic gain-of-function mechanism as illustrated in Figure 4-2. Since both, a simple loss-of-function and a sole gain-of-function toxicity seem unlikely, it is hypothesized that UBQLN2-linked ALS/FTD is driven by a coalescence of both [293].

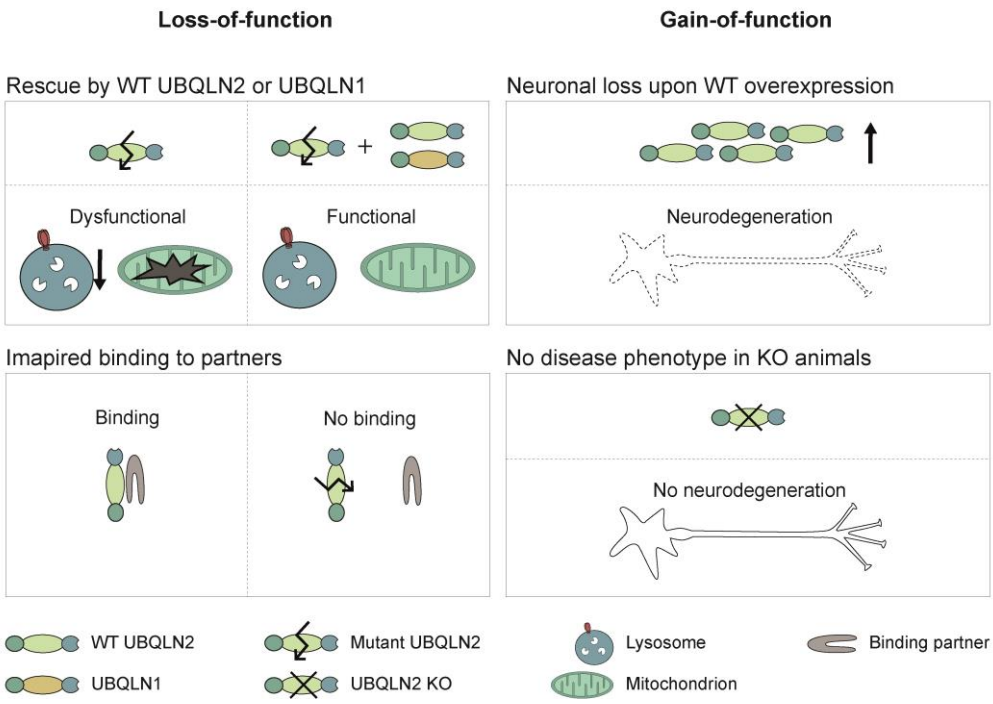


**Figure 4-2: Illustration of indications from the literature arguing either for a loss- or a gain-of-function of mutant UBQLN2.**
Rescue of defects observed in UBQLN2 mutants by UBQLN1 or WT UBQLN2 indicate a loss-of-function mutation. Impaired interaction of mutant UBQLN2 with typical binding partner also support a loss-of-function mechanism. On the other side, neuronal loss upon WT overexpression but no detection of neurodegeneration in UBQLN2 KO animals suggest a gain-of-function mechanism.

## 4.5 FUS S439 phosphorylation and its disease relevance

The initial objective of the phosphoproteomic experiment was to identify changes in phosphorylation in MAP1B. However, an interesting finding that emerged from deeper analysis of this data set was the significant dephosphorylation of pS439 in FUS in patient-derived UBQLN2 mutant cells. This phosphosite was reported before, for example in the context of breast cancer, but did not receive any attention [294, 295]. The situation is different for phosphosites in the low-complexity domain of FUS, which mediates LLPS [296]. Changes in phosphorylation in the low-complexity domain are suggested to lead to reduced phase separation and aggregation eventually seeding FUS inclusions in ALS/FTD [297]. The S439 phosphosite, however, is located in FUS' zinc finger domain, the domain which is–together with the RRM domain–responsible for RNA-binding [266, 298]. Due to its localization in such a relevant domain, changes in FUS S439 phosphorylation could have severe consequences. However, a note of caution is needed, since validation of changes in pS439 are limited to observations seen in Phos-tag™ gels. Phos-tag™ gels allow to detect general changes in phosphorylation. In this work, reduced phosphorylation of FUS was uncovered in patient-derived cells carrying mutant UBQLN2. While no other FUS phosphosite was found to be significantly changed in the phosphoproteomic data set, we speculate that the observed

phosphorylated band represents FUS phosphorylated at S439. Its down-regulation in the mutant cells further argues for this assumption. Yet, it remains to be independently demonstrated that the observed band indeed depicts FUS phosphorylated at S439. Thus, this is an important issue for future research. In this regard the development of a phospho-specific antibody able to detect phosphorylation of FUS S439 is of high importance. Such an antibody would facilitate the validation of FUS pS439 dephosphorylation in patient-derived UBQLN2 mutant cells. Furthermore, it would allow the examination of this site in patient material of UBQLN2-linked but also other ALS/FTD cases as well as in ALS/FTD animal models.

## 4.6 Consequences of altered FUS S439 phosphorylation and effects on MAP1B

Since no phospho-specific FUS antibody targeting pS439 is yet available, we aimed to decipher if altered phosphorylation of FUS S439 results in any changes of FUS-RNA-binding. For this, electrophoretic mobility shift assay (EMSA) experiments with the phospho-mimetic S439E, the phospho-deficient S439A and the WT FUS protein variant were performed. *In vitro* unphosphorylated WT FUS as well as the S439A variant showed clear binding to a known FUS RNA substrate: the SON pre-mRNA consisting of a stem-loop and a downstream GUU [266]. Strikingly, the phospho-mimetic S439E variant did not bind this substrate. According to these data, we inferred that phosphorylation of S439 affects FUS' RNA-binding capacity. This is also in line with a recent publication emphasizing the importance of phosphorylation events in RBPs in regulating RNA-binding and splicing [299]. However, our finding is somewhat limited by the investigation of only one RNA substrate model. FUS was reported to bind a large variety of RNA motifs possibly in different manners [266]. It cannot be concluded that phosphorylation of FUS S439 has the identical effect on its binding to all substrates. In contrary, it even seems possible that changes in phosphorylation of S439 are a deciding factor influencing which RNA substrate does or does not bind to FUS.

We hypothesized that FUS mediates the increase of MAP1B observed in UBQLN2 mutant lines. In cell culture experiments, overexpressing HA-tagged WT FUS in FUS KD cells reversed elevated MAP1B levels. On the other hand, overexpression of HA-tagged FUS S439A was not capable of reducing MAP1B abundance. Thus, we provide evidence that alterations in FUS S439 phosphorylation influence MAP1B protein levels. In more detail, S439 phosphorylation, alleged to be present in non-disease conditions, is associated with steady-state MAP1B levels, whereas FUS hypophosphorylation results in elevated MAP1B abundance. These findings raise the question how MAP1B abundance is regulated by changes in FUS S439 phosphorylation. There are several possible explanations. For example, a direct regulation via an interaction of FUS and *MAP1B* mRNA that is dependent on the

phosphorylation of S439 is conceivable. This option is supported by studies, demonstrating the capacity of FUS to bind *MAP1B* mRNA and to regulate its translation [92, 263]. In this case, it would also remain to be clarified whether S439A phosphorylation results in increased or decreased binding of *MAP1B* mRNA and what consequences this might have on its translation. On the other hand, it is also plausible that MAP1B abundance changes are a downstream effect of alterations of another FUS target. Accordingly, this is an important issue for future research. The binding capacity of FUS variants (WT and S439E) to *MAP1B* mRNA could easily be assessed by EMSA experiments which would provide crucial insights in this aspect.

The observed impact of FUS S439 phosphorylation on its RNA-binding capacity offers an explanation for the different effects of reduced FUS levels. On first sight it appears conflicting, that we found decreased MAP1B levels upon knockdown of FUS in a UBQLN2 KO background, while detecting an elevation of MAP1B abundance in a WT background after depleting FUS. To resolve this discrepancy, the FUS S439 phosphorylation state needs to be considered. Hypophosphorylation of FUS S439 in ALS/FTD-patient-derived cells indicate that FUS is phosphorylated in WT cells. Assuming similar appearance of FUS in UBQLN2 KO cells as in UBQLN2 mutant cells, FUS is hypophosphorylated at S439 in UBQLN2 KO cells. Accordingly, in UBQLN2 KO cells, the hypophosphorylated FUS form was reduced, while in WT cells the phosphorylated form was depleted (Figure 4-3). Importantly, this explanation is based on a number of assumptions and requires further inspection.

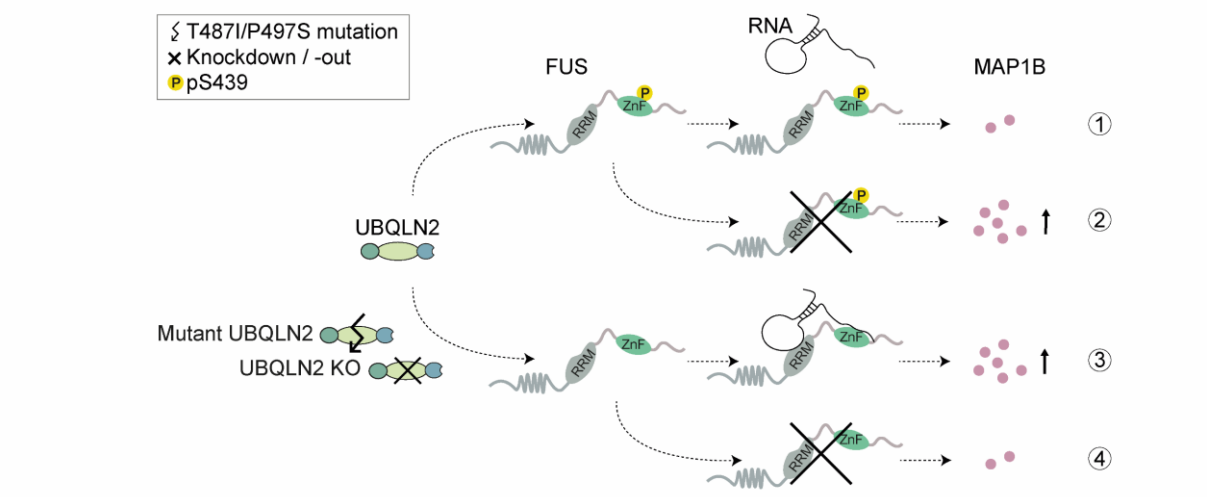


**Figure 4-3: Schematic model illustrating effects of UBQLN2 modifications on FUS phosphorylation and changes in MAP1B abundance upon FUS alterations.**
**(1)** FUS-RNA-binding is impaired in UBQLN2 WT cells where S439 is constitutively phosphorylated. **(2)** Depletion of FUS in a WT UBQLN2 background results in elevated MAP1B levels. **(3)** FUS S439 is hypophosphorylated in T487I and P497S UBQLN2 mutants which show increased MAP1B protein levels, also detected upon UBQLN2 depletion. **(4)** Depletion of FUS in a UBQLN2 KO background rescues the MAP1B phenotype.

## 4.7 UBQLN2 mutations affect FUS phosphorylation

In this work, we provide evidence for a hypophosphorylation of FUS S439 as a consequence of ALS/FTD-associated mutations in UBQLN2. However, how UBQLN2 mutations result in this change in phosphorylation remains elusive. From the data presented here, it can only be assumed that this dephosphorylation is due to a loss-of-function of UBQLN2. Nonetheless, several factors support the hypothesis that UBQLN2 indeed can influence FUS phosphorylation. In fact, UBQLN2 was reported to undergo LLPS and to localize to stress granules [169]. Thereby, UBQLN2 is known to be able to locate to a cellular compartment, where also FUS is found. Furthermore, UBQLN2 was reported to associate with FUS in stress granules and regulate FUS-RNA interaction [170]. Accordingly, those findings support our hypothesis that UBQLN2 can influence FUS phosphorylation, possibly promoting it even through a direct interaction with FUS. In addition, the observation by Alexander et al., showing that ALS/FTD-linked mutations in UBQLN2 impair its association with FUS and thus its ability in regulating FUS-RNA-binding, further underpins our findings [170]. Besides changes in FUS phosphorylation mediated possibly through a direct interaction of FUS and UBQLN2, also a more indirect regulation is conceivable. Since UBQLN2 facilitates the proteasomal degradation of multiple proteins as an Ub-shuttle factor, it seems plausible that mutations in UBQLN2 alter the degradation of kinases or phosphatases. In turn, resulting changes in kinase or phosphatase protein levels could cause alterations in phosphorylation of target proteins. In fact, mutated or depleted UBQLN2 was already associated with changes in phosphorylation in the past. For example, knockdown of UBQLN2 decreased the phosphorylation of the mTORC1 target eIF4E-binding protein 1 (4EBP1) [300]. Similarly, diminished phosphorylation of 4EBP but also of S6 kinase and the protein kinase B (Akt), targets of mTORC1 and 2 respectively, were detected in drosophila with dUbqn ablation [160]. Finally, a recent study showed that imbalance of UBQLN2 results also in altered tau phosphorylation [301]. Overall, available literature concurs with our hypothesis that UBQLN2 mutations lead to hypophosphorylated FUS at pS439. However, so far it can only be speculated how mutations in UBQLN2 induce this outcome (Figure 4-4). Thus, future studies will be required to determine the mechanism, how ALS/FTD-linked UBQLN2 mutations result in pS439 dephosphorylation. The availability of a phospho-specific antibody targeting pS439 would facilitate the achievement of this aim extremely by allowing to screen for kinases and phosphatases regulating this specific phosphorylation.

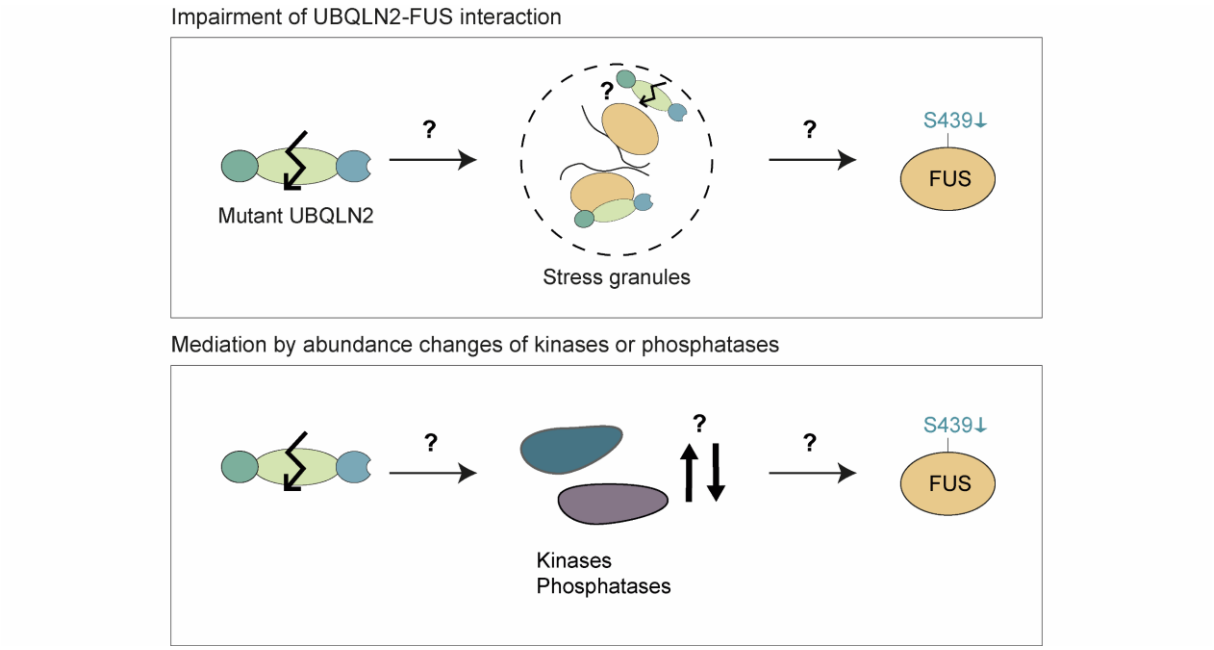


**Figure 4-4: Illustration of two possible scenarios how mutations in UBQLN2 result in FUS pS439 dephosphorylation.**
WT UBQLN2 was reported to bind FUS in stress granules. Mutant UBQLN2 possible perturbs this interaction somehow resulting in changes in FUS pS439. Besides this comparatively direct mechanism, mutated UBQLN2 might result in changed abundance levels of kinases or phosphatases responsible for FUS S439 phosphorylation.

# 5 References


1. GBD 2016 Motor Neuron Disease Collaborators, *Global, regional, and national burden of motor neuron diseases 1990-2016: a systematic analysis for the Global Burden of Disease Study 2016.* Lancet Neurol, 2018. **17**(12): p. 1083-1097.
2. Brown, R.H., Jr. and A. Al-Chalabi, *Amyotrophic Lateral Sclerosis.* N Engl J Med, 2017. **377**(16): p. 1602.
3. Niedermeyer, S., M. Murn, and P.J. Choi, *Respiratory Failure in Amyotrophic Lateral Sclerosis.* Chest, 2019. **155**(2): p. 401-408.
4. Lomen-Hoerth, C., et al., *Are amyotrophic lateral sclerosis patients cognitively normal?* Neurology, 2003. **60**(7): p. 1094-7.
5. Ringholz, G.M., et al., *Prevalence and patterns of cognitive impairment in sporadic ALS.* Neurology, 2005. **65**(4): p. 586-90.
6. Bang, J., S. Spina, and B.L. Miller, *Frontotemporal dementia.* Lancet, 2015. **386**(10004): p. 1672-82.
7. Olney, N.T., S. Spina, and B.L. Miller, *Frontotemporal Dementia.* Neurol Clin, 2017. **35**(2): p. 339-374.
8. Lomen-Hoerth, C., *Clinical phenomenology and neuroimaging correlates in ALS-FTD.* J Mol Neurosci, 2011. **45**(3): p. 656-62.
9. Neumann, M., et al., *Ubiquitinated TDP-43 in frontotemporal lobar degeneration and amyotrophic lateral sclerosis.* Science, 2006. **314**(5796): p. 130-3.
10. Arai, T., et al., *TDP-43 is a component of ubiquitin-positive tau-negative inclusions in frontotemporal lobar degeneration and amyotrophic lateral sclerosis.* Biochem Biophys Res Commun, 2006. **351**(3): p. 602-11.
11. Deng, H.X., et al., *FUS-immunoreactive inclusions are a common feature in sporadic and non-SOD1 familial amyotrophic lateral sclerosis.* Ann Neurol, 2010. **67**(6): p. 739-48.
12. Neumann, M., et al., *A new subtype of frontotemporal lobar degeneration with FUS pathology.* Brain, 2009. **132**(Pt 11): p. 2922-31.
13. Ling, S.C., M. Polymenidou, and D.W. Cleveland, *Converging mechanisms in ALS and FTD: disrupted RNA and protein homeostasis.* Neuron, 2013. **79**(3): p. 416-38.
14. Olszewska, D.A., et al., *Genetics of Frontotemporal Dementia.* Curr Neurol Neurosci Rep, 2016. **16**(12): p. 107.
15. Rohrer, J.D., et al., *The heritability and genetics of frontotemporal lobar degeneration.* Neurology, 2009. **73**(18): p. 1451-6.
16. Chow, T.W., et al., *Inheritance of frontotemporal dementia.* Arch Neurol, 1999. **56**(7): p. 817-22.
17. Byrne, S., et al., *Rate of familial amyotrophic lateral sclerosis: a systematic review and meta-analysis.* J Neurol Neurosurg Psychiatry, 2011. **82**(6): p. 623-7.
18. Casterton, R.L., R.J. Hunt, and M. Fanto, *Pathomechanism Heterogeneity in the Amyotrophic Lateral Sclerosis and Frontotemporal Dementia Disease Spectrum: Providing Focus Through the Lens of Autophagy.* J Mol Biol, 2020. **432**(8): p. 2692-2713.
19. Ji, A.L., et al., *Genetics insight into the amyotrophic lateral sclerosis/frontotemporal dementia spectrum.* J Med Genet, 2017. **54**(3): p. 145-154.
20. Kumar, V., et al., *Delineating the relationship between amyotrophic lateral sclerosis and frontotemporal dementia: Sequence and structure-based predictions.* Biochim Biophys Acta, 2016. **1862**(9): p. 1742-54.
21. Radford, R.A., et al., *The established and emerging roles of astrocytes and microglia in amyotrophic lateral sclerosis and frontotemporal dementia.* Front Cell Neurosci, 2015. **9**: p. 414.
22. Shahheydari, H., et al., *Protein Quality Control and the Amyotrophic Lateral Sclerosis/Frontotemporal Dementia Continuum.* Front Mol Neurosci, 2017. **10**: p. 119.
23. Broustal, O., et al., *FUS mutations in frontotemporal lobar degeneration with amyotrophic lateral sclerosis.* J Alzheimers Dis, 2010. **22**(3): p. 765-9.

24. Huey, E.D., et al., *FUS and TDP43 genetic variability in FTD and CBS.* Neurobiol Aging, 2012. **33**(5): p. 1016 e9-17.
25. Kabashi, E., et al., *TARDBP mutations in individuals with sporadic and familial amyotrophic lateral sclerosis.* Nat Genet, 2008. **40**(5): p. 572-4.
26. Kovacs, G.G., et al., *TARDBP variation associated with frontotemporal dementia, supranuclear gaze palsy, and chorea.* Mov Disord, 2009. **24**(12): p. 1843-7.
27. Kwiatkowski, T.J., Jr., et al., *Mutations in the FUS/TLS gene on chromosome 16 cause familial amyotrophic lateral sclerosis.* Science, 2009. **323**(5918): p. 1205-8.
28. Sreedharan, J., et al., *TDP-43 mutations in familial and sporadic amyotrophic lateral sclerosis.* Science, 2008. **319**(5870): p. 1668-72.
29. Vance, C., et al., *Mutations in FUS, an RNA processing protein, cause familial amyotrophic lateral sclerosis type 6.* Science, 2009. **323**(5918): p. 1208-1211.
30. Rosen, D.R., et al., *Mutations in Cu/Zn superoxide dismutase gene are associated with familial amyotrophic lateral sclerosis.* Nature, 1993. **362**(6415): p. 59-62.
31. Nishimura, A.L., et al., *A mutation in the vesicle-trafficking protein VAPB causes late-onset spinal muscular atrophy and amyotrophic lateral sclerosis.* Am J Hum Genet, 2004. **75**(5): p. 822-31.
32. Maruyama, H., et al., *Mutations of optineurin in amyotrophic lateral sclerosis.* Nature, 2010. **465**(7295): p. 223-6.
33. Kim, H.J., et al., *Mutations in prion-like domains in hnRNPA2B1 and hnRNPA1 cause multisystem proteinopathy and ALS.* Nature, 2013. **495**(7442): p. 467-473.
34. Cirulli, E.T., et al., *Exome sequencing in amyotrophic lateral sclerosis identifies risk genes and pathways.* Science, 2015. **347**(6229): p. 1436-41.
35. Deng, H.X., et al., *Mutations in UBQLN2 cause dominant X-linked juvenile and adult-onset ALS and ALS/dementia.* Nature, 2011. **477**(7363): p. 211-5.
36. Fecto, F., et al., *SQSTM1 mutations in familial and sporadic amyotrophic lateral sclerosis.* Arch Neurol, 2011. **68**(11): p. 1440-6.
37. Rubino, E., et al., *SQSTM1 mutations in frontotemporal lobar degeneration and amyotrophic lateral sclerosis.* Neurology, 2012. **79**(15): p. 1556-62.
38. Watts, G.D., et al., *Inclusion body myopathy associated with Paget disease of bone and frontotemporal dementia is caused by mutant valosin-containing protein.* Nat Genet, 2004. **36**(4): p. 377-81.
39. Mol, M.O., et al., *Novel TUBA4A Variant Associated With Familial Frontotemporal Dementia.* Neurol Genet, 2021. **7**(3): p. e596.
40. Perrone, F., et al., *Investigating the role of ALS genes CHCHD10 and TUBA4A in Belgian FTD-ALS spectrum patients.* Neurobiol Aging, 2017. **51**: p. 177 e9-177 e16.
41. Smith, B.N., et al., *Exome-wide rare variant analysis identifies TUBA4A mutations associated with familial ALS.* Neuron, 2014. **84**(2): p. 324-31.
42. Baker, M., et al., *Mutations in progranulin cause tau-negative frontotemporal dementia linked to chromosome 17.* Nature, 2006. **442**(7105): p. 916-9.
43. Hutton, M., et al., *Association of missense and 5'-splice-site mutations in tau with the inherited dementia FTDP-17.* Nature, 1998. **393**(6686): p. 702-5.
44. Cruts, M., et al., *Null mutations in progranulin cause ubiquitin-positive frontotemporal dementia linked to chromosome 17q21.* Nature, 2006. **442**(7105): p. 920-4.
45. Skibinski, G., et al., *Mutations in the endosomal ESCRTIII-complex subunit CHMP2B in frontotemporal dementia.* Nat Genet, 2005. **37**(8): p. 806-8.
46. Borroni, B., et al., *Heterozygous TREM2 mutations in frontotemporal dementia.* Neurobiol Aging, 2014. **35**(4): p. 934 e7-10.
47. Williams, K.L., et al., *CCNF mutations in amyotrophic lateral sclerosis and frontotemporal dementia.* Nat Commun, 2016. **7**: p. 11253.
48. Nguyen, H.P., C. Van Broeckhoven, and J. van der Zee, *ALS Genes in the Genomic Era and their Implications for FTD.* Trends Genet, 2018. **34**(6): p. 404-423.
49. Liscic, R.M., et al., *From basic research to the clinic: innovative therapies for ALS and FTD in the pipeline.* Mol Neurodegener, 2020. **15**(1): p. 31.
50. Ayala, Y.M., et al., *Structural determinants of the cellular localization and shuttling of TDP-43.* J Cell Sci, 2008. **121**(Pt 22): p. 3778-85.

51. Zinszner, H., et al., *TLS (FUS) binds RNA in vivo and engages in nucleo-cytoplasmic shuttling.* J Cell Sci, 1997. **110 ( Pt 15)**: p. 1741-50.
52. Bampton, A., et al., *The role of hnRNPs in frontotemporal dementia and amyotrophic lateral sclerosis.* Acta Neuropathol, 2020. **140**(5): p. 599-623.
53. Kato, M. and S.L. McKnight, *The low-complexity domain of the FUS RNA binding protein self-assembles via the mutually exclusive use of two distinct cross-β cores.* Proceedings of the National Academy of Sciences, 2021. **118**(42): p. e2114412118.
54. Morohoshi, F., et al., *Genomic structure of the human RBP56/hTAFII68 and FUS/TLS genes.* Gene, 1998. **221**(2): p. 191-8.
55. Ou, S.H., et al., *Cloning and characterization of a novel cellular protein, TDP-43, that binds to human immunodeficiency virus type 1 TAR DNA sequence motifs.* J Virol, 1995. **69**(6): p. 3584-96.
56. Casafont, I., et al., *TDP-43 localizes in mRNA transcription and processing sites in mammalian neurons.* J Struct Biol, 2009. **167**(3): p. 235-41.
57. Lalmansingh, A.S., C.J. Urekar, and P.P. Reddi, *TDP-43 is a transcriptional repressor: the testis-specific mouse acrv1 gene is a TDP-43 target in vivo.* J Biol Chem, 2011. **286**(13): p. 10970-82.
58. Freibaum, B.D., et al., *Global Analysis of TDP-43 Interacting Proteins Reveals Strong Association with RNA Splicing and Translation Machinery.* Journal of Proteome Research, 2010. **9**(2): p. 1104-1120.
59. Bertolotti, A., et al., *hTAF(II)68, a novel RNA/ssDNA-binding protein with homology to the pro-oncoproteins TLS/FUS and EWS is associated with both TFIID and RNA polymerase II.* EMBO J, 1996. **15**(18): p. 5022-31.
60. Bronisz, A., et al., *The multifunctional protein fused in sarcoma (FUS) is a coactivator of microphthalmia-associated transcription factor (MITF).* J Biol Chem, 2014. **289**(1): p. 326-34.
61. Dhar, S.K., et al., *FUsed in sarcoma is a novel regulator of manganese superoxide dismutase gene transcription.* Antioxid Redox Signal, 2014. **20**(10): p. 1550-66.
62. Yang, L., et al., *Self-assembled FUS binds active chromatin and regulates gene transcription.* Proc Natl Acad Sci U S A, 2014. **111**(50): p. 17809-14.
63. Tan, A.Y., et al., *TLS/FUS (translocated in liposarcoma/fused in sarcoma) regulates target gene transcription via single-stranded DNA response elements.* Proc Natl Acad Sci U S A, 2012. **109**(16): p. 6030-5.
64. Schwartz, J.C., et al., *FUS binds the CTD of RNA polymerase II and regulates its phosphorylation at Ser2.* Genes Dev, 2012. **26**(24): p. 2690-5.
65. Lagier-Tourenne, C., et al., *Divergent roles of ALS-linked proteins FUS/TLS and TDP-43 intersect in processing long pre-mRNAs.* Nat Neurosci, 2012. **15**(11): p. 1488-97.
66. Avendano-Vazquez, S.E., et al., *Autoregulation of TDP-43 mRNA levels involves interplay between transcription, splicing, and alternative polyA site selection.* Genes Dev, 2012. **26**(15): p. 1679-84.
67. Ayala, Y.M., et al., *TDP-43 regulates its mRNA levels through a negative feedback loop.* EMBO J, 2011. **30**(2): p. 277-88.
68. Bose, J.K., et al., *TDP-43 overexpression enhances exon 7 inclusion during the survival of motor neuron pre-mRNA splicing.* J Biol Chem, 2008. **283**(43): p. 28852-9.
69. Buratti, E., et al., *Nuclear factor TDP-43 and SR proteins promote in vitro and in vivo CFTR exon 9 skipping.* EMBO J, 2001. **20**(7): p. 1774-84.
70. Fiesel, F.C., et al., *TDP-43 regulates global translational yield by splicing of exon junction complex component SKAR.* Nucleic Acids Res, 2012. **40**(6): p. 2668-82.
71. Ling, J.P., et al., *TDP-43 repression of nonconserved cryptic exons is compromised in ALS-FTD.* Science, 2015. **349**(6248): p. 650-5.
72. Mercado, P.A., et al., *Depletion of TDP 43 overrides the need for exonic and intronic splicing enhancers in the human apoA-II gene.* Nucleic Acids Res, 2005. **33**(18): p. 6000-10.
73. Polymenidou, M., et al., *Long pre-mRNA depletion and RNA missplicing contribute to neuronal vulnerability from loss of TDP-43.* Nat Neurosci, 2011. **14**(4): p. 459-68.

74. Sephton, C.F., et al., *Identification of neuronal RNA targets of TDP-43-containing ribonucleoprotein complexes.* J Biol Chem, 2011. **286**(2): p. 1204-15.
75. Tollervey, J.R., et al., *Characterizing the RNA targets and position-dependent splicing regulation by TDP-43.* Nat Neurosci, 2011. **14**(4): p. 452-8.
76. Rappsilber, J., et al., *Large-scale proteomic analysis of the human spliceosome.* Genome Res, 2002. **12**(8): p. 1231-45.
77. Meissner, M., et al., *Proto-oncoprotein TLS/FUS is associated to the nuclear matrix and complexed with splicing factors PTB, SRm160, and SR proteins.* Exp Cell Res, 2003. **283**(2): p. 184-95.
78. Zhou, Z., et al., *Comprehensive proteomic analysis of the human spliceosome.* Nature, 2002. **419**(6903): p. 182-5.
79. Hoell, J.I., et al., *RNA targets of wild-type and mutant FET family proteins.* Nat Struct Mol Biol, 2011. **18**(12): p. 1428-31.
80. Udagawa, T., et al., *FUS regulates AMPA receptor function and FTLD/ALS-associated behaviour via GluA1 mRNA stabilization.* Nat Commun, 2015. **6**: p. 7098.
81. Yokoi, S., et al., *3'UTR Length-Dependent Control of SynGAP Isoform alpha2 mRNA by FUS and ELAV-like Proteins Promotes Dendritic Spine Maturation and Cognitive Function.* Cell Rep, 2017. **20**(13): p. 3071-3084.
82. Rogelj, B., et al., *Widespread binding of FUS along nascent RNA regulates alternative splicing in the brain.* Sci Rep, 2012. **2**: p. 603.
83. Dalla Costa, I., et al., *The functional organization of axonal mRNA transport and translation.* Nat Rev Neurosci, 2021. **22**(2): p. 77-91.
84. Nagano, S., et al., *TDP-43 transports ribosomal protein mRNA to regulate axonal local translation in neuronal axons.* Acta Neuropathologica, 2020. **140**(5): p. 695-713.
85. Chu, J.-F., et al., *TDP-43 Regulates Coupled Dendritic mRNA Transport-Translation Processes in Co-operation with FMRP and Staufen1.* Cell Reports, 2019. **29**(10): p. 3118-3133.e6.
86. Kanai, Y., N. Dohmae, and N. Hirokawa, *Kinesin transports RNA: isolation and characterization of an RNA-transporting granule.* Neuron, 2004. **43**(4): p. 513-25.
87. Fujii, R. and T. Takumi, *TLS facilitates transport of mRNA encoding an actin-stabilizing protein to dendritic spines.* Journal of Cell Science, 2005. **118**(24): p. 5755-5765.
88. Yoshimura, A., et al., *Myosin-Va facilitates the accumulation of mRNA/protein complex in dendritic spines.* Curr Biol, 2006. **16**(23): p. 2345-51.
89. Kim, S.H., et al., *Amyotrophic lateral sclerosis-associated proteins TDP-43 and FUS/TLS function in a common biochemical complex to co-regulate HDAC6 mRNA.* J Biol Chem, 2010. **285**(44): p. 34097-105.
90. Kamelgarn, M., et al., *ALS mutations of FUS suppress protein translation and disrupt the regulation of nonsense-mediated decay.* Proc Natl Acad Sci U S A, 2018. **115**(51): p. E11904-E11913.
91. Sevigny, M., et al., *FUS contributes to mTOR-dependent inhibition of translation.* J Biol Chem, 2020. **295**(52): p. 18459-18473.
92. Blokhuis, A.M., et al., *Comparative interactomics analysis of different ALS-associated proteins identifies converging molecular pathways.* Acta Neuropathol, 2016. **132**(2): p. 175-196.
93. Darnell, J.C., et al., *FMRP stalls ribosomal translocation on mRNAs linked to synaptic function and autism.* Cell, 2011. **146**(2): p. 247-61.
94. Li, Z., et al., *The fragile X mental retardation protein inhibits translation via interacting with mRNA.* Nucleic Acids Res, 2001. **29**(11): p. 2276-83.
95. Lu, R., et al., *The fragile X protein controls microtubule-associated protein 1B translation and microtubule stability in brain neuron development.* Proc Natl Acad Sci U S A, 2004. **101**(42): p. 15201-6.
96. Majumder, P., et al., *Co-regulation of mRNA translation by TDP-43 and Fragile X Syndrome protein FMRP.* Acta Neuropathol, 2016. **132**(5): p. 721-738.
97. Jain, S., et al., *ATPase-Modulated Stress Granules Contain a Diverse Proteome and Substructure.* Cell, 2016. **164**(3): p. 487-98.

98. Groen, E.J., et al., *ALS-associated mutations in FUS disrupt the axonal distribution and function of SMN.* Hum Mol Genet, 2013. **22**(18): p. 3690-704.
99. Tischbein, M., et al., *The RNA-binding protein FUS/TLS undergoes calcium-mediated nuclear egress during excitotoxic stress and is required for GRIA2 mRNA processing.* J Biol Chem, 2019. **294**(26): p. 10194-10210.
100. Vance, C., et al., *ALS mutant FUS disrupts nuclear localization and sequesters wild-type FUS within cytoplasmic stress granules.* Hum Mol Genet, 2013. **22**(13): p. 2676-88.
101. Johnson, B.S., et al., *TDP-43 is intrinsically aggregation-prone, and amyotrophic lateral sclerosis-linked mutations accelerate aggregation and increase toxicity.* J Biol Chem, 2009. **284**(30): p. 20329-39.
102. Dormann, D., et al., *ALS-associated fused in sarcoma (FUS) mutations disrupt Transportin-mediated nuclear import.* EMBO J, 2010. **29**(16): p. 2841-57.
103. Liu-Yesucevitz, L., et al., *Tar DNA binding protein-43 (TDP-43) associates with stress granules: analysis of cultured cells and pathological brain tissue.* PLoS One, 2010. **5**(10): p. e13250.
104. Dormann, D. and C. Haass, *TDP-43 and FUS: a nuclear affair.* Trends Neurosci, 2011. **34**(7): p. 339-48.
105. Bosco, D.A., et al., *Mutant FUS proteins that cause amyotrophic lateral sclerosis incorporate into stress granules.* Human Molecular Genetics, 2010. **19**(21): p. 4160-4175.
106. Gasset-Rosa, F., et al., *Cytoplasmic TDP-43 De-mixing Independent of Stress Granules Drives Inhibition of Nuclear Import, Loss of Nuclear TDP-43, and Cell Death.* Neuron, 2019. **102**(2): p. 339-357 e7.
107. Paschal, B.M. and R.B. Vallee, *Retrograde transport by the microtubule-associated protein MAP 1C.* Nature, 1987. **330**(6144): p. 181-183.
108. Schroer, T.A., E.R. Steuer, and M.P. Sheetz, *Cytoplasmic dynein is a minus end-directed motor for membranous organelles.* Cell, 1989. **56**(6): p. 937-946.
109. Vale, R.D., T.S. Reese, and M.P. Sheetz, *Identification of a novel force-generating protein, kinesin, involved in microtubule-based motility.* Cell, 1985. **42**(1): p. 39-50.
110. Keates, R.A.B. and R.H. Hall, *Tubulin requires an accessory protein for self assembly into microtubules.* Nature, 1975. **257**(5525): p. 418-421.
111. Murphy, D.B. and G.G. Borisy, *Association of high-molecular-weight proteins with microtubules and their role in microtubule assembly in vitro.* Proceedings of the National Academy of Sciences, 1975. **72**(7): p. 2696-2700.
112. L'Hernault, S.W. and J.L. Rosenbaum, *Chlamydomonas alpha-tubulin is posttranslationally modified by acetylation on the epsilon-amino group of a lysine.* Biochemistry, 1985. **24**(2): p. 473-8.
113. Takemura, R., et al., *Increased microtubule stability and alpha tubulin acetylation in cells transfected with microtubule-associated proteins MAP1B, MAP2 or tau.* J Cell Sci, 1992. **103 ( Pt 4)**: p. 953-64.
114. Gundersen, G.G., M.H. Kalnoski, and J.C. Bulinski, *Distinct populations of microtubules: tyrosinated and nontyrosinated alpha tubulin are distributed differently in vivo.* Cell, 1984. **38**(3): p. 779-89.
115. Brown, A., et al., *Composite microtubules of the axon: quantitative analysis of tyrosinated and acetylated tubulin along individual axonal microtubules.* J Cell Sci, 1993. **104 ( Pt 2)**: p. 339-52.
116. Kapitein, L.C. and C.C. Hoogenraad, *Building the Neuronal Microtubule Cytoskeleton.* Neuron, 2015. **87**(3): p. 492-506.
117. Alonso, A.C., et al., *Role of abnormally phosphorylated tau in the breakdown of microtubules in Alzheimer disease.* Proc Natl Acad Sci U S A, 1994. **91**(12): p. 5562-6.
118. Wagner, U., et al., *Cellular phosphorylation of tau by GSK-3 beta influences tau binding to microtubules and microtubule organisation.* J Cell Sci, 1996. **109 ( Pt 6)**: p. 1537-43.
119. Dubey, J., N. Ratnakaran, and S.P. Koushika, *Neurodegeneration and microtubule dynamics: death by a thousand cuts.* Front Cell Neurosci, 2015. **9**: p. 343.

120. De Vos, K.J., et al., *Familial amyotrophic lateral sclerosis-linked SOD1 mutants perturb fast axonal transport to reduce axonal mitochondria content.* Human Molecular Genetics, 2007. **16**(22): p. 2720-2728.
121. Williamson, T.L. and D.W. Cleveland, *Slowing of axonal transport is a very early event in the toxicity of ALS–linked SOD1 mutants to motor neurons.* Nature Neuroscience, 1999. **2**(1): p. 50-56.
122. Nicolas, A., et al., *Genome-wide Analyses Identify KIF5A as a Novel ALS Gene.* Neuron, 2018. **97**(6): p. 1268-1283 e6.
123. Munch, C., et al., *Point mutations of the p150 subunit of dynactin (DCTN1) gene in ALS.* Neurology, 2004. **63**(4): p. 724-6.
124. Wu, C.H., et al., *Mutations in the profilin 1 gene cause familial amyotrophic lateral sclerosis.* Nature, 2012. **488**(7412): p. 499-503.
125. Meyer, T., et al., *Early-onset ALS with long-term survival associated with spastin gene mutation.* Neurology, 2005. **65**(1): p. 141-3.
126. Jentsch, S., *The ubiquitin-conjugation system.* Annu Rev Genet, 1992. **26**: p. 179-207.
127. Martinez-Fonts, K., et al., *The proteasome 19S cap and its ubiquitin receptors provide a versatile recognition platform for substrates.* Nat Commun, 2020. **11**(1): p. 477.
128. Bhattacharyya, S., et al., *Regulated protein turnover: snapshots of the proteasome in action.* Nat Rev Mol Cell Biol, 2014. **15**(2): p. 122-33.
129. Rousseau, A. and A. Bertolotti, *Regulation of proteasome assembly and activity in health and disease.* Nat Rev Mol Cell Biol, 2018. **19**(11): p. 697-712.
130. Feng, Y., et al., *The machinery of macroautophagy.* Cell Res, 2014. **24**(1): p. 24-41.
131. Nishimura, T. and S.A. Tooze, *Emerging roles of ATG proteins and membrane lipids in autophagosome formation.* Cell Discov, 2020. **6**(1): p. 32.
132. Martens, S. and D. Fracchiolla, *Activation and targeting of ATG8 protein lipidation.* Cell Discov, 2020. **6**: p. 23.
133. Stolz, A., A. Ernst, and I. Dikic, *Cargo recognition and trafficking in selective autophagy.* Nat Cell Biol, 2014. **16**(6): p. 495-501.
134. Yim, W.W.-Y. and N. Mizushima, *Lysosome biology in autophagy.* Cell Discovery, 2020. **6**(1): p. 6.
135. Urushitani, M., et al., *Proteasomal inhibition by misfolded mutant superoxide dismutase 1 induces selective motor neuron death in familial amyotrophic lateral sclerosis.* J Neurochem, 2002. **83**(5): p. 1030-42.
136. Puttaparthi, K., et al., *Aggregate formation in the spinal cord of mutant SOD1 transgenic mice is reversible and mediated by proteasomes.* J Neurochem, 2003. **87**(4): p. 851-60.
137. Allen, S., et al., *Analysis of the Cytosolic Proteome in a Cell Culture Model of Familial Amyotrophic Lateral Sclerosis Reveals Alterations to the Proteasome, Antioxidant Defenses, and Nitric Oxide Synthetic Pathways*.* Journal of Biological Chemistry, 2003. **278**(8): p. 6371-6383.
138. Sellier, C., et al., *Loss of C9ORF72 impairs autophagy and synergizes with polyQ Ataxin-2 to induce motor neuron dysfunction and cell death.* EMBO J, 2016. **35**(12): p. 1276-97.
139. Jung, J., et al., *Multiplex image-based autophagy RNAi screening identifies SMCR8 as ULK1 kinase activity and gene expression regulator.* Elife, 2017. **6**.
140. Sullivan, P.M., et al., *The ALS/FTLD associated protein C9orf72 associates with SMCR8 and WDR41 to regulate the autophagy-lysosome pathway.* Acta Neuropathologica Communications, 2016. **4**(1): p. 51.
141. Rothenberg, C., et al., *Ubiquilin functions in autophagy and is degraded by chaperone-mediated autophagy.* Hum Mol Genet, 2010. **19**(16): p. 3219-32.
142. Marín, I., *The ubiquilin gene family: evolutionary patterns and functional insights.* BMC Evolutionary Biology, 2014. **14**(1): p. 63.
143. Uhlén, M., et al., *Tissue-based map of the human proteome.* Science, 2015. **347**(6220): p. 1260419.
144. Walters, K.J., et al., *Structural studies of the interaction between ubiquitin family proteins and proteasome subunit S5a.* Biochemistry, 2002. **41**(6): p. 1767-77.

145. Wu, A.L., et al., *Ubiquitin-related proteins regulate interaction of vimentin intermediate filaments with the plasma membrane.* Mol Cell, 1999. **4**(4): p. 619-25.
146. Kleijnen, M.F., et al., *The hPLIC Proteins May Provide a Link between the Ubiquitination Machinery and the Proteasome.* Molecular Cell, 2000. **6**(2): p. 409-419.
147. Elsasser, S., et al., *Proteasome subunit Rpn1 binds ubiquitin-like protein domains.* Nat Cell Biol, 2002. **4**(9): p. 725-30.
148. Funakoshi, M., et al., *Budding yeast Dsk2p is a polyubiquitin-binding protein that can interact with the proteasome.* Proceedings of the National Academy of Sciences, 2002. **99**(2): p. 745-750.
149. Saeki, Y., et al., *Identification of ubiquitin-like protein-binding subunits of the 26S proteasome.* Biochem Biophys Res Commun, 2002. **296**(4): p. 813-9.
150. Kaye, F.J., et al., *A family of ubiquitin-like proteins binds the ATPase domain of Hsp70-like Stch.* FEBS Letters, 2000. **467**(2): p. 348-355.
151. Hjerpe, R., et al., *UBQLN2 Mediates Autophagy-Independent Protein Aggregate Clearance by the Proteasome.* Cell, 2016. **166**(4): p. 935-949.
152. Zhang, K., et al., *UBQLN2-HSP70 axis reduces poly-Gly-Ala aggregates and alleviates behavioral defects in the C9ORF72 animal model.* Neuron, 2021. **109**(12): p. 1949-1962.e6.
153. Olzmann, J.A., R.R. Kopito, and J.C. Christianson, *The mammalian endoplasmic reticulum-associated degradation system.* Cold Spring Harb Perspect Biol, 2013. **5**(9).
154. Kim, T.Y., et al., *Herp enhances ER-associated protein degradation by recruiting ubiquilins.* Biochem Biophys Res Commun, 2008. **369**(2): p. 741-6.
155. Lim, P.J., et al., *Ubiquilin and p97/VCP bind erasin, forming a complex involved in ERAD.* J Cell Biol, 2009. **187**(2): p. 201-17.
156. Xia, Y., et al., *Pathogenic mutation of UBQLN2 impairs its interaction with UBXD8 and disrupts endoplasmic reticulum-associated protein degradation.* J Neurochem, 2014. **129**(1): p. 99-106.
157. N'Diaye, E.N., et al., *PLIC proteins or ubiquilins regulate autophagy-dependent cell survival during nutrient starvation.* EMBO Rep, 2009. **10**(2): p. 173-9.
158. Deng, Z., et al., *Autophagy Receptors and Neurodegenerative Diseases.* Trends Cell Biol, 2017. **27**(7): p. 491-504.
159. Herhaus, L., et al., *TBK1-mediated phosphorylation of LC3C and GABARAP-L2 controls autophagosome shedding by ATG4 protease.* EMBO reports, 2020. **21**(1): p. e48317.
160. Senturk, M., et al., *Ubiquilins regulate autophagic flux through mTOR signalling and lysosomal acidification.* Nat Cell Biol, 2019. **21**(3): p. 384-396.
161. Wu, J.J., et al., *ALS/FTD mutations in UBQLN2 impede autophagy by reducing autophagosome acidification through loss of function.* Proc Natl Acad Sci U S A, 2020. **117**(26): p. 15230-15241.
162. Pfanner, N., B. Warscheid, and N. Wiedemann, *Mitochondrial proteins: from biogenesis to functional networks.* Nature Reviews Molecular Cell Biology, 2019. **20**(5): p. 267-284.
163. Itakura, E., et al., *Ubiquilins Chaperone and Triage Mitochondrial Membrane Proteins for Degradation.* Mol Cell, 2016. **63**(1): p. 21-33.
164. Whiteley, A.M., et al., *Ubiquilin1 promotes antigen-receptor mediated proliferation by eliminating mislocalized mitochondrial proteins.* eLife, 2017. **6**: p. e26435.
165. Whiteley, A.M., et al., *Global proteomics of Ubqln2-based murine models of ALS.* J Biol Chem, 2021. **296**: p. 100153.
166. Lin, B.C., et al., *ALS/FTD mutations in UBQLN2 are linked to mitochondrial dysfunction through loss-of-function in mitochondrial protein import.* Hum Mol Genet, 2021. **30**(13): p. 1230-1246.
167. Tolay, N. and A. Buchberger, *Comparative profiling of stress granule clearance reveals differential contributions of the ubiquitin system.* Life Sci Alliance, 2021. **4**(5).
168. Maxwell, B.A., et al., *Ubiquitination is essential for recovery of cellular activities after heat shock.* Science, 2021. **372**(6549): p. eabc3593.

169. Dao, T.P., et al., *Ubiquitin Modulates Liquid-Liquid Phase Separation of UBQLN2 via Disruption of Multivalent Interactions.* Mol Cell, 2018. **69**(6): p. 965-978 e6.
170. Alexander, E.J., et al., *Ubiquilin 2 modulates ALS/FTD-linked FUS-RNA complex dynamics and stress granule formation.* Proc Natl Acad Sci U S A, 2018. **115**(49): p. E11485-E11494.
171. Kaye, F.J. and T.B. Shows, *Assignment of ubiquilin2 (UBQLN2) to human chromosome xp11. 23-->p11.1 by GeneBridge radiation hybrids.* Cytogenet Cell Genet, 2000. **89**(1-2): p. 116-7.
172. Fahed, A.C., et al., *UBQLN2 mutation causing heterogeneous X-linked dominant neurodegeneration.* Annals of neurology, 2014. **75**(5): p. 793-798.
173. Gellera, C., et al., *Ubiquilin 2 mutations in Italian patients with amyotrophic lateral sclerosis and frontotemporal dementia.* Journal of Neurology, Neurosurgery & Psychiatry, 2013. **84**(2): p. 183.
174. Teyssou, E., et al., *Novel UBQLN2 mutations linked to amyotrophic lateral sclerosis and atypical hereditary spastic paraplegia phenotype through defective HSP70-mediated proteolysis.* Neurobiol Aging, 2017. **58**: p. 239.e11-239.e20.
175. Millecamps, S., et al., *Mutations in UBQLN2 are rare in French amyotrophic lateral sclerosis.* Neurobiol Aging, 2012. **33**(4): p. 839.e1-3.
176. Synofzik, M., et al., *Screening in ALS and FTD patients reveals 3 novel UBQLN2 mutations outside the PXX domain and a pure FTD phenotype.* Neurobiol Aging, 2012. **33**(12): p. 2949.e13-7.
177. Daoud, H., et al., *UBQLN2 mutations are rare in French and French-Canadian amyotrophic lateral sclerosis.* Neurobiol Aging, 2012. **33**(9): p. 2230.e1-2230.e5.
178. Williams, K.L., et al., *UBQLN2/ubiquilin 2 mutation and pathology in familial amyotrophic lateral sclerosis.* Neurobiol Aging, 2012. **33**(10): p. 2527.e3-10.
179. Özoğuz, A., et al., *The distinct genetic pattern of ALS in Turkey and novel mutations.* Neurobiol Aging, 2015. **36**(4): p. 1764.e9-1764.e18.
180. Huang, X., S. Shen, and D. Fan, *No Evidence for Pathogenic Role of UBQLN2 Mutations in Sporadic Amyotrophic Lateral Sclerosis in the Mainland Chinese Population.* PLoS One, 2017. **12**(1): p. e0170943.
181. Dillen, L., et al., *Explorative genetic study of UBQLN2 and PFN1 in an extended Flanders-Belgian cohort of frontotemporal lobar degeneration patients.* Neurobiol Aging, 2013. **34**(6): p. 1711.e1-5.
182. Williams, K.L., et al., *UBQLN2/ubiquilin 2 mutation and pathology in familial amyotrophic lateral sclerosis.* Neurobiol Aging, 2012. **33**(10): p. 2527 e3-10.
183. Chang, L. and M.J. Monteiro, *Defective Proteasome Delivery of Polyubiquitinated Proteins by Ubiquilin-2 Proteins Containing ALS Mutations.* PLoS One, 2015. **10**(6): p. e0130162.
184. Osaka, M., D. Ito, and N. Suzuki, *Disturbance of proteasomal and autophagic protein degradation pathways by amyotrophic lateral sclerosis-linked mutations in ubiquilin 2.* Biochem Biophys Res Commun, 2016. **472**(2): p. 324-31.
185. Gorrie, G.H., et al., *Dendritic spinopathy in transgenic mice expressing ALS/dementia-linked mutant UBQLN2</em&gt.* Proceedings of the National Academy of Sciences, 2014. **111**(40): p. 14524.
186. Sharkey, L.M., et al., *Mutant UBQLN2 promotes toxicity by modulating intrinsic self-assembly.* Proceedings of the National Academy of Sciences, 2018. **115**(44): p. E10495.
187. Zhang, W., et al., *Impaired 26S Proteasome Assembly Precedes Neuronal Loss in Mutant UBQLN2 Rats.* Int J Mol Sci, 2021. **22**(9).
188. Chen, T., et al., *Mutant UBQLN2P497H in motor neurons leads to ALS-like phenotypes and defective autophagy in rats.* Acta Neuropathologica Communications, 2018. **6**(1): p. 122.
189. Chen, T., et al., *UBQLN2 Promotes the Production of Type I Interferon via the TBK1-IRF3 Pathway.* Cells, 2020. **9**(5).

190. Gilpin, K.M., L. Chang, and M.J. Monteiro, *ALS-linked mutations in ubiquilin-2 or hnRNPA1 reduce interaction between ubiquilin-2 and hnRNPA1.* Hum Mol Genet, 2015. **24**(9): p. 2565-77.
191. Guil, S., J.C. Long, and J.F. Cáceres, *hnRNP A1 relocalization to the stress granules reflects a role in the stress response.* Molecular and cellular biology, 2006. **26**(15): p. 5744-5758.
192. Dao, T.P., et al., *ALS-Linked Mutations Affect UBQLN2 Oligomerization and Phase Separation in a Position- and Amino Acid-Dependent Manner.* Structure, 2019. **27**(6): p. 937-951 e5.
193. Kim, S.H., et al., *Mutation-dependent aggregation and toxicity in a Drosophila model for UBQLN2-associated ALS.* Hum Mol Genet, 2018. **27**(2): p. 322-337.
194. Riley, J.F., et al., *ALS-linked mutations impair UBQLN2 stress-induced biomolecular condensate assembly in cells.* J Neurochem, 2021. **159**(1): p. 145-155.
195. Borisy, G.G., et al., *Purification of tubulin and associated high molecular weight proteins from porcine brain and characterization of microtubule assembly in vitro.* Ann N Y Acad Sci, 1975. **253**: p. 107-32.
196. Mohan, R. and A. John, *Microtubule-associated proteins as direct crosslinkers of actin filaments and microtubules.* IUBMB Life, 2015. **67**(6): p. 395-403.
197. Utreras, E., et al., *Microtubule-associated protein 1B interaction with tubulin tyrosine ligase contributes to the control of microtubule tyrosination.* Dev Neurosci, 2008. **30**(1-3): p. 200-10.
198. Qiang, L., et al., *Tau Does Not Stabilize Axonal Microtubules but Rather Enables Them to Have Long Labile Domains.* Current Biology, 2018. **28**(13): p. 2181-2189.e4.
199. Leung, C.L., et al., *Microtubule actin cross-linking factor (MACF): a hybrid of dystonin and dystrophin that can interact with the actin and microtubule cytoskeletons.* J Cell Biol, 1999. **147**(6): p. 1275-86.
200. Yang, Y., et al., *An essential cytoskeletal linker protein connecting actin microfilaments to intermediate filaments.* Cell, 1996. **86**(4): p. 655-65.
201. Barlan, K., W. Lu, and Vladimir I. Gelfand, *The Microtubule-Binding Protein Ensconsin Is an Essential Cofactor of Kinesin-1.* Current Biology, 2013. **23**(4): p. 317-322.
202. Hooikaas, P.J., et al., *MAP7 family proteins regulate kinesin-1 recruitment and activation.* J Cell Biol, 2019. **218**(4): p. 1298-1318.
203. Siahaan, V., et al., *Kinetically distinct phases of tau on microtubules regulate kinesin motors and severing enzymes.* Nature Cell Biology, 2019. **21**(9): p. 1086-1092.
204. Tortosa, E., L.C. Kapitein, and C.C. Hoogenraad, *Microtubule Organization and Microtubule-Associated Proteins (MAPs)*, in *Dendrites: Development and Disease*, K. Emoto, et al., Editors. 2016, Springer Japan: Tokyo. p. 31-75.
205. Gao, Y.L., et al., *Tau in neurodegenerative disease.* Ann Transl Med, 2018. **6**(10): p. 175.
206. Halpain, S. and L. Dehmelt, *The MAP1 family of microtubule-associated proteins.* Genome Biol, 2006. **7**(6): p. 224.
207. Orbán-Németh, Z., et al., *Microtubule-associated Protein 1S, a Short and Ubiquitously Expressed Member of the Microtubule-associated Protein 1 Family *.* Journal of Biological Chemistry, 2005. **280**(3): p. 2257-2265.
208. Hammarback, J.A., et al., *MAP1B is encoded as a polyprotein that is processed to form a complex N-terminal microtubule-binding domain.* Neuron, 1991. **7**(1): p. 129-139.
209. Langkopf, A., et al., *Microtubule-associated proteins 1A and LC2. Two proteins encoded in one messenger RNA.* Journal of Biological Chemistry, 1992. **267**(23): p. 16561-16566.
210. Ramkumar, A., B.Y. Jong, and K.M. Ori-McKenney, *ReMAPping the microtubule landscape: How phosphorylation dictates the activities of microtubule-associated proteins.* Dev Dyn, 2018. **247**(1): p. 138-155.
211. Schoenfeld, T.A., et al., *MAP 1A and MAP 1B are structurally related microtubule associated proteins with distinct developmental patterns in the CNS.* J Neurosci, 1989. **9**(5): p. 1712-30.

212. Asai, D.J., et al., *Microtubule-associated proteins (MAPs): a monoclonal antibody to MAP 1 decorates microtubules in vitro but stains stress fibers and not microtubules in vivo.* Proc Natl Acad Sci U S A, 1985. **82**(5): p. 1434-8.
213. Bloom, G.S., F.C. Luca, and R.B. Vallee, *Microtubule-associated protein 1B: identification of a major component of the neuronal cytoskeleton.* Proceedings of the National Academy of Sciences of the United States of America, 1985. **82**(16): p. 5404-5408.
214. Calvert, R. and B.H. Anderton, *A microtubule-associated protein (MAP1) which is expressed at elevated levels during development of the rat cerebellum.* Embo j, 1985. **4**(5): p. 1171-6.
215. Riederer, B., R. Cohen, and A. Matus, *MAP5: a novel brain microtubule-associated protein under strong developmental regulation.* J Neurocytol, 1986. **15**(6): p. 763-75.
216. Tucker, R.P., C.C. Garner, and A. Matus, *In situ localization of microtubule-associated protein mRNA in the developing and adult rat brain.* Neuron, 1989. **2**(3): p. 1245-56.
217. Black, M.M., T. Slaughter, and I. Fischer, *Microtubule-associated protein 1b (MAP1b) is concentrated in the distal region of growing axons.* J Neurosci, 1994. **14**(2): p. 857-70.
218. DiTella, M.C., et al., *MAP-1B/TAU functional redundancy during laminin-enhanced axonal growth.* J Cell Sci, 1996. **109 ( Pt 2)**: p. 467-77.
219. Gonzalez-Billault, C., J. Avila, and A. Caceres, *Evidence for the role of MAP1B in axon formation.* Mol Biol Cell, 2001. **12**(7): p. 2087-98.
220. Nothias, F., et al., *Expression of a phosphorylated isoform of MAP1B is maintained in adult central nervous system areas that retain capacity for structural plasticity.* J Comp Neurol, 1996. **368**(3): p. 317-34.
221. Emery, D.L., et al., *Bilateral growth-related protein expression suggests a transient increase in regenerative potential following brain trauma.* J Comp Neurol, 2000. **424**(3): p. 521-31.
222. Book, A.A., et al., *Altered expression of microtubule-associated proteins in cat trochlear motoneurons after peripheral and central lesions of the trochlear nerve.* Exp Neurol, 1996. **138**(2): p. 214-26.
223. Collins, M.O., et al., *Proteomic analysis of in vivo phosphorylated synaptic proteins.* J Biol Chem, 2005. **280**(7): p. 5972-82.
224. The UniProt Consortium, *UniProt: the universal protein knowledgebase in 2021.* Nucleic Acids Res, 2021. **49**(D1): p. D480-d489.
225. Ulloa, L., J. Avila, and J. Diaz-Nido, *Heterogeneity in the phosphorylation of microtubule-associated protein MAP1B during rat brain development.* J Neurochem, 1993. **61**(3): p. 961-72.
226. García-Pérez, J., J. Avila, and J. Díaz-Nido, *Implication of cyclin-dependent kinases and glycogen synthase kinase 3 in the phosphorylation of microtubule-associated protein 1B in developing neuronal cells.* J Neurosci Res, 1998. **52**(4): p. 445-52.
227. Ulloa, L., et al., *Localization of differentially phosphorylated isoforms of microtubule-associated protein 1B in cultured rat hippocampal neurons.* Neuroscience, 1994. **61**(2): p. 211-23.
228. Díaz-Nido, J., et al., *A casein kinase II-related activity is involved in phosphorylation of microtubule-associated protein MAP-1B during neuroblastoma cell differentiation.* Journal of Cell Biology, 1988. **106**(6): p. 2057-2065.
229. Ulloa, L., J. Díaz-Nido, and J. Avila, *Depletion of casein kinase II by antisense oligonucleotide prevents neuritogenesis in neuroblastoma cells.* Embo j, 1993. **12**(4): p. 1633-40.
230. Barbier, P., et al., *Role of Tau as a Microtubule-Associated Protein: Structural and Functional Aspects.* 2019. **11**(204).
231. Pedrotti, B. and K. Islam, *Microtubule associated protein 1B (MAP1B) promotes efficient tubulin polymerisation in vitro.* FEBS Lett, 1995. **371**(1): p. 29-31.
232. Vandecandelaere, A., et al., *Differences in the regulation of microtubule dynamics by microtubule-associated proteins MAP1B and MAP2.* Cell Motil Cytoskeleton, 1996. **35**(2): p. 134-46.

233. Goold, R.G., R. Owen, and P.R. Gordon-Weeks, *Glycogen synthase kinase 3beta phosphorylation of microtubule-associated protein 1B regulates the stability of microtubules in growth cones.* J Cell Sci, 1999. **112 ( Pt 19)**: p. 3373-84.
234. Barnat, M., et al., *The GSK3-MAP1B pathway controls neurite branching and microtubule dynamics.* Mol Cell Neurosci, 2016. **72**: p. 9-21.
235. Tortosa, E., et al., *MAP1B regulates microtubule dynamics by sequestering EB1/3 in the cytosol of developing neuronal cells.* Embo j, 2013. **32**(9): p. 1293-306.
236. Moritz, A., et al., *Metabotropic glutamate receptor 4 interacts with microtubule-associated protein 1B.* Biochem Biophys Res Commun, 2009. **390**(1): p. 82-6.
237. Hanley, J.G., et al., *The protein MAP-1B links GABA(C) receptors to the cytoskeleton at retinal synapses.* Nature, 1999. **397**(6714): p. 66-9.
238. Palenzuela, R., et al., *MAP1B Light Chain Modulates Synaptic Transmission via AMPA Receptor Intracellular Trapping.* J Neurosci, 2017. **37**(41): p. 9945-9963.
239. Gandini, M.A., et al., *CaV2.2 channel cell surface expression is regulated by the light chain 1 (LC1) of the microtubule-associated protein B (MAP1B) via UBE2L3-mediated ubiquitination and degradation.* Pflügers Archiv - European Journal of Physiology, 2014. **466**(11): p. 2113-2126.
240. O'Brien, J.E., et al., *Interaction of Voltage-gated Sodium Channel Nav1.6 (SCN8A) with Microtubule-associated Protein Map1b*.* Journal of Biological Chemistry, 2012. **287**(22): p. 18459-18466.
241. Eriksson, M., et al., *MAP1B binds to the NMDA receptor subunit NR3A and affects NR3A protein concentrations.* Neurosci Lett, 2010. **475**(1): p. 33-7.
242. Kim, S.H., et al., *Direct interaction and functional coupling between human 5-HT6 receptor and the light chain 1 subunit of the microtubule-associated protein 1B (MAP1B-LC1).* PLoS One, 2014. **9**(3): p. e91402.
243. Sun, H., et al., *Modulation of 5-HT3 receptor desensitization by the light chain of microtubule-associated protein 1B expressed in HEK 293 cells.* J Physiol, 2008. **586**(3): p. 751-62.
244. Billups, D., et al., *GABAC receptor sensitivity is modulated by interaction with MAP1B.* J Neurosci, 2000. **20**(23): p. 8643-50.
245. Mann, S.S. and J.A. Hammarback, *Molecular characterization of light chain 3. A microtubule binding subunit of MAP1A and MAP1B.* J Biol Chem, 1994. **269**(15): p. 11492-7.
246. Harrison, B., et al., *DAPK-1 binding to a linear peptide motif in MAP1B stimulates autophagy and membrane blebbing.* J Biol Chem, 2008. **283**(15): p. 9999-10014.
247. Marchbank, K., et al., *MAP1B Interaction with the FW Domain of the Autophagic Receptor Nbr1 Facilitates Its Association to the Microtubule Network.* Int J Cell Biol, 2012. **2012**: p. 208014.
248. Arasaki, K., et al., *MAP1B-LC1 prevents autophagosome formation by linking syntaxin 17 to microtubules.* EMBO Rep, 2018. **19**(8).
249. Tretyakova, I., et al., *Nuclear export factor family protein participates in cytoplasmic mRNA trafficking.* J Biol Chem, 2005. **280**(36): p. 31981-90.
250. Fujiwara, Y., et al., *Microtubule association of a neuronal RNA-binding protein HuD through its binding to the light chain of MAP1B.* Biochimie, 2011. **93**(5): p. 817-22.
251. Mirisis, A.A. and T.J. Carew, *The ELAV family of RNA-binding proteins in synaptic plasticity and long-term memory.* Neurobiology of Learning and Memory, 2019. **161**: p. 143-148.
252. Jensen, P.H., et al., *Microtubule-associated protein 1B is a component of cortical Lewy bodies and binds alpha-synuclein filaments.* J Biol Chem, 2000. **275**(28): p. 21500-7.
253. Wang, Z., et al., *DJ-1 can inhibit microtubule associated protein 1 B formed aggregates.* Mol Neurodegener, 2011. **6**: p. 38.
254. Chan, S.L., et al., *MAP1B rescues LRRK2 mutant-mediated cytotoxicity.* Mol Brain, 2014. **7**: p. 29.
255. Hasegawa, M., T. Arai, and Y. Ihara, *Immunochemical evidence that fragments of phosphorylated MAP5 (MAP1B) are bound to neurofibrillary tangles in Alzheimer's disease.* Neuron, 1990. **4**(6): p. 909-18.

256. Ulloa, L., et al., *Microtubule-associated protein 1B (MAP1B) is present in glial cells phosphorylated different than in neurones.* Glia, 1994. **10**(4): p. 266-75.
257. Johnson-Kerner, B.L., et al., *Giant axonal neuropathy: An updated perspective on its pathology and pathogenesis.* Muscle & Nerve, 2014. **50**(4): p. 467-476.
258. Ding, J., et al., *Microtubule-associated protein 1B: a neuronal binding partner for gigaxonin.* J Cell Biol, 2002. **158**(3): p. 427-33.
259. Allen, E., et al., *Gigaxonin-controlled degradation of MAP1B light chain is critical to neuronal survival.* Nature, 2005. **438**(7065): p. 224-8.
260. Romano, M., F. Feiguin, and E. Buratti, *TBPH/TDP-43 modulates translation of Drosophila futsch mRNA through an UG-rich sequence within its 5'UTR.* Brain Research, 2016. **1647**: p. 50-56.
261. Coyne, A.N., et al., *Futsch/MAP1B mRNA is a translational target of TDP-43 and is neuroprotective in a Drosophila model of amyotrophic lateral sclerosis.* J Neurosci, 2014. **34**(48): p. 15962-74.
262. Zalfa, F., et al., *The fragile X syndrome protein FMRP associates with BC1 RNA and regulates the translation of specific mRNAs at synapses.* Cell, 2003. **112**(3): p. 317-27.
263. Imperatore, J.A., et al., *FUS Recognizes G Quadruplex Structures Within Neuronal mRNAs.* Front Mol Biosci, 2020. **7**: p. 6.
264. Rappsilber, J., M. Mann, and Y. Ishihama, *Protocol for micro-purification, enrichment, pre-fractionation and storage of peptides for proteomics using StageTips.* Nat Protoc, 2007. **2**(8): p. 1896-906.
265. Strohm, L., et al., *Multi-omics profiling identifies a deregulated FUS-MAP1B axis in ALS/FTD–associated UBQLN2 mutants.* Life Science Alliance, 2022. **5**(11): p. e202101327.
266. Loughlin, F.E., et al., *The Solution Structure of FUS Bound to RNA Reveals a Bipartite Mode of RNA Recognition with Both Sequence and Shape Specificity.* Mol Cell, 2019. **73**(3): p. 490-504.e6.
267. Wu, Q., et al., *Pathogenic Ubqln2 gains toxic properties to induce neuron death.* Acta Neuropathologica, 2015. **129**(3): p. 417-428.
268. Sharkey, L.M., et al., *Modeling UBQLN2-mediated neurodegenerative disease in mice: Shared and divergent properties of wild type and mutant UBQLN2 in phase separation, subcellular localization, altered proteostasis pathways, and selective cytotoxicity.* Neurobiol Dis, 2020. **143**: p. 105016.
269. Bannwarth, S., et al., *A mitochondrial origin for frontotemporal dementia and amyotrophic lateral sclerosis through CHCHD10 involvement.* Brain, 2014. **137**(Pt 8): p. 2329-45.
270. Chaussenot, A., et al., *Screening of CHCHD10 in a French cohort confirms the involvement of this gene in frontotemporal dementia with amyotrophic lateral sclerosis patients.* Neurobiology of Aging, 2014. **35**(12): p. 2884.e1-2884.e4.
271. Genin, E.C., et al., *CHCHD10 mutations promote loss of mitochondrial cristae junctions with impaired mitochondrial genome maintenance and inhibition of apoptosis.* EMBO Molecular Medicine, 2016. **8**(1): p. 58-72.
272. Sasaki, S. and M. Iwata, *Mitochondrial Alterations in the Spinal Cord of Patients With Sporadic Amyotrophic Lateral Sclerosis.* Journal of Neuropathology & Experimental Neurology, 2007. **66**(1): p. 10-16.
273. Magrané, J., et al., *Abnormal mitochondrial transport and morphology are common pathological denominators in SOD1 and TDP43 ALS mouse models.* Human Molecular Genetics, 2013. **23**(6): p. 1413-1424.
274. Wang, W., et al., *The ALS disease-associated mutant TDP-43 impairs mitochondrial dynamics and function in motor neurons.* Human Molecular Genetics, 2013. **22**(23): p. 4706-4719.
275. Onesto, E., et al., *Gene-specific mitochondria dysfunctions in human TARDBP and C9ORF72 fibroblasts.* Acta Neuropathologica Communications, 2016. **4**(1): p. 47.
276. Stribl, C., et al., *Mitochondrial Dysfunction and Decrease in Body Weight of a Transgenic Knock-in Mouse Model for TDP-43*.* Journal of Biological Chemistry, 2014. **289**(15): p. 10769-10784.

277. Halloran, M., et al., *Amyotrophic lateral sclerosis-linked UBQLN2 mutants inhibit endoplasmic reticulum to Golgi transport, leading to Golgi fragmentation and ER stress.* Cell Mol Life Sci, 2020. **77**(19): p. 3859-3873.
278. Chen, Q.Y., et al., *Exosomal Proteins and miRNAs as Mediators of Amyotrophic Lateral Sclerosis.* Frontiers in Cell and Developmental Biology, 2021. **9**.
279. Frühbeis, C., et al., *Extracellular vesicles as mediators of neuron-glia communication.* Frontiers in Cellular Neuroscience, 2013. **7**.
280. Gagliardi, D., et al., *Extracellular vesicles and amyotrophic lateral sclerosis: from misfolded protein vehicles to promising clinical biomarkers.* Cellular and Molecular Life Sciences, 2021. **78**(2): p. 561-572.
281. Liu, X. and J.L. Henty-Ridilla, *Multiple roles for the cytoskeleton in ALS.* Experimental Neurology, 2022. **355**: p. 114143.
282. Zhang, Y.Q., et al., *Drosophila Fragile X-Related Gene Regulates the MAP1B Homolog Futsch to Control Synaptic Structure and Function.* Cell, 2001. **107**(5): p. 591-603.
283. Bora, G., et al., *Microtubule-associated protein 1B dysregulates microtubule dynamics and neuronal mitochondrial transport in spinal muscular atrophy.* Hum Mol Genet, 2021. **29**(24): p. 3935-3944.
284. Bowerman, M., et al., *Pathogenic commonalities between spinal muscular atrophy and amyotrophic lateral sclerosis: Converging roads to therapeutic development.* European Journal of Medical Genetics, 2018. **61**(11): p. 685-698.
285. Shi, Q., et al., *Tubulin Polymerization Promoting Protein, Ringmaker, and MAP1B Homolog Futsch Coordinate Microtubule Organization and Synaptic Growth.* Frontiers in Cellular Neuroscience, 2019. **13**.
286. Baas, P.W., et al., *Stability properties of neuronal microtubules.* Cytoskeleton, 2016. **73**(9): p. 442-460.
287. Fanara, P., et al., *Stabilization of hyperdynamic microtubules is neuroprotective in amyotrophic lateral sclerosis.* The Journal of biological chemistry, 2007. **282**(32): p. 23465-23472.
288. Villarroel-Campos, D. and C. Gonzalez-Billault, *The MAP1B case: An old MAP that is new again.* Developmental Neurobiology, 2014. **74**(10): p. 953-971.
289. Carrel, L. and H.F. Willard, *X-inactivation profile reveals extensive variability in X-linked gene expression in females.* Nature, 2005. **434**(7031): p. 400-404.
290. Wang, S., M. Tatman, and M.J. Monteiro, *Overexpression of UBQLN1 reduces neuropathology in the P497S UBQLN2 mouse model of ALS/FTD.* Acta Neuropathol Commun, 2020. **8**(1): p. 164.
291. Huang, B., et al., *Increased Ubqln2 expression causes neuron death in transgenic rats.* Journal of Neurochemistry, 2016. **139**(2): p. 285-293.
292. Le, N.T., et al., *Motor neuron disease, TDP-43 pathology, and memory deficits in mice expressing ALS-FTD-linked UBQLN2 mutations.* Proc Natl Acad Sci U S A, 2016. **113**(47): p. E7580-e7589.
293. Lin, B.C., et al., *UBQLN proteins in health and disease with a focus on UBQLN2 in ALS/FTD.* The FEBS Journal, 2021. **n/a**(n/a).
294. Guipaud, O., et al., *An in vitro enzymatic assay coupled to proteomics analysis reveals a new DNA processing activity for Ewing sarcoma and TAF(II)68 proteins.* PROTEOMICS, 2006. **6**(22): p. 5962-5972.
295. Mertins, P., et al., *Proteogenomics connects somatic mutations to signalling in breast cancer.* Nature, 2016. **534**(7605): p. 55-62.
296. Murthy, A.C., et al., *Molecular interactions underlying liquid−liquid phase separation of the FUS low-complexity domain.* Nature Structural & Molecular Biology, 2019. **26**(7): p. 637-648.
297. Monahan, Z., et al., *Phosphorylation of the FUS low-complexity domain disrupts phase separation, aggregation, and toxicity.* EMBO J, 2017. **36**(20): p. 2951-2967.
298. Iko, Y., et al., *Domain Architectures and Characterization of an RNA-binding Protein, TLS*.* Journal of Biological Chemistry, 2004. **279**(43): p. 44834-44840.

299. Vieira-Vieira, C.H., et al., *Proteome-wide quantitative RNA-interactome capture identifies phosphorylation sites with regulatory potential in RBM20.* Molecular Cell, 2022. **82**(11): p. 2069-2083.e8.
300. Coffey, R.T., et al., *Ubiquilin-mediated Small Molecule Inhibition of Mammalian Target of Rapamycin Complex 1 (mTORC1) Signaling.* J Biol Chem, 2016. **291**(10): p. 5221-33.
301. Gerson, J.E., et al., *Disrupting the Balance of Protein Quality Control Protein UBQLN2 Accelerates Tau Proteinopathy.* The Journal of Neuroscience, 2022. **42**(9): p. 1845.

# Acknowledgements

*Little by little, one travels far."*

-J.R.R. Tolkien / Spanish Saying

Ich möchte mich von Herzen bei all denen bedanken, die mich während der letzten 5 Jahre auf unterschiedlichster Weise unterstützt haben.

Ein besonderer Dank gilt **Chris**, der mir nicht nur die Möglichkeit gegeben hat in seiner Arbeitsgruppe meine Doktorarbeit durchzuführen, sondern zu jeder Tageszeit für mich erreichbar war und stehts ein offenes Ohr für mich hatte. Vor allem hat er mich durch seine große Begeisterung für unsere Forschung immer wieder motiviert und inspiriert.

Ein großer Dank geht an all meinen **Kooperationspartner** sowohl für die wertvollen Beiträge zu meinem Projekt als auch für die gemeinsamen Projekte und allen **Mitgliedern der Prüfungskommission** für ihre kostbare Zeit.

Ausgesprochen dankbar bin ich meinen aktuellen (**Alex, Nessi, JJ, K, Debjani, Sophie und Alina$^2$**) und ehemaligen (**Franzi, Lu und Susa**) Kollegen des Behrendslabs, von welchen viele für mich so viel mehr als nur Kollegen geworden sind. Eine so intensive Zeit wie die des PhDs schweißt einen auf eine ganz besondere Art und Weise zusammen. Ich habe mich jeden einzelnen Tag gefreut ins Labor zu kommen, weil ich dort Zeit mit euch verbringen konnte. Wir haben nicht nur gemeinsam versucht Protokolle zu optimieren, die Masse zum Laufen zu bringen, Fehler zu identifizieren oder Proben aus dem Müllereimer zu fischen, sondern haben zusammen gelacht, geweint, getanzt, gesungen, sind gewandert und so vieles mehr.

Sehr dankbar bin ich auch den Mitgliedern der Eddie-, Steiner-, Fisch- und Haass-Gruppe, sowie Sabine für Ratschläge, Versorgung mit Reagenzien und Equipment und tollen Unterhaltungen. Insbesondere möchte ich mich bei Eddie, Mareike und Henni für ihre Hilfe bei den Rattenneuronen bedanken.

Danke liebe **Radl-Gang**: auch scheinbare Kleinigkeiten, wie unsere gemeinsame Radlfahrt oder unseren morgendlichen Kaffee/Tee haben jeden Tag bereichert.

In Bezug auf meine Thesis möchte ich mich nochmals besonders bei **Susa, K, Annika, Alex, Johannes und Nadine** für das Gegenlesen von Textabschnitten, das freundliche Kritisieren meiner Grafiken oder ihren Input zur Form und Organisation bedanken.

Ein ganz besonderer Dank geht an meine wundervollen Freunde. **Annika**, die schon seit meiner Schulzeit immer für mich da ist. **Joules und Maddin**, für die gemütlichen Feierabend-Biere der letzten Jahre und eure tolle Freundschaft. **Nadine**, für die spaßigen Tanznächte,

unendlichen Spaziergängen und Dinner-Dates. **Nele**, für regelmäßige München-Besuche, spontane Spaziergänge, die liebevollen Karten und das tolle Survival-Paket. **Linda**, für die vielen Lunch-Dates, Grillabende und natürlich für deinen unermüdlichen Einsatz für meinen Finger. Und schließlich **Maria**, meine Lieblings-Streberin, mit der ich so viele spaßige Momente verbringe, sie mich aber auch immer wieder anspornt mein Bestes zu geben.

Ohne die Unterstützung und den Halt meiner Familie wäre ich nie so weit gekommen. Vielen Dank **Lilli, Artur, Sarah & Bernd und Jasmin & Matthias**. Danke für euren unerschöpflichen Glauben an mich und euer Verständnis, wenn ich bei der ein oder anderen Familienfeier mal wieder nicht dabei sein konnte. Auch bei **Marianne** und **Gerhard** möchte ich mich herzlich für ihr großes Verständnis und ihre Unterstützung bedanken.

Ein letzter Dank geht an **Alex**. Danke, dass du für mich nach München gekommen bist. Danke, dass du dir täglich all meine unendlichen Laborprobleme angehört hast, mir in den stressigen Phasen, also quasi immer, den Rücken freigehalten hast, mir Halt gibst, uneingeschränkt an mich glaubst und mich bei allem unterstützt was ich in Angriff nehme.

# Affidavit

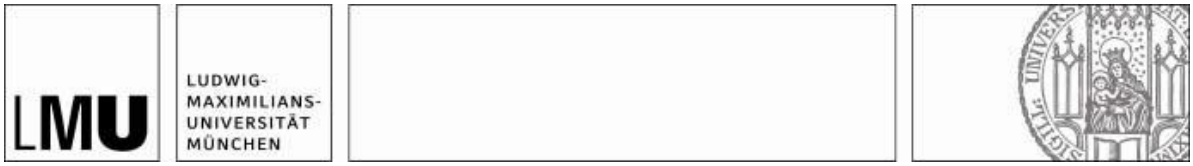


## Eidesstattliche Versicherung

Strohm, Laura

Name, Vorname

Ich erkläre hiermit an Eides statt, dass ich die vorliegende Dissertation mit dem Thema

"Dissecting the role of UBQLN2 in amyotrophic lateral sclerosis and frontotemporal dementia using multi-omics profiling"

selbständig verfasst, mich außer der angegebenen keiner weiteren Hilfsmittel bedient und alle Erkenntnisse, die aus dem Schrifttum ganz oder annähernd übernommen sind, als solche kenntlich gemacht und nach ihrer Herkunft unter Bezeichnung der Fundstelle einzeln nachgewiesen habe.

Ich erkläre des Weiteren, dass die hier vorgelegte Dissertation nicht in gleicher oder in ähnlicher Form bei einer anderen Stelle zur Erlangung eines akademischen Grades eingereicht wurde.

Dettenhausen, 02.04.2023 — Laura Strohm

Ort, Datum — Unterschrift Doktorandin/Doktorand